The Activation of Mitogen-Activated Protein Kinases in the Optic Nerve Head in a Model of Ocular Hypertension

Teresa Mammone

A thesis submitted to the University of Adelaide in fulfilment of

Masters of Philosophy (Ophthalmology)

In

The Discipline of Ophthalmology & Visual Sciences, School of Medicine

August 2017

CONTENTS

ABSTRACT

Glaucoma is a neurological blinding eye disease, which results from the death of retinal ganglion cells. Although the pathogenesis of glaucoma remains unknown, changes in the tissue microenvironment of the optic nerve head (ONH), where insults are believed to be initiated, will cause signalling alterations in local cells. One important type of signalling involved in the control of cellular functions is protein phosphorylation. This is controlled by the balance between protein kinases and protein phosphatases, which add and remove phosphate groups respectively. One particularly important group of protein kinases is the mitogen-activated protein kinase (MAPK) family, whose activity is known to be altered in neurological diseases.

The first aim of this thesis was to determine whether specific MAPK family members (P42/44 MAPK, SAPK/JNK MAPK and P38 MAPK) were altered in a laser-induced ocular hypertension model, used to simulate the pressure elevation often associated with glaucoma. Techniques used for analysis included immunohistochemistry to observe changes in histopathological activation and location, Western immunoblotting to quantify changes in protein level expression, and real time reverse-transcriptase polymerase chain reaction to establish whether there were any changes in MAPK gene expression.

Total P42/44 MAPK expression was unaffected after intraocular pressure elevation, but a significant increase in its activation was detected in astrocytes in the ONH after 6-24 hours. Active SAPK/JNK was present throughout treated and untreated RGC axons, but accumulated in the ONH at 6-24 hours after pressure elevation, signifying axon transport disruption. P38 MAPK was expressed by a population of microglial cells throughout the retina, ONH and optic nerve, which were significantly increased in number following elevated intraocular pressure. However, this enzyme was only significantly activated in microglia after more than 3 days and

then not in the retina, where it was solely activated in retinal ganglion cell perikarya. These data imply both upregulation and activation of MAPK in the ocular hypertension model, in several distinct locations.

Levels of particular phosphoproteins are readily affected by minor perturbations in cellular homeostasis, as will occur when an animal is killed for tissue procurement. Thus, the second aim of this thesis was to identify whether activated MAPKs could be stabilised in procured tissues by perfusing animals with saline containing phosphatase inhibitors before fixation. Immunohistochemical analysis was used to observe differences in specific staining of phosphorylated MAPKs. The addition of phosphatase inhibitors to the perfusate had no significant effect on control animals or animals where there was a robust demonstration of tissue damage, but this procedure significantly reduced variability and improved clarity of outcome in labelling for activated MAPKs in animals with less extensive tissue damage, likely by stabilising levels of these phosphoproteins. These data suggest that phosphatase inhibitors stabilised phosphorylated MAPK levels and enabled a clearer dissemination of the activation of these enzymes, particularly when associated tissue damage was not extensive.

Having determined that MAPKs isoenzymes were activated in the ONH after sustained ocular hypertension, future work will concentrate on determining whether manipulation of these enzymes could play a useful role in the management of diseases such as glaucoma.

DECLARATION

I certify that this work contains no material which has been accepted for the award of any other degree or diploma in my name, in any university or other tertiary institution and, to the best of my knowledge and belief, contains no material previously published or written by another person, except where due reference has been made in the text. In addition, I certify that no part of this work will, in the future, be used in a submission in my name, for any other degree or diploma in any university or other tertiary institution without the prior approval of the University of Adelaide and where applicable, any partner institution responsible for the joint-award of this degree. I give consent to this copy of my thesis when deposited in the University Library, being made available for loan and photocopying, subject to the provisions of the Copyright Act 1968. I acknowledge that copyright of published works contained within this thesis resides with the copyright holder(s) of those works. I also give permission for the digital version of my thesis to be made available on the web, via the University's digital research repository, the Library Search and also through web search engines, unless permission has been granted by the University to restrict access for a period of time.

Teresa Mammone November 2017

Re: A1655487, School of Medicine, AHEGS Thesis Abstract

Wood, John (Health)

Wed 9/08/2017 1:14 PM

To:graduate centre <graduate.centre@adelaide.edu.au>;

Cc:Mammone, Teresa (Health) <Teresa.Mammone@sa.gov.au>;

1 attachment

Copy of ahegs-thesis-abstract-A1655487.xlsx;

To Graduate Centre

cc Teresa Mammone

I have looked through the attached AHEGS abstract for Teresa Mammone and I am happy with this.

Thank you and best wishes

John W

Abstract:
The aim of this thesis was to investigate the activation of mitogen activated protein kinases (MAPKs) in the optic nerve head in a laser-induced model of ocular hypertension (OHT).
Activation of three distinct sub-groups of MAPKs: P42/44 MAPK, SAPK/JNK and P38 MAPK was proven, by immunohistochemistry, Western immunoblot and reverse-transcriptase polymerase chain reaction.
In addition to this, a more sensitive method of detection for activated MAPKs was developed in order to identify whether the magnitude of the observed activations in the ONH were directly proportional to the degree of tissue damage in the model.

John P. M. Wood, D.Phil,
Senior Research Scientist,
Ophthalmic Research Laboratories,
Level 7, Adelaide Health and Medical Sciences Building,
The University of Adelaide,
North Terrace,
Adelaide,
South Australia 5000

PO Box 14, Rundle Mall,
South Australia 5000

Tel: +61 8 8313 7183

Email: john.wood2@sa.gov.au
john.wood@adelaide.edu.au

From: Teresa Mammone <teresa.mammone@adelaide.edu.au>
Sent: Wednesday, 9 August 2017 1:04 PM
To: graduate centre
Cc: Wood, John (Health)
Subject: A1655487, School of Medicine, AHEGS Thesis Abstract

Hi Dr Wood,

Attached is the AHEGS thesis abstract.

Please review and confirm, by reply of email, you are satisfied with the wording and submission of this abstract and thesis.

Regards
Teresa Mammone

ACKNOWLEDGMENT

The financial support of the Bright Focus Foundation, the Ophthalmic Research Institute of Australia and the National Health and Medical Research Council of Australia are gratefully acknowledged.

My heartfelt appreciation and sincere gratitude goes to the many people who have supported me in achieving the work presented here. Firstly, to Dr John Wood my principle supervisor, for his support, guidance and review of my work, which at times was no doubt challenging. And Dr Glyn Chidlow, for his positive critique. Their mentorship and knowledge in the scientific discipline of ophthalmology is exceptional.

To my work colleague, Mark Daymon, for his support, technical guidance in histology and friendship. Your years of wisdom and guidance through life's journey have provided much reassurance and laughter after the long and challenging working weeks.

To Professor Robert Casson and the supportive network of the Ophthalmic Research Laboratory Julia Winnick, thank you for your support and guidance.

To the Neuropathology Laboratory, Jim, Kathy, Bernice, Yvonne, Serg, Sven, Sofie and Dr Barbara Koszyca, thank you. The competitive nature of our morning tea cryptic crosswords will always be a fond memory.

To my parents Antonio and Maria, brothers Francesco and Vincenzo and sister Christina. My sister-in laws Rita and Katrina, and my beautify nephews and nieces, Anthony, Valentina, Amelia, Alessandro and Aria. You provided much support and laughter when I needed it the most.

A special mention and my gratitude go to the many people I have had the privilege of meeting though this work and developed life-time friendships. In particular to Dr Andreas Ebneter, thank you for your assistance in establishing and teaching me the glaucoma model. For all the fun we have shared both here in Adelaide and in Switzerland. I would also like to thank Alisa Kruger and Rebecca Spence for your words of wisdom and encouragement.

ABBREVIATIONS

AD; Alzheimer's disease

APP; Amyloid precursor protein

CNS; Central nervous system

HD; High damage

IOP; Intraocular pressure

LD; Low damage

MAPK; Mitogen-activated protein kinase

MPIs; Minus phosphatase inhibitors

NBF; Neutral buffered formalin containing 4 % formaldehyde

OHT ; Ocular hypertension

ONH; Optic nerve head

P38 MAPK ; P38 mitogen-activated protein kinase

P42/44 MAPK; Extracellular signal-regulated kinases (ERK)

PIs; Phosphatase inhibitors

POAG; Primary open-angle glaucoma

PPIs; Plus phosphatase inhibitors

RGC; Retinal ganglion cells

SAPK/JNK; Stress-activated protein kinase/c-Jun N-terminal kinases

INTRODUCTION

Glaucoma is characterised as an optic neuropathy, often associated with an increased intraocular pressure (IOP). This condition represents one of the leading causes of age-related blindness. More than 60.5 million people globally were diagnosed with glaucoma in 2010, and incidences of this disease are expected to increase to 79.6 million by 2020 (Quigley and Broman 2006). Glaucoma manifests itself as structural damage to the optic nerve and retinal ganglion cell (RGC) death by apoptosis. There are different forms of glaucoma: primary and secondary, open-angle and angle-closure. The most common form is primary open-angle glaucoma (POAG). POAG is categorized by an increase in IOP due to a dysfunction in aqueous humour production by ciliary epithelium and its outflow through the trabecular meshwork (Kokotas et al. 2012). Primary angle-closure glaucoma is characterised by a sudden increase in IOP due to blockage or narrowing of the angle between the iris and the cornea (Cedrone et al. 2008). Secondary open-angle glaucoma and secondary angle-closure glaucoma result from situations such as ocular injury, trauma, inflammation or tumour (Rohrbach et al. 2005). In contrast, normal tension glaucoma is not associated with an increased IOP. The pathogenesis of normal tension glaucoma is poorly understood, but is hypothesised to involve vascular insufficiency at the optic nerve head (ONH) (Harada et al. 2007). Congenital forms of glaucoma, often present in infants or early childhood, have also been described (Casson et al. 2012, Kokotas et al. 2012, Ray and Mookherjee 2009).

Anatomy of the visual system

To understand the development and pathology of glaucoma, a brief insight into the structure of the eye and visual pathway is required (Figure 1). The eye is made up of three outer layers,

the sclera forms the outer-most layer, encapsulating the globe, and is made of strong collagen fibres. The choroid is made up of a rich tissue supply of blood vessels. The vitreous humour fills the posterior chamber, while the lens and aqueous humour (produced by the ciliary body), occupy the anterior chamber. The retina, which lines the inner layer of the eye, is made up of distinct layers of cells (Figure 2A).

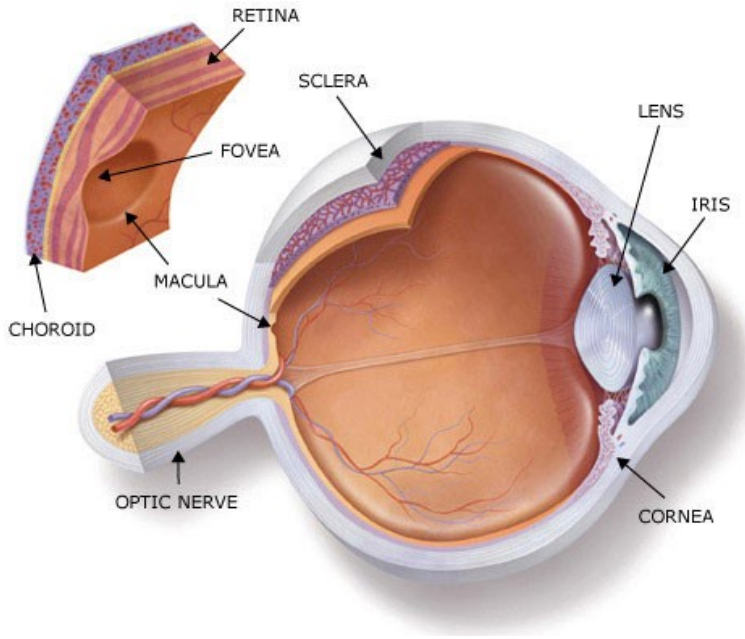

Figure 1. Anatomy of the eye. http://www.aapos.org/terms/conditions/22

The layers of the retina play a critical role in the detection and processing of incidental light, and the subsequent relay of visual information from the eye to the brain. Within the retina, light signals are detected by photoreceptors and transmitted as nerve impulses via bipolar cells to the RGCs. Within this linear pathway of neurons, laterally interconnecting horizontal and amacrine cells provide synaptic input (Figure 2B).

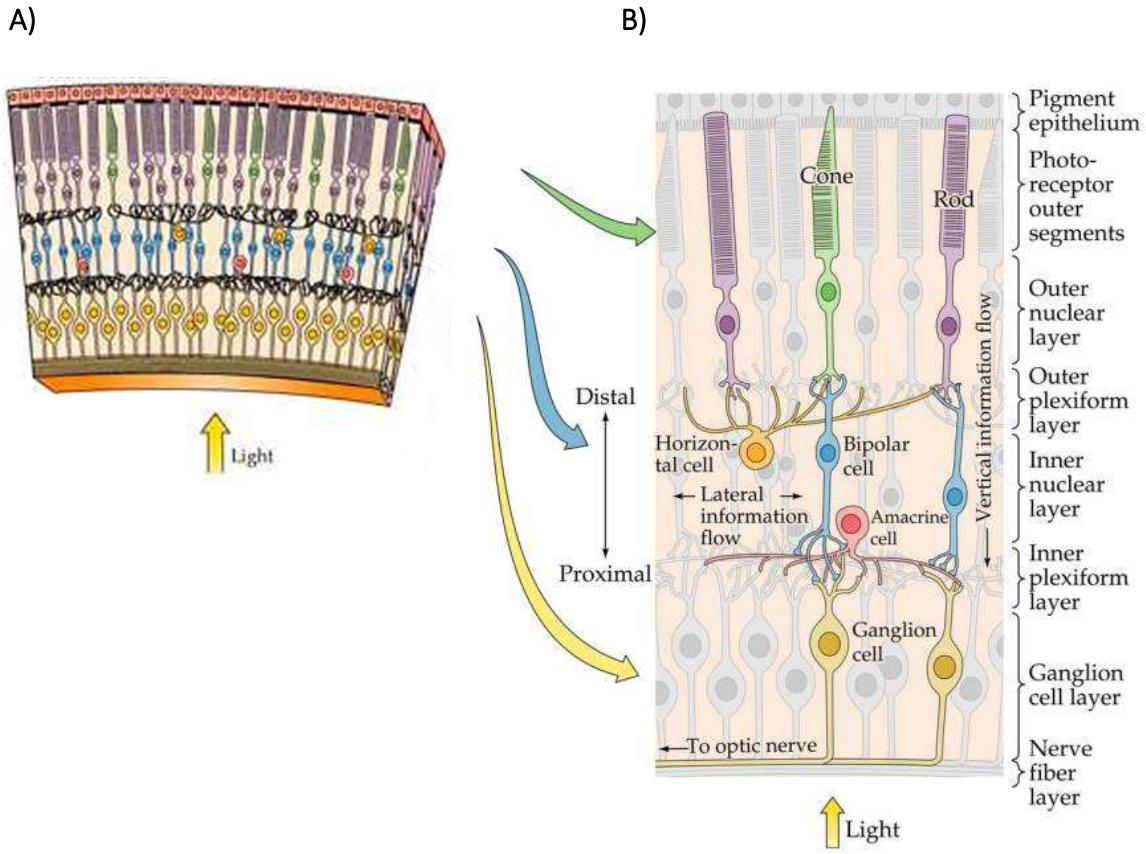

Figure 2. A) Structure of the retina. B) Diagram of the retinal cell layers. The pathway of cellular transmission begins with the photoreceptors at the distal end of the retinal layers and gets transmitted through the many layers before the information is sent along the nerve fiber layer, optic nerve, and ultimately to the brain (Purves D 2001).

The retina is also comprised of glial cells which play an important role in maintaining the structure and function of the retina (Vecino et al. 2016). The glial cell population is made up of three major types of cells: astrocytes, microglia and Müller cells. Müller cells are the principle type of glial cell within the retina. Their main function is in metabolic, ionic and extracellular support for neurons (Nomura-Komoike et al. 2016). Astrocytes provide structural support for the blood retinal barrier and retinal vascularisation (Wang et al. 2002). Microglia are located throughout the different retinal layers and optic nerve. They can be found in two

different states of function, resting or active. In their active state their function relates mainly to their macrophage action. This action is complemented by the secretion of chemical signals contributing to inflammation, cell death and cell survival (Wang et al. 2016).

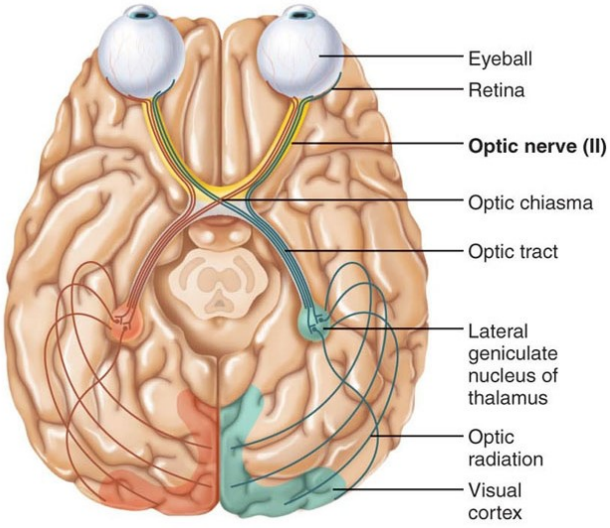

Figure 3. Visual pathways from the eye to the brain along the optic nerve. Nerve impulses are transported along the optic nerve, cross over at the optic chiasm and continue to the visual cortex through the optic tract.

RGCs transmit visual information via long, initially unmyelinated axons to several relay centres of the brain, including the lateral geniculate nucleus, suprachiasmatic nucleus and pretectal nucleus (Figure 3). Over 1.1 million RGC axons converge to form the optic nerve and these exit the retina at the ONH (Figure 4). The ONH is a sieve-like structure in humans made up of a network of collagen fibres, forming multilayer sheets, termed the lamina cribrosa, through which axons pass prior to becoming myelinated. Rodents do not possess a genuine lamina cribrosa of collagen fibres. Instead, they have a robust densely-packed network of astrocytes that has been termed a glial lamina (Howell et al. 2007). Optic nerves from each eye partially (humans) or almost completely (rodents) cross over and project to the opposite side

of the brain at the optic chiasm. The continuation of each optic nerve beyond the optic chiasm is known as the optic tract (Figure 3).

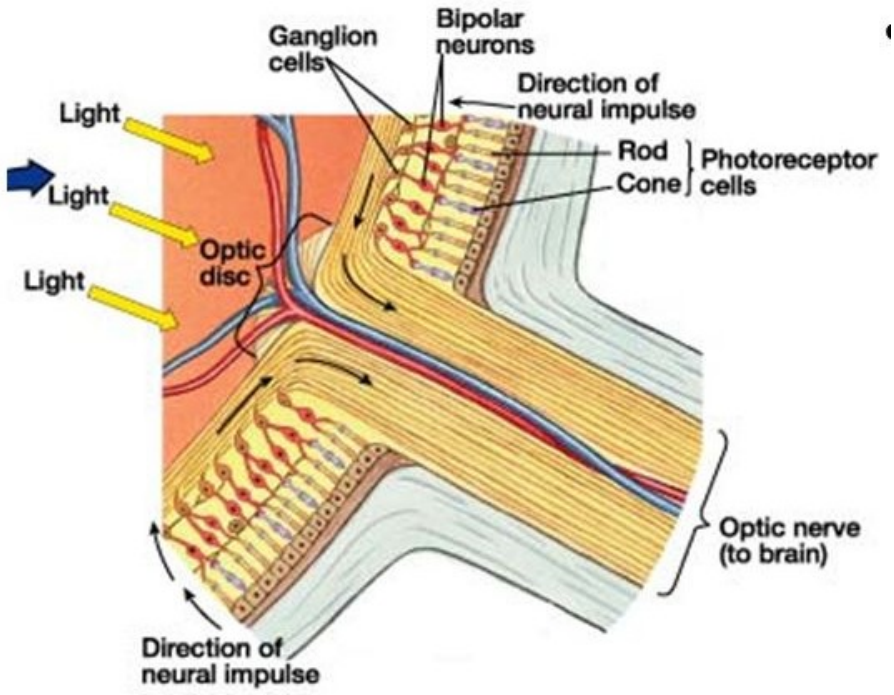

Figure 4. The ONH. RGC axons converge at the site of the ONH and enter the optic nerve on their way to the brain.

In order to study the biomechanics of glaucoma, researchers have made use of various models which mimic features associated with the disease. These models provide the framework used by researchers to look at potentially relevant pathology.

Models

Since there is no single experimental glaucoma model which can fully simulate the human disease, then the value of any given paradigm to a researcher must be selected, according to economic and/or practical issues and the specific experimental needs and hypotheses under investigation. To this end, a variety of in vivo (Table 1, adapted from Bouhenni et al. 2012) and

in vitro paradigms (Table 2) exist. These models either represent similar conditions in other animals, or attempt to mimic single or multiple aspects of the human disease. The use of such models assists in providing more detailed knowledge and understanding of the disorder, as well as aiming to ultimately identify different targets for therapy.

Available experimental models of glaucoma can be classified as acute, chronic, primary or secondary (Levin 2001). The acute model generally describes a sudden and substantial rise in IOP above systolic blood pressure, resulting in a likely ischemic effect on the retina, whereas the chronic system confers a relatively slow rise in pressure over time (Fitzgerald et al. 2009). Additionally, a primary model describes the direct effects of an injury, but a secondary paradigm can also delineate the effects of an insult at locations which are displaced from the initial injury site (Levkovitch-Verbin et al. 2003).

Each type of model is usually established in a different way and often concentrates upon specific aspects of pathological development which relate to glaucoma; eg acute elevation of IOP causes rapid ischemic effects to the inner retina (Adachi et al. 1996), whereas, chronic ocular hypertension (OHT), as conferred, for example, by lasering of the trabecular meshwork and episcleral veins (Levkovitch-Verbin et al. 2002) induces optic nerve dysfunction and subsequent RGC death.

Table 1. Examples of in vivo animal models

Glaucoma type	Animal	Model mode, mechanism	Reference
Primary open-angle glaucoma	Monkey	Laser photocoagulation of trabecular meshwork, reduced outflow	(Toris et al. 2000)
		Intracameral injection of latex microspheres, trabecular meshwork blockage	(Weber and Zelenak 2001)
		Intracameral injection of autologous fixed red blood cells, trabecular meshwork blockage	(Quigley and Addicks 1980)
	Mouse	Transgenic, alpha-1 subunit of collagen type I	(Mabuchi et al. 2004)
	Rat	Transgenic, eye mutations	(Sawaguchi et al. 2005)
	Zebrafish	Subconjunctival injection of betamethasone	(McMahon et al. 2004)
	Rabbit	Posterior chamber injection of α-chymotrypsin, trabecular meshwork blockage	(Melena et al. 1997)
Primary angle-closure glaucoma	Rat	Laser photocoagulation of translimbal region, reduced outflow	(Levkovitch-Verbin et al. 2002)
	Mouse	Laser photocoagulation of episcleral veins, reduced outflow	(Gross et al. 2003)
		Water loading, decreased outflow facility	(McDonald et al. 1969)
	Rabbit	Laser photocoagulation of trabecular meshwork, obstruction of outflow	(Johnson et al. 1999)
Primary congenital glaucoma	Rabbit	Spontaneous inheritance, WAG strain	(Fox et al. 1969, Hanna et al. 1962)
	Rat	Transgenic mutation	(Addison and How 1926)
	Mouse	Transgenic, gene mutation	
Normal tension	Mouse	Immunization against damage cell markers and RGC loss	(Shields 2008, Harada et al. 2007)
Autoimmune	Rat	Autoimmune	(Joachim et al. 2009)
	Rat	Optic nerve transaction, RGC loss from axonal injury	(Berkelaar et al. 1994)

Related in vitro studies allow researchers to investigate cellular responses and characterise the structure, function, and metabolic status of cells in culture from direct treatment (Table 2). Such in vitro models include explants of tissue, primary retinal cultures and transformed cell lines, often from rodent, human or porcine sources. Techniques such as

immuno-panning or culturing under specific conditions (for example with specific combinations of growth factors or on specific basal matrices), allow the isolation of certain cell types (Zhang et al. 2002). Injury models for in vitro studies can mainly be classified as either chemical or physical. As suggested, the former refers to the chemical manipulation of the culture medium to provoke a specific injurious response eg, hydrogen peroxide or sodium azide to cause oxidative stress or metabolic compromise, respectively (Wood et al. 2012). The use of hyperbaric pressure or hypoxia chambers to create physical insults are also useful in studying the stress responses of cells, by inducing alterations in atmospheric pressure or changes in bathing oxygen levels, respectively, in the cellular environment (Aihara et al. 2014).

Table 2. Examples of in vitro retinal culture models

Type	Source	Model, mechanism	Reference
Explants	Chicken embryo	Retina, long term photoreceptor cell study	(Thangaraj et al. 2011)
	Porcine retina	RGC response	(Luo et al. 2001)
		Retina mixed cells, through enzyme digestion	(Sander and Nauman 2010)
Primary cultures	Rat	Mixed retinal cultures	(Wood et al. 2012)
		RGC cultures	(Iwamoto et al. 2013, Pang et al. 2007)
		RGC- using patch-clamp, to study receptors through electrophysiological response	(Ullian et al. 2004)
		Retinal pigment epithelial cultures	(Pang et al. 2007)
Cell lines	Murinae	BV-2-microglial cell line, and inflammatory response	(Pittman et al. 1993)
	Rat	Adrenal medulla-PC12 cells, can be manipulated to differentiate into neuron-like cells	(Dang et al. 2014)
Cortical Neurons	Rat embryonic-day 17 gestation	Neuronal cell response to stimuli	(Martin et al. 2011)
		Immunomagnetic purification of cells	(Sappington et al. 2003)

RGC death

In the previous sections we have identified that healthy functioning RGCs are fundamental for good vision. Damage to, or death of these cells plays a critical role in the progression of glaucoma and the resultant visual loss. There are a range of characterised modes of cell death, but they are all believed to comprise a continuum, bounded by two distinct forms: (1) necrosis, by which damage to the cell, often resulting from inflammation, toxins, or external factors, causes sudden death; (2) apoptosis, by which a more subtle perturbation to the cellular environment occurs, leading to the activation of numerous cellular pathways and ultimately auto-destruction ("suicide") of the cell in a programmed manner (Degterev and Yuan 2008). It is believed that RGC death in glaucoma predominantly occurs through apoptosis, as has been observed in various experimental models of the disease (Agar et al. 2006, Levkovitch-Verbin 2015, Nakazawa et al. 2006) as well as in histological tissue from glaucoma patients (Chidlow et al. 2007).

It is likely that there are numerous stimuli that trigger the apoptotic pathway of RGC death in glaucoma (Lee et al. 2011). Factors are generally categorised as vascular (changes in nutrient supply), mechanical (physical alterations at the ONH), autoimmune (immune response acting against its own substrates), mitochondrial (alteration in energy supply for cells to function correctly) and neuroinflammatory (inflammation in neuronal tissue). It has been hypothesised that the breakdown of both the vascular supply and axonal transport to the retina of essential neurotrophins taken up in the brain, deprives the RGC body, or soma, of essential survival factors and this leads to apoptotic death of these cells. This not only suggests that axonal degeneration precedes RGC soma death, but also that interruptions in the supply of such factors can compromise RGC integrity (Nickells 1996, Munemasa and Kitaoka 2013). An imbalance in physiological levels of available neurotransmitters in the retina, including

excitatory glutamate or inhibitory γ-aminobutyric acid (GABA), as a response to hypoxic or ischemic injury, can also contribute to the induction of RGC death (Schmidt et al. 2004). Increased factors such as vascular endothelial growth factor as found in glaucoma are the result of changes in vascular supply, again possibly causing hypoxic conditions in the retina and contributed to by pre-clinical conditions such as diabetic retinopathy, central retinal vein occlusion and carotid artery obstructive disease (Ergorul et al. 2008, Horsley and Kahook 2010, Hu et al. 2002).

The site at which RGC axons enter the optic nerve is the ONH and this seems to be the primary location of insult in glaucoma. With over 1.1 million RGC axons converging at this site, it is obvious that any local detrimental influences will have a wide-ranging effect (Hernandez 2000).

In early stage glaucoma, it is thought that compression of the laminar sheets and bulging of the lamina cribrosa occurs (Edwards and Good 2001). These structural changes result in physical alterations to the supportive tissue, and also likely have influences on local blood flow (Figure 5). These facets of the injury give rise to notions of a “mechanical theory” and a “vascular theory” for the basis of glaucoma (Flammer et al. 2002). Whatever the root cause, it is clear that all of these events contribute in some manner to the developing axonopathy. Moreover, the increasing damage to axons at the ONH contributes to ganglion cell death and subsequent changes in vision.

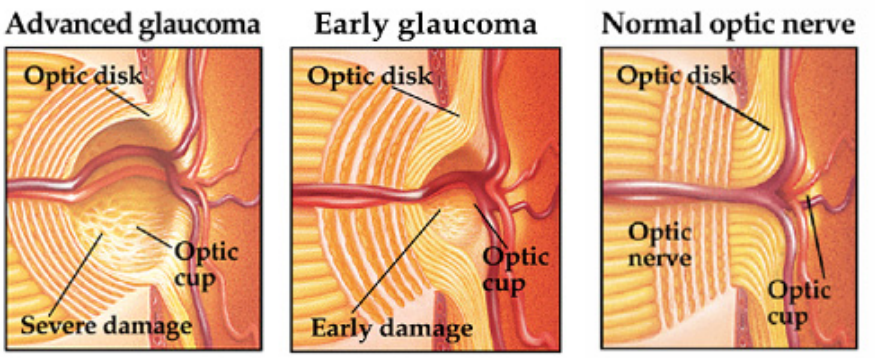

Figure 5. Changes in the ONH as seen in glaucoma.

By understanding the mechanisms by which RGC death can occur, we can derive insights into possible means by which these cells are caused to die in situ. In particular, axonal transport disruption in RGCs can have wide-ranging effects to the whole cell. With this in mind, analysis of pathological events in optic nerve axons as a result of experimental injury induction may provide useful information in the search for causes of RGC death.

Protein phosphorylation

Phosphorylation is the process by which a phosphate group (PO_4^{3-}) is added to a protein, as a post-translational modification, usually to positively or negatively regulate its activity or function. This regulation process is achieved by kinases or phosphatases, which phosphorylate or dephosphorylate proteins respectively.

The site-specific location of phosphorylation in an individual protein is highly conserved and usually occurs on any one of the serine, threonine, tyrosine or histidine residues. This leads to protein conformational changes and forms a mechanism by which signal transduction can occur. The modulation of kinases or phosphatases are by second messengers such as cyclic adenosine monophosphate, calcium ions (Ca^{2+}), or extracellular chemical signals such as

growth factors. Situations which cause non-physiological elevations in intracellular signalling moieties such as Ca^{2+}, can cause an imbalance in the relative activation of kinases relative to phosphatases. Signalling changes as a result of homeostatic disturbances in cells in the early stages of neurological stresses can stimulate changes in protein (de)phosphorylation. Such changes are likely to occur in tissue elements of the ONH as a response to mechanical, vascular or metabolic insults in glaucoma. Thus, investigation into changes in protein phosphorylation could prove useful in disseminating pathology involved in glaucomatous loss of RGC. One class of protein kinases known to be activated in stressed or diseased tissue, is the mitogen-activated protein kinase (MAPK) family. The role of these enzymes in RGC loss in glaucoma, however, remains unclear at present.

MAPK

The MAPK family plays a critical role in the implementation and maintenance of many cellular processes (Pearson et al. 2001). MAPKs are catalytically inactive in their expressed forms. They themselves require phosphorylation at (a number of) specific sites to gain activation. These enzymes exist as components of phosphorylation cascades, where activation of one member after detection of a stimulus, such as a stress response for example, will lead to phosphorylation of a number of other MAPKs in sequence, before a specific cellular response is initiated (Burkhard and Shapiro 2010). The activation of MAPK reaction pathways, via extracellular and intracellular stimuli including peptide growth factors, cytokines, hormones and stress activators results in the downstream regulation of such diverse processes as cell proliferation, differentiation, migration and apoptosis (Figure 6). MAPKs, therefore, play intimate roles in both cell survival and death (Johnson and Lapadat 2002).

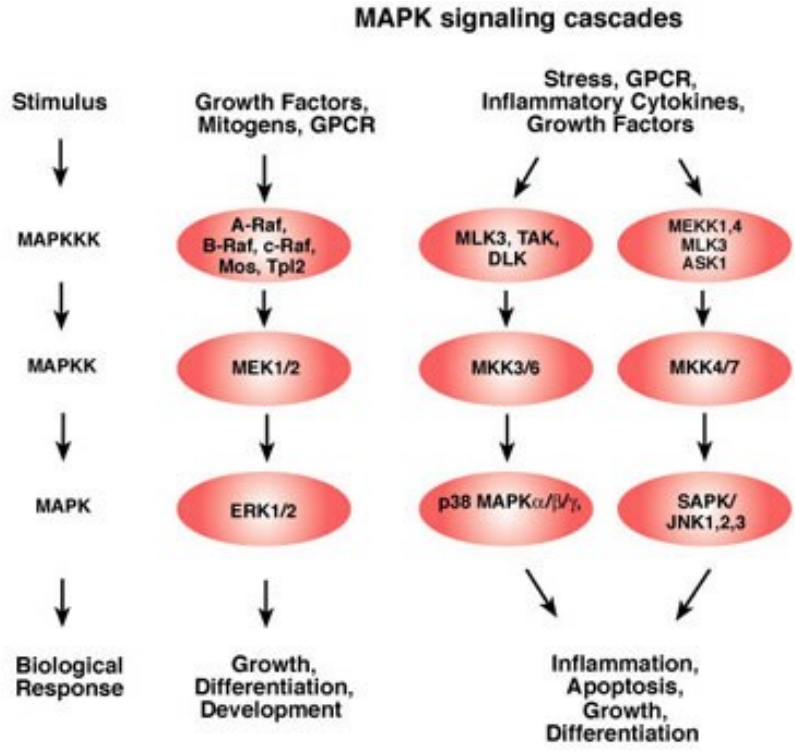

Figure 6. MAPK signalling pathway. Source http://www.cellsignal.com

There are several well-described members of the MAPK family, including the extracellular signal related kinases P42/44 MAPK (also referred to as ERK1/2), stress activated protein kinase/c-Jun N-terminal Kinase (SAPK/JNK) and P38 MAPK. P42/44 MAPK plays a key role in cell proliferation and differentiation (Roth et al. 2003). Initially located in the cytoplasm, activation of this enzyme through the phosphorylation cascade causes its temporary translocation to the nucleus, to affect downstream gene regulation. Each cell is susceptible to different thresholds of P42/44 MAPK activation, and this will determine the requisite cell fate (Chambard et al. 2007). Like all cellular processes, the translocation, phosphorylation and dephosphorylation of P42/44 MAPK requires stringent regulation and a harmonious balance for normal cellular function. However, as demonstrated by Stanciu et al, prolonged activation

of P42/44 MAPK in the nucleus of an in vitro neuronal model causes cell cycle arrest, neuronal toxicity, and eventually cell death will result (Stanciu and DeFranco 2002).

SAPK/JNK, a stress-activated protein kinase, can be induced by inflammatory cytokines, UV radiation, DNA damage, hypoxia and environmental and oxidative stress (Bennett et al. 2001). Amongst other functions, SAPK/JNK enzymes regulate activities of both mitochondrial proteins and nuclear proteins including c-jun and p52 (Vlahopoulos and Zoumpourlis 2004, Irving and Bamford 2002). There are three known genes that encode for SAPK/JNK, and these produce 10 enzyme isoforms: four JNK1 isoforms, four JNK2 isoforms and two JNK3 isoforms. Each group of isoforms has a specific role/mode of action. JNK1 and JNK2 are ubiquitous, whereas JNK3 is restricted to the central nervous system (CNS) (Kuan et al. 2003). SAPK/JNK has been shown to be activated in numerous cerebral ischemia models, and this group of enzymes is also, therefore, implicated in neuronal apoptosis (Irving and Bamford 2002). Kuan and colleagues, for example, used a JNK3 gene knockout model to specifically study the role of neuronal JNK3 in cerebral ischemia (Kuan et al. 2003). Whereas wild-type mice have shown neuronal loss in response to an hypoxic injury, the JNK3 knockout animals were far less damaged, suggesting JNK3 is critical in the downstream activation of stress-induced neuronal apoptosis.

Like SAPK/JNK, the P38 MAPK group of enzymes are sensitive to stress stimuli and pro-inflammatory cytokines. The P38 MAPK gene is translated as four isoforms (α, β, γ, and δ), which are ubiquitously expressed. P38 MAPK isoforms play a role in cell differentiation, apoptosis and autophagy. This enzyme has been reported to drive neurite outgrowth during cell differentiation of the PC12 cell line (Takeda and Ichijo 2002). P38 MAPK is thought to be particularly important in the inflammatory response, with strong evidence showing that upon activation of P38 MAPK, production of pro-inflammatory cytokines, such as tumour necrosis

factor and interleukin are stimulated (Walshe et al. 2011, Yong et al. 2009). P38 MAPK has been linked to the pathogenesis of neurodegenerative diseases where inflammation is known to play a part, such as Alzheimer's disease (AD) (Kim and Choi 2010, Culbert et al. 2006). Indeed, this enzyme group has been shown to be unregulated in the brains of transgenic models of AD (Munoz and Ammit 2010). Agthong et al. demonstrated that P38 MAPK inhibitors significantly protected dorsal root ganglion nerves in rats with sciatic nerve transections (Agthong et al. 2012). These data demonstrated that P38 MAPK has an involvement in sensory neuron loss. They also suggest that this enzyme could play a similar role in stressed RGCs. Indeed, Dapper has demonstrated an up-regulation of P38 MAPK in retinas of eyes with increased IOP (Dapper et al. 2013). P38 MAPK has also been shown to be involved in RGC death directly (Kikuchi et al. 2000). These data point to the fact that MAPKs may play a role in the pathological mechanisms associated with glaucoma.

Neuroprotection as a treatment strategy for glaucoma

When IOP is elevated in glaucoma patients, rapid and sustained lowering of IOP ensures that optic neuropathy and accompanying RGC loss are controlled, but more importantly, this also ensures that visual function is maintained. Pharmacological treatment of eyes with topically-applied, ocular hypotensive drugs forms the front-line in the treatment of POAG patients. Prostaglandin analogues are the most widely prescribed drugs currently. Other classes of drugs include β-adrenergic receptor antagonists, carbonic anhydrase inhibitors, α_2-adrenergic receptor agonists and anti-cholinergics. In certain circumstances, management of IOP with topical medications is not sufficient to halt disease progression, and laser treatment or incisional surgery is considered.

In some POAG patients, pharmacological lowering of raised IOP does not prevent disease progression as it is likely that its cause is multifactorial (Fechtner and Weinreb 1994). Similarly, in patients with normal tension glaucoma, targeting IOP is often of little benefit (Wax and Tezel 2009). For these reasons, the development of compounds that prevent visual loss via non-IOP lowering mechanisms is vital. One strategy that is being explored in many neurodegenerative diseases is the delivery of compounds which directly target non-healthy, sick, or dying neurons. This strategy is termed neuroprotection. Neuroprotection, in the context of glaucoma, is defined as the relative preservation of RGC structure and/or function (Casson et al. 2012). The most successful neuroprotective agent to date in the laboratory setting has been the drug memantine. Memantine is a selective, uncompetitive *N*-methyl-D-aspartic acid receptor antagonist, and has displayed marked protection of RGCs in several animal models of glaucoma, including primates (Yucel et al. 2006). However, randomised phase II clinical trials failed to show any effectiveness in human glaucoma patients (Danesh-Meyer 2011), which illustrates the difficulty in translating laboratory successes to the clinic.

Since the mechanisms of RGC death in glaucoma are still undefined, it follows that agents with more than one mode of action may prove to be the most beneficial. Indeed, if either single compounds, or a cocktail of compounds together could be found which can directly protect RGCs and also lower IOP, then this would represent an excellent practical treatment for glaucoma. Current treatment strategies for future and current sufferers of glaucoma are limited. For this reason, it is important that novel research for the development of diverse therapeutic avenues be undertaken. Previous research into other neurodegenerative disorders has provided knowledge of tissue pathways which could also prove critical in glaucoma. With this in mind, investigation into the activation of protein kinases

such as the MAPK family could provide a key area for research, and this could lead to novel therapeutic strategies.

HYPOTHESIS AND AIMS

Data suggests the MAPK activation could be involved in RGC pathology. It is therefore proposed to investigate the activation of MAPKs in a well-described model of experimental glaucoma and disseminate if in fact the ONH is the initial site of insult resulting in RGC loss. The following investigations are therefore proposed:

Aim 1; Chapter 1

To employ a rodent model of chronic OHT to identify novel protein kinase involvement in ganglion cell pathology, i.e. that of MAPKs. Firstly, to characterise pathological changes occurring in the model and secondly to determine changes in MAPK location and activation status within the ONH. These data will identify whether stimulation of particular MAPK isoforms potentially contribute to specific pathological outcomes for RGCs.

Aim 2; Chapter 2

To develop a novel approach to improve the stability of phosphoproteins i.e. selected specific phosphorylated MAPK isoenzymes, during tissue procurement for immunohistochemical analysis.

CHAPTER 1

Statement of Authorship

Title of Paper:	Expression and activation of MAPK in the ONH in a rat model of ocular hypertension.
Publication Status:	Submitted for Publication, under review
Publication Details:	Molecular and cellular neuroscience

Principal Author

Name of Principle Author (candidate):	Teresa Mammone
Contribution to the Paper:	Experimental work, manuscript preparation
Overall percentage (%):	85%
Certification:	This paper reports on original research I conducted during the period of my Higher Degree by Research candidature and is not subject to any obligations or contractual agreements with a third party that would constrain its inclusion in this thesis. I am the primary author of this paper.

Signature:

Date: 09-08-17

Co-Author Contributions

By signing the Statement of Authorship, each author certifies that:

i. the candidate's stated contribution to the publication is accurate (as detailed above);
ii. permission is granted for the candidate in include the publication in the thesis; and
iii. the sum of all co-author contributions is equal to 100% less the candidate's stated contribution.

Name of Co-Author:	John Wood
Contribution to the paper:	Conception and design of study, manuscript preparation

Signature:

Date: 09-08-17

Name of Co-Author:	Glyn Chidlow
Contribution to the paper:	Conception of study, manuscript editing

Signature:

Date: 09-08-17

Name of Co-Author:	Robert Casson
Contribution to the paper:	Provision of laboratory space and equipment, manuscript editing
Signature:	
Date:	09-08-17

EXPRESSION AND ACTIVATION OF MAPK IN THE ONH IN A RAT MODEL OF OCULAR HYPERTENSION

Teresa Mammone [a,b], Glyn Chidlow [a,b], Robert J. Casson [a,b], John P. M. Wood [a,b]

[a]Ophthalmic Research Laboratories, Central Adelaide Local Health Network, Level 7 Adelaide Health & Medical Sciences Building, University of Adelaide, Adelaide, South Australia, Australia

[b]Department of Ophthalmology and Visual Sciences, University of Adelaide, Adelaide, South Australia, Australia

Corresponding author: John P. M. Wood

Email: john.wood2@sa.gov.au

'Tel: +61 8 8313 7183

Other authors: teresa.mammone@sa.gov.au

glyn.chidlow@sa.gov.au

robert.casson@adelaide.edu.au

Conflicts of interest: None

ABSTRACT

Background: Glaucoma is a leading cause of irreversible blindness and manifests as an age-related, progressive optic neuropathy with associated RGC loss. MAPKs (P42/44 MAPK, SAPK/JNK, P38 MAPK) are known to be activated in a variety of retinal disease models and likely contribute to the mechanisms of RGC death. Although MAPKs have been suggested to play roles in the development of retinal pathology, however, their action in the ONH, where the initial insult to RGC axons likely resides in glaucoma, remains unexplored.

Methods: An experimental paradigm representing glaucoma was established by induction of chronic OHT via laser-induced coagulation of the trabecular meshwork in Sprague-Dawley rats. MAPKs were subsequently investigated over the following days for expression and activity alterations, using RT-PCR, immunohistochemistry and Western immunoblot.

Results: P42/44 MAPK expression was unaltered after IOP elevation, but there was a significant activation of this enzyme in ONH astrocytes after 6-24 hours. Activated SAPK/JNK was present throughout healthy RGC axons but after IOP elevation or mechanical injury via optic nerve crush, it accumulated at the ONH, likely due to RGC axon transport disruption. P38 MAPK was expressed by a population of microglia which were significantly increased in number following IOP elevation. However it was only significantly activated in microglia after 3 days, and then only in the ONH and optic nerve; in the retina it was solely activated in RGC perikarya.

Conclusions: In conclusion, each of the MAPKs showed a specific spatio-temporal expression and activation pattern in the retina, ONH and optic nerve as a result of IOP elevation. These findings likely reflect the roles of the individual enzymes, and the cells in which they reside, in the developing pathology following IOP elevation. These data have implications for understanding the mechanisms of ocular pathology in diseases such as glaucoma.

Keywords: P42/44 MAPK; P38 MAPK; SAPK/JNK; ONH; Axonal injury; Glaucoma; OHT; MAPK; Phosphorylation

Glaucoma, the leading causes of irreversible blindness worldwide (Quigley and Broman 2006), is often associated with increased IOP. It is characterised as a related group of neurodegenerative diseases with structural damage to the optic nerve resulting in loss of RGCs and their axons (Casson et al. 2012). It is believed that RGCs become stressed in glaucoma as a result of altered mechanical and/or vascular influences at the ONH, the anatomical site where RGC axons converge (Burgoyne 2011, Flammer et al. 1999, Hernandez 2000, Osborne et al. 1999). Whatever the initial cause of the stress to RGCs, localised tissue outcomes are thought to include perturbations in metabolic functioning, cessation of axon transport and failure of cellular homeostatic mechanisms (Chidlow et al. 2007). Such events will destabilise intracellular signalling and impact activity of enzymes such as protein kinases, which are physiologically tightly regulated.

The MAPKs comprise a group of structurally similar enzymes that phosphorylate a diverse array of target substrates to control many cellular functions including proliferation, differentiation, migration, secretion, apoptosis and inflammation (Cargnello and Roux 2011, Cowan and Storey 2003). Classical activation of MAPKs occurs when they are themselves phosphorylated; this process most often derives from the upstream stimulation of a complex, three-tiered cascade of separate protein kinases (Johnson and Lapadat 2002, Zeke et al. 2016). Three separate groups of the MAPK family are well defined: P42/44 MAPK; ERK1 and ERK2 (Roskoski 2012), SAPK/JNK; JNK-1, JNK-2, JNK-3 (Mehan et al. 2011) and P38 MAPKs (P38α, P38β, P38γ, P38δ) (Cuenda and Rousseau 2007). In broad terms, SAPK/JNK and P38 MAPK isoforms are primarily stimulated by stress-related effectors or cytokines to cause inflammatory responses, autophagy or apoptosis, while the P42/44 MAPK pathway is

stimulated by mitogens or growth factors resulting in cell cycle progression, cell proliferation or differentiation. Because of their widespread expression in the CNS (Flood et al. 1998), their key roles in cellular functioning, the diversity of signals to which they respond, and the numerous known substrates for their kinase action (Cargnello and Roux 2011), MAPKs have been implicated in the pathophysiology of many CNS disorders (Grewal et al. 1999, Hetman and Gozdz 2004, Kim and Choi 2010). Indeed, roles for this enzyme family have been described in AD, Parkinson's disease and Amyotrophic lateral sclerosis. Additionally, MAPKs have also been shown to have roles in animal models of metabolic stress and ischemia in the CNS (Shackelford and Yeh 2006, Sugino et al. 2000, Ozawa et al. 1999).

Previous studies have elucidated that members of each of the three major groups of MAPKs are present in the retina. Both activated (by way of phosphorylation) and non-activated P42/44 MAPKs localise to non-neuronal Müller cells, astrocytes and the retinal pigmented epithelium (Zhou et al. 2007, Nakazawa et al. 2002) where they are believed to mediate the effects of endogenous growth factors, such as vascular endothelial growth factor. P38 MAPK and SAPK/JNK, however, are mainly present in their non-activated (non-phosphorylated) forms and are associated with neurons such as RGCs and bipolar cells (Zhou et al. 2007, Nakazawa et al. 2002). MAPKs have been shown to respond to different stressors within the retina. For example, MAPKs are activated in response to N-methyl-D-aspartate (Munemasa et al. 2005, Manabe and Lipton 2003) or glutamate injections (Zhou et al. 2007), retinal ischemia (Roth et al. 2003, Kim et al. 2016) optic nerve transection (Nitzan et al. 2006, Nakazawa et al. 2002, Kikuchi et al. 2000), experimentally-elevated IOP (Dapper et al. 2013), endotoxin-induced uveitis (Takeda and Ichijo 2002) and experimental diabetes (Ye et al. 2012). Furthermore, Tezel and Wax (Tezel et al. 2003) found increased activation of P42/44 MAPK, as well as both P38

MAPK and SAPK/JNK, in retinal glia and inner retinal neurons, respectively, in human glaucoma patients.

Despite the diversity of studies investigating MAPK in the injured retina there is very little published information regarding the role of this family of enzymes at the ONH, which is believed to represent the likely primary site of injury for RGC axons in glaucoma (Chidlow et al. 2011b, Howell et al. 2007, Osborne et al. 1999). We therefore sought to carry out a detailed spatio-temporal investigation into the potential activation of MAPKs in the ONH of rats subjected to our model of elevated OHT. The responses of MAPKs in the retina and optic nerve were also determined, partly to build up a more complete picture of the role of these enzymes in our model and partly to check agreement with previous models of retinal injury.

MATERIALS AND METHODS

Materials

All chemicals were purchased from Sigma-Aldrich (Castle Hill, New South Wales, Australia), unless otherwise stated. A full list of antibodies used in the study is listed in Table 1 with primer sequences shown in Table 2. Antibodies specific to each of P42/44 MAPK, SAPK/JNK and P38 MAPK, or their phosphorylated forms, were reactive with all isoforms associated with that respective MAPK group: anti-P42/44 MAPK recognised P42 MAPK (ERK2) and P44 MAPK (ERK1) and therefore detected proteins of masses 42 and 44 kD; anti-SAPK/JNK recognised all ten separate isoforms - derived as either 46 or 54 kD forms from each of five mRNAs (JNK1α, JNK1β, JNK2α, JNK2β, JNK3) - and therefore positively labelled both 46 and 54 kD protein species on Western immunoblots; anti-P38 MAPK recognised the four isoforms of this enzyme (P38α, P38β, P38γ, P38δ) and therefore detected targets as a single protein band of 38 kD. Results of Western immunoblotting and immunohistochemistry for phospho-MAPKs were confirmed by comparing results shown against data obtained with separate, alternate antibodies (not shown; Cell Signaling Technologies; phospho-P38 MAPK, cat #4511; phospho-P42/44 MAPK, cat #9106; phospho-SAPK/JNK, cat #9255). Control cell samples containing both positive and negative control samples for each respective MAPK group were purchased through Cell Signaling Technologies (Danvers, MA, USA) via an Australian distributor (Genesearch, Arundel, Queensland, Australia; P38 MAPK, cat #9213; P42/44 MAPK, cat #9194; SAPK/JNK, cat #9253).

Previous work has reliably detected each group of (phospho-)MAPKs by immunohistochemistry in formalin-fixed, paraffin-embedded in situ ductal breast carcinoma

sections (Davidson et al. 2006). In the present study, tissue sections of ductal breast carcinoma were procured from positive control paraffin blocks provided by the Surgical Diagnostic Facility of SA Pathology (Adelaide, South Australia, Australia). This tissue, therefore, served as a positive control for the immunolabelling techniques employed and for the sensitivity of each antibody.

Table 1. Antibodies used in the study

Name	Cat No./ Clone#	Host	Company	Dilution IHC	Dilution IF	Dilution WB
Amyloid Precursor Protein	22C11#	Mouse	Gift-C. Masters	1:1,000	1:250*/ 1:1,000	
β-Actin	A5441	Mouse	Sigma-Aldrich			1;10,000
βIII-Tubulin	MAB1637	Mouse	Millipore		1:500*	1:1,000
Brn 3a	C-20#	Goat	Santa Cruz	1:3,000	1:3,000	
Iba1	Ab107159	Goat	Abcam		1:500*	
npNFH	SMI32#	Mouse	Sternberger	1:15,000		
Oligo 2	AB9610	Rabbit	Chemicon	1:1,000		
P38 MAPK	8690	Rabbit	CST	1:300		1:500
P44/42 MAPK	9102	Rabbit	CST	1:2,000	1:1,500	1:1,000
Phospho-P38 MAPK	4631	Rabbit	CST	1:300	1:300	1:500
Phospho-P44/42 MAPK	4376	Rabbit	CST	1:2,000	1:1,500	1:1,000
Phospho-SAPK/JNK	9251	Rabbit	CST	1:300	1:300	1:250
SAPK/JNK	9258	Rabbit	CST	1:300	1:300	1:250
S100	MAB079-1	Mouse	Millipore		1:1,000*	
γ-Synuclein	CPTC-SNCG-1	Mouse	DSHB		1:40*	
Vimentin	V9#	Mouse	DAKO		1:1,000*	

CST- Cell signalling technologies, IHC- immunohistochemistry, IF- immunofluorescence, WB-Western immunoblot, * denotes concentration for a 2 step reaction

Table 2. Primer sequences used for real-time RT-PCR

mRNA	Primer sequence	Product size (bp)	GeneBank Accession number
GAPDH	5'-TGCACCACCAACTGCTTAGC-'3 5'-GGCATGGACTGTGGTCATGAG-3'	87	M19533
P44 MAPK	5'-TGGCTTTCTGACCGAGTATGTG-'3 5'-ATTTGGTGTAGCCCTTGGAGTT'-3	80	NM_017347
P42 MAPK	5'-TTGGTCAGGACAAGGGCTCA-'3 5'-CTCGGAACGGCTCAAAGGA-'3	127	NM_053842
SAPK	5'-GCTGCTTTTGATACAGTTCTTGG-'3 5'-AGTTCACGGTAGGCTCTCTTTG-3'	98	NM_001270544, NM_001270556, NM_053829
P38 MAPK	5'-CTGGAAGATGTCGCAGGAGAG-'3 5'-CCTTTTGGCGTGAATGATGG-'3	208	NM_031020

Animals and Procedures

Adult female Sprague-Dawley rats (approximately 250 g) were housed in a temperature- and humidity-controlled room, with a 12 h light, 12 h dark cycle, and were provided with food and water ad libitum. All procedures were performed under anesthesia (100 mg/kg ketamine / 10 mg/kg xylazine), and all efforts were made to minimize suffering.

The OHT model which we employed produces a chronic elevation of IOP via translimbal laser photocoagulation to the trabecular meshwork (Levkovitch-Verbin et al. 2002). This model fulfils a number of the key glaucoma disease criteria of sectorial RGC loss, early ONH axonal damage, exclusivity of RGC death, lack of a significant retinal inflammatory response and correlation between RGC loss and IOP exposure (Casson et al. 2012, Chidlow et al. 2011b, Howell et al. 2007, Osborne et al. 1999). IOP elevations are greater than those

observed in open angle glaucoma, but similar to those seen in experimental primate glaucoma, a commonality among the observed pathologies is high. To establish the model of experimental OHT, raised IOP was induced in the right eye of each animal by laser photocoagulation of the trabecular meshwork using a modification of a published method (Levkovitch-Verbin et al. 2002). Specifically, a continuous wave, frequency-doubled neodymium:yttrium-aluminium garnet (Nd:YAG) 532 nm laser supplied by Ellex R&D Pty Ltd (Adelaide, South Australia, Australia) with the following settings: 300 mW, 0.6 s duration, 50 µm spot diameter, was directed at approximately 80 % of the radial trabecular meshwork as viewed through a slit lamp apparatus. In addition, three of the four episcleral veins were also targeted using the following settings: 260 mW; 0.6 s duration; 100 µm spot diameter. Prior to induction of OHT, the IOP was recorded to obtain a baseline reading using a hand held, rebound tonometer (TonoLab; Icare Finland, Espoo, Finland). For the shorter time points, IOP measurements were recorded once at the time of death (1, 3, and 6 h). For the longer time points (greater than 6 h), IOP measurements were recorded once daily for the duration of the experiment or up to 5 days of treatment at which point IOP measurements were taken every alternate day. All animals demonstrated an adequate IOP elevation (minimum increase in IOP in treated versus control eye of 10 mmHg).

To perform optic nerve crush, a previously described method was employed (Chidlow et al. 2012). In brief, the superior muscle complex was identified, divided and the optic nerve was subsequently exposed by blunt dissection. The exposed optic nerve was then crushed at a distance of approximately 3 mm posterior to the globe for 20 s by employing number 5 forceps. Ophthalmoscopic fundus examination identified any animals with vascular impairment resulting from surgery; any such animals were discarded. A total of 6 rats were subjected to optic nerve crush and these were killed after 1 day.

Tissue harvesting of ONH for protein and RNA extraction

Rats were killed by transcardial perfusion with physiological saline under deep anaesthesia. Eyes were immediately enucleated and ONH samples were prepared using the following method: the anterior portion and vitreous from each eye were removed. The remaining eye-cup was subsequently dissected into a flattened whole-mount in the shape of a "maltese-cross". A biopsy punch of 2 mm in diameter (Stiefel Laboratories, Brentford, United Kingdom, cat # BIOPSY-5918) was then utilized to separate the ONH area from the remainder of the ocular tissue. The initial 1 mm length of optic nerve was also included within each sample, as was a central portion of the retina. ONH samples were placed in 400 µl of TRI-reagent (Sigma-Aldrich) and then sonicated. Subsequently, both total protein and total RNA were extracted by following the manufacturer's method.

Tissue processing for paraffin embedding

Rats were deeply anaesthetised before being transcardially perfused with physiological saline. Eyes were enucleated and immersion fixed. Initially, 10 % (w/v) neutral buffered formalin (containing 4 % formaldehyde; NBF) was used as the fixative, but more consistent immunohistochemistry and better tissue preservation resulted from using Davidson's fixative (2 parts formalin (37-40 %) solution, 3 parts ethanol (95 %), 1 part glacial acetic acid and 3 parts water); the latter fixative was therefore used for all studies (see supplemental Figure 3). Fixation was for 24 h followed by routine processing for paraffin embedding. Eyes were marked in a specific and recorded location to ensure correct orientation during embedding and 5 µm serial sections were cut using a rotary microtome.

Immunohistochemistry

Ocular sections including retina, ONH and optic nerve were deparaffinised in xylene followed by 100 % ethanol before being treated for 25 min with 0.5 % (v/v) hydrogen peroxide to block endogenous peroxidase activity. For antigen retrieval, sections were heated until boiling before being microwaved for 10 min in sodium citrate buffer (10 mM; pH 6.0) or EDTA (1 mM EDTA, 0.05 % Tween 20 and pH 8.0). Tissue sections were then blocked in phosphate buffer saline (PBS; 137 mM NaCl, 5.4 mM KCl, 1.28 mM NaH_2PO_4, 7 mM Na_2HPO_4; pH 7.4) containing 3 % normal horse serum (PBS-NHS), followed by overnight incubation at room temperature in primary antibody diluted in 3 % PBS-NHS (see Table 1). Subsequent incubations were carried out first with appropriate biotinylated secondary antibodies (Vector Labs, California, United States) at a dilution of 1:250 in 3 % PBS-NHS for 30 min, and then with streptavidin horseradish peroxidase conjugate (Pierce, United States, Illinois, cat # 21127) at a dilution of 1:1000 in 3 % PBS-NHS for 1 h. Colour development was achieved using 3',3'-diaminobenzidine and hydrogen peroxide for 5 min at which time the reaction was stopped by submersion in water. Sections were counterstained with haematoxylin, dehydrated and cleared in histolene before mounting with DPX mountant. When differentiating between ONH and optic nerve in analysis of labelling, ONH was defined as ending where the zone of myelination of the optic nerve begins (Ebneter et al. 2010).

Fluorescent double-labelling was used to determine co-localisation of antigens with known cell-specific markers. Visualisation of one antigen was achieved using a 3-step procedure (primary antibody, biotinylated secondary antibody, streptavidin-conjugated AlexaFluor 488 or 594), while the second antigen was labelled by a concurrent 2-step

procedure (primary antibody, secondary antibody conjugated to AlexaFluor 594 or 488; the "opposite" fluoro-tag to that used for the first antigen). Sections were prepared as previously described. Sodium citrate buffer or EDTA were used for antigen retrieval and blocking carried out with 3 % (v/v) PBS-NHS. Sections were incubated overnight at room temperature with both primary antibodies concurrently (see Table 1). On the following day, sections were incubated with the requisite AlexaFluor-conjugated secondary antibody specific to label the 2-step antigen (Molecular Probes, Thermo Fisher Scientific, Massachusetts, United States; 1:250) together with the biotinylated secondary (1:250) for 30 min at room temperature specific for the 3-step antigen. This was followed by incubation with streptavidin-conjugate AlexaFluor 488 or 594 (Molecular Probes; 1:500) for 1 h. Nuclear labelling was achieved with 500 ng/ml 4',6-Diamidino-2-phenylindole, dihydrochloride (DAPI) in PBS for 5 min. Sections were mounted with fluorescence-specific mounting medium (Dako, Sydney, New South Wales, Australia) and examined with a confocal fluorescence microscope.

Where appropriate, quantification of labelled cells was carried out as follows. For P38 MAPK-labelled cells in the retina, counts were taken across whole sections from periphery to periphery, which were approximately through the central axis since they included the optic nerve and ONH. Counts were taken from sections double-labelled with Iba1; only P38 MAPK cells within the retinal limiting membranes which were also labelled with Iba1 were counted. At least 10 eyes were counted in this manner at each time-point. In optic nerve sections, all P38 MAPK-immunoreactive cells were also labelled with Iba1. Counts were many-fold more numerous than retina and were taken per optic nerve section at 200x magnification. A stage micrometer/eyepiece graticule combination was used to

quantify distance, and counts acquired were adjusted to unit area (mm^2) accordingly. At least 10 eyes were counted per time-point, as per the retina.

Real-time RT-PCR

Real-time reverse-transcription polymerase chain reaction (RT-PCR) studies were carried out as described previously (Chidlow et al. 2008). In brief, ONHs were carefully dissected and sonicated in 400 ul TRI-reagent and samples prepared for total RNA extraction as per manufacturer's instructions. First strand cDNA was then synthesised from each of the DNase-treated RNA sample. Real-time RT-PCR reactions were carried out in 96-well optical reaction plates (Bio-Rad, Sydney, New South Wales, Australia) using the cDNA equivalent of 10 ng total RNA per sample as well as IQ SYBR Green supermix (Bio-Rad), 400 nM of forward and reverse primers and 4 mM magnesium chloride, in a total volume of 20 µl. Thermal cycling conditions were 95°C for 3 min followed by 40 cycles of amplification comprising 95°C for 12 s, 63°C for 30 s and 72°C for 30 s. For the oligonucleotide primer sequences, see Table 2. Results obtained from real-time RT-PCR were quantified by relative quantification of gene expression via the analysis of comparative threshold cycles (C_T) in each case; this was further corrected for amplification efficiency of each combination of primer sets of 95 % or greater and a single melt curve expressed identifying only one target accounting for any secondary primer formation (Chidlow et al. 2012). For statistical analysis, the null hypothesis tested was that C_T differences between target and GAPDH, as selected for housekeeping genes did not differ between control or experimental samples.

Western immunoblotting

ONH protein samples were prepared from TRI-reagent extracts as per the manufacturer's protocol. Extracted proteins were solubilised in homogenisation buffer (20 mM Tris-HCl, pH 7.4; containing 2 mM EDTA, 0.5 mM EGTA, 1 mM dithiothreitol, 50 µg/ml leupeptin, 50 µg/ml pepstatin A, 50 µg/ml aprotinin, and 0.1 mM phenylmethylsulfonyl fluoride). An equal volume of sample buffer (62.5 mM Tris-HCl, pH 7.4, containing 4 % (v/v) SDS, 10 % (v/v) glycerol, 10 % (v/v) β-mercaptoethanol, and 0.002 % (w/v) bromophenol blue) was then added and samples heated to 80 ^{o}C for 6 min. Electrophoresis was performed using 10 % denaturing polyacrylamide gels for protein separation. After electrophoresis, proteins were transferred to polyvinylidine fluoride (PVDF) membranes (Bio-Rad) for immuno detection. Membranes were blocked in tris-buffered saline (TBS; 10 mM Tris-HCl, pH 7.4, 140 mM NaCl plus 0.1 % (v/v) Tween 20 (TBST) containing 5 % (w/v) non-fat dried skimmed milk powder (TBST-NDSM) before being incubated with the appropriate primary antibodies (see Table 1), diluted in TBST-NDSM for 3 h at room temperature. Relevant biotinylated secondary antibodies (Vector; 1:1,000 for 30 min) were applied followed by streptavidin horseradish peroxidase conjugate (Pierce; 1:1,000 for 1 h). Chromogenic detection of antibody labelling was achieved using 3-amino-9-ethylcarbazole. Reactions were stopped by immersion of membranes in 0.01 % (w/v) sodium azide. Detection of β-actin was assessed in all samples to normalise total protein levels. Control cell extracts containing both positive and negative controls specific to each (phospho-) MAPK were assessed in order to confirm that detected target weights for each antibody were of the correct molecular mass. Labelled membranes were scanned with a conventional flat-bed scanner and analysed for densitometry using Adobe Photoshop software (Adobe Systems Inc, San Jose, California, United States).

Following subtraction of background labelling, values for target proteins were normalised for levels of β-actin. Statistical analysis was performed as outlined.

Experimental design and statistics

A total of 20 rats were treated in their right eye only per time-point of analysis. These were broken down as follows: 6 rats were used to prepare ONH samples for real-time RT-PCR and Western immunoblot, 6 for retina and optic nerve Western blot samples and 8 for histology and immunohistochemical labelling. All analyses were carried out by comparing treated eyes/samples with appropriate contralateral controls. Data were analysed for significance using a two sample paired student t-test followed by a Bonferroni correction; the null hypothesis being that there was no difference in the specific parameter under investigation when comparing treated with contralateral control eyes. Data were expressed as mean percentage of control value, plus standard error of the mean. A "*P*" value of <0.05 was considered significant.

RESULTS

Validation of the model

A model of chronic OHT that had been established previously (Ebneter et al. 2012) was employed in the study (supplemental Figure 1). IOP peaked at one day after laser treatment (treated eye, 34.1 ± 0.8 mmHg; non-treated eye, 9.0 ± 0.2 mmHg) but generally remained significantly elevated for up to two weeks (supplemental Figure 1A), thus, although there was an initial spike in IOP, this elevation was, at least in part, sustained for the duration of the study. The spatio-temporal pattern of damage in each eye was assessed in a number of ways, including analysing loss of axon-specific proteins from optic nerve samples (eg. βIII-tubulin; supplemental Figure 1B), loss of RGC perikarya in transverse retinal sections as denoted by Brn3a-labelling (supplemental Figure 1C), and detecting axonal abnormalities in labelling for non-phosphorylated 200 kD neurofilament (npNFH; SMI32) in sections of optic chiasm and nerve (supplemental Figure 1D). Thus, the model employed showed a sustained, chronic elevation of IOP and a pattern of damage consistent with that shown in previous studies (Chidlow et al. 2011b, Ebneter et al. 2010, Ebneter et al. 2011).

Validation of the MAPK antibodies

In order to confirm the correct reactivity of the MAPK antibodies used in the study, labelling specificity tests were carried out (supplemental Figure 2). Sections of in situ ductal breast carcinoma showed positive immunolabelling for each of the MAPK and phosphorylated-MAPK (p-MAPK) isoenzymes under investigation (A, P42/44 MAPK, p-P42/44 MAPK; B, SAPK/JNK, p-SAPK/JNK; C, P38 MAPK, p-P38 MAPK), as described previously (Davidson et al.

2006). Furthermore, commercially-obtained control immunoblot extracts for each of the antibodies (see Methods section for details) were positively and appropriately labelled by the requisite antibody pairs: P42/44 MAPK was labelled in stimulated and unstimulated control Jurkat cell extracts, whereas p-P42/44 MAPK was only present in the stimulated control extract (detected proteins with mass of 42 and 44 kD); SAPK/JNK was labelled in both stimulated and unstimulated control HEK293 cell extracts, whereas p-SAPK/JNK was only present in the stimulated control extract (detected protein species with masses of 46 and 54 kD); P38 MAPK was labelled in both stimulated and unstimulated control C-6 glioma cell extracts (apparent protein mass of 40 kD), whereas p-P38 MAPK was only present in the stimulated control extract (apparent mass of 43 kD). Correct labelling with all six antibodies in appropriate, previously-described tissue sections as well as identification of protein species with the correct molecular masses in control cell extracts confirmed that the tested antibodies identified the correct protein antigens.

Choice of fixative for ocular studies

NBF was initially selected as the fixative, but subsequent immunohistochemistry revealed substantial inconsistencies in labelling for p-P42/44 MAPK (supplemental Figure 3A-D) and p-SAPK/JNK (supplemental Figure 3E-F) in control retinal sections. For p-P42/44 MAPK, labelling outcomes varied from no detection in some eyes, (supplemental Figure 3A), faint labelling in cell perikarya of the inner plexiform layer in some eyes (supplemental Figure 3B) and in some cases, clear putative Müller cell labelling (supplemental Figure 3C). This labelling variation did not appear to relate to any discernible factor (eg. age of animal). In contrast, use of Davidson's fixative allowed clear and consistent labelling for p-P42/44 MAPK

in putative Müller cells in all untreated retinas (supplemental Figure 3D). In the case of p-SAPK/JNK, fixation with NBF meant that no labelling was detected in sections (supplemental Figure 3E), whereas fixation with Davidson's revealed clear antibody labelling in the retinal nerve fibre layer (supplemental Figure 3F). Based on these tests, Davidson's fixative was selected for use throughout this study since it provided a consistency which was required, in order to determine changes in possible labelling for these and other antibodies as a result of IOP elevation.

P42/44 MAPK

Expression levels of P42/44 MAPK mRNA and protein: These were evaluated in ONH extracts by real-time RT-PCR and Western immunoblotting, respectively. Since the two genes for P42 and P44 MAPK (*MAPK1* and *MAPK3* genes, respectively) are separately transcribed, the individual level of each respective mRNA species was able to be determined. Data showed that there were no significant differences in expression for either gene at any time-point after induction of OHT, relative to contralateral untreated eyes (Figure 1A). P42 and P44 MAPK proteins were detected on the same Western immunoblots. This was because the antibodies used labelled both proteins as a clearly identifiable protein pair on Western immunoblots; the protein with the higher molecular mass corresponded to P44 MAPK and the lower to P42 MAPK. Example blots are shown for ONH samples taken from animals subjected to unilateral elevation of IOP for 6 hours, 3 days and 7 days (Figure 1B). P44 MAPK protein was clearly present at higher tonic levels than P42 MAPK. Total protein levels for both P42 and P44 MAPK were unaltered in ONH extracts as a result of elevating IOP (Figure 1C). In contrast, the active, phosphorylated forms of both P42 and P44 MAPK were

significantly elevated in the ONH from 6 hours after laser treatment (175.8 ± 36.6 % and 158.8 ± 23.3 % of untreated contralateral levels, respectively). Moreover, levels of both p-P42 MAPK and p-P44 MAPK in treated ONH extracts continued to increase up to and beyond 7 days, when they were at 332.9 ± 89.7 % and 304.9 ± 61.0 % of untreated contralateral values, respectively (Figures 1C, D).

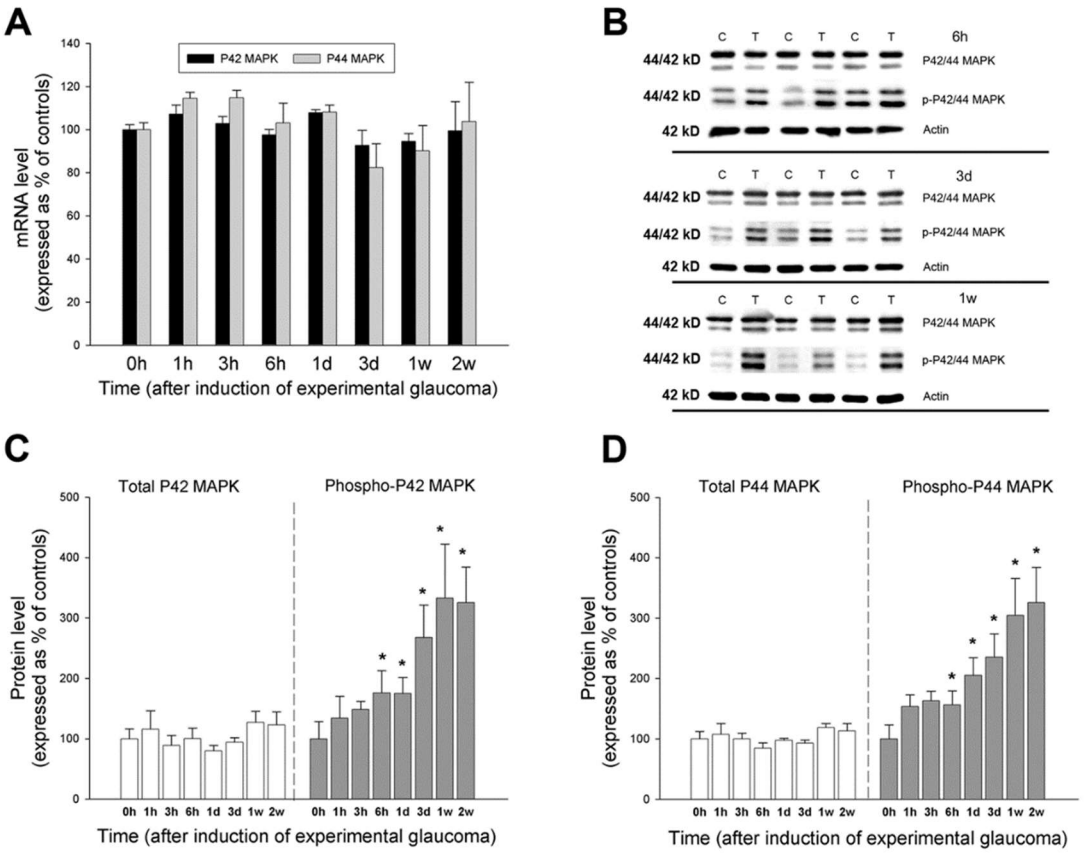

Figure 1. Expression of mRNA and protein products for P42/44 MAPK at different times after induction of elevated IOP. (A) mRNA levels of both P42 and P44 MAPK, as determined by real-time RT-PCR, expressed as a percentage of the untreated, contralateral eye normalised to GAPDH. Data are expressed as mean percentage values ± SEM (*n*=6 animals) in each case. (B) Western immunoblots shown for P42/44 MAPK and the phosphorylated forms for three representative animals (C, control eye; T, treated eye) for each of three time-points after induction of elevated IOP (6 hours, 3 days, 1 week). β-actin immunoblots are also shown for the same samples, as gel-loading controls. (C, D) Quantification of Western immunoblot data (C, total P42 MAPK/phospho-P42 MAPK; D, total P44 MAPK/phospho-P44 MAPK), relative to levels of β-actin (as gel-loading control). For each animal, results were calculated as relative percentage levels of the requisite MAPK in treated versus control eyes; data are expressed as mean ± SEM values in each case. **P* <0.05, when compared with sham, non-treated animals (time zero), by two sample paired t-test followed by a Bonferroni correction.

Immunolabelling in ONH: Immunolabelling of P42/44 MAPK revealed the presence of this enzyme within the ONH of control animals (Figure 2A). The signal was mainly associated with glial cells at the vitreal face and some cells situated between some axon bundles through the lamina region. There was no obvious alteration in localisation for the total form of this enzyme at any time point after elevation of IOP (Figures 2B, 2C). The active, phosphorylated form of the enzyme was not detectable in the control ONH (Figures 2D, J). At 1 hour post-IOP elevation (Figure 2E), however, faint increased labelling was detected at the nerve margins; this was increased markedly by 6 hours (Figure 2F) and continued to increase over time such that at 1 day post-laser, most of the non-axonal tissue in this region was labelled for p-P42/44 MAPK (Figures 2G, 2K). This pattern of labelling remained at 3 days (Figure 2H) and 7 days (Figures 2I, 2L) post-IOP elevation, although labelling was less focal and the intensity was somewhat decreased after the peak at 1 day. Double-immunofluorescence labelling confirmed that p-P42/44 MAPK in the ONH was associated with vimentin-positive glial cells after 1 day of elevated IOP (Figures 3A-F). As further confirmation of the glial-based activation of p-P42/44 MAPK, no co-localisation was observed with the axonal marker βIII-tubulin (Figure 3G-I).

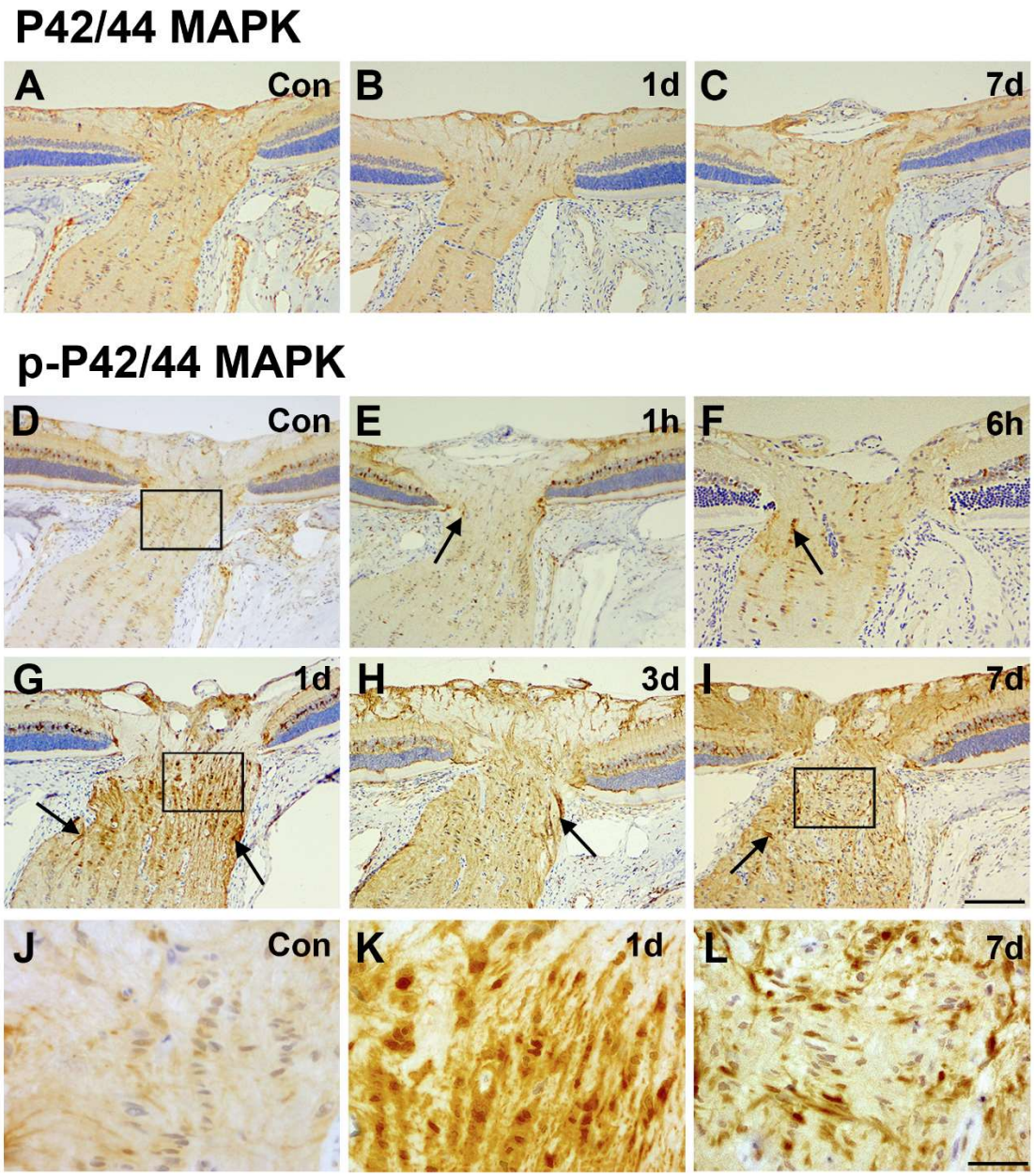

Figure 2. Immunohistochemical localisation of P42/44 MAPK and p-P42/44 MAPK in the ONH of animals subjected to unilateral elevation of IOP. The ONH region labelled for P42/44 MAPK in untreated eyes (A) and eyes subjected to elevated IOP for 1 day (B) or 7 days (C). There are no evident changes in the localisation of this enzyme after treatment. Localisation of p-P42/44 MAPK in the ONH region in untreated eyes (D) and in eyes subjected to elevated IOP for 1 hour (E), 6 hours (F), 1 day (G), 3 days (H) or 7 days (I). More detailed images (x4 relative zoom) of demarcated, labelled regions from control (D), 1 day (G) and 7 day (I) nerve heads are also shown in (J), (K) and (L), respectively. From 1 hour after induction of elevated IOP, there is an evident increase in p-P42/44 MAPK-immunoreactivity in focal elements in the ONH (arrows). Increased labelling persists at 7 days, although from 3 days onwards the immunoreactivity is less focal. Scale bars, 100µm (A-I); 25µm (J-L).

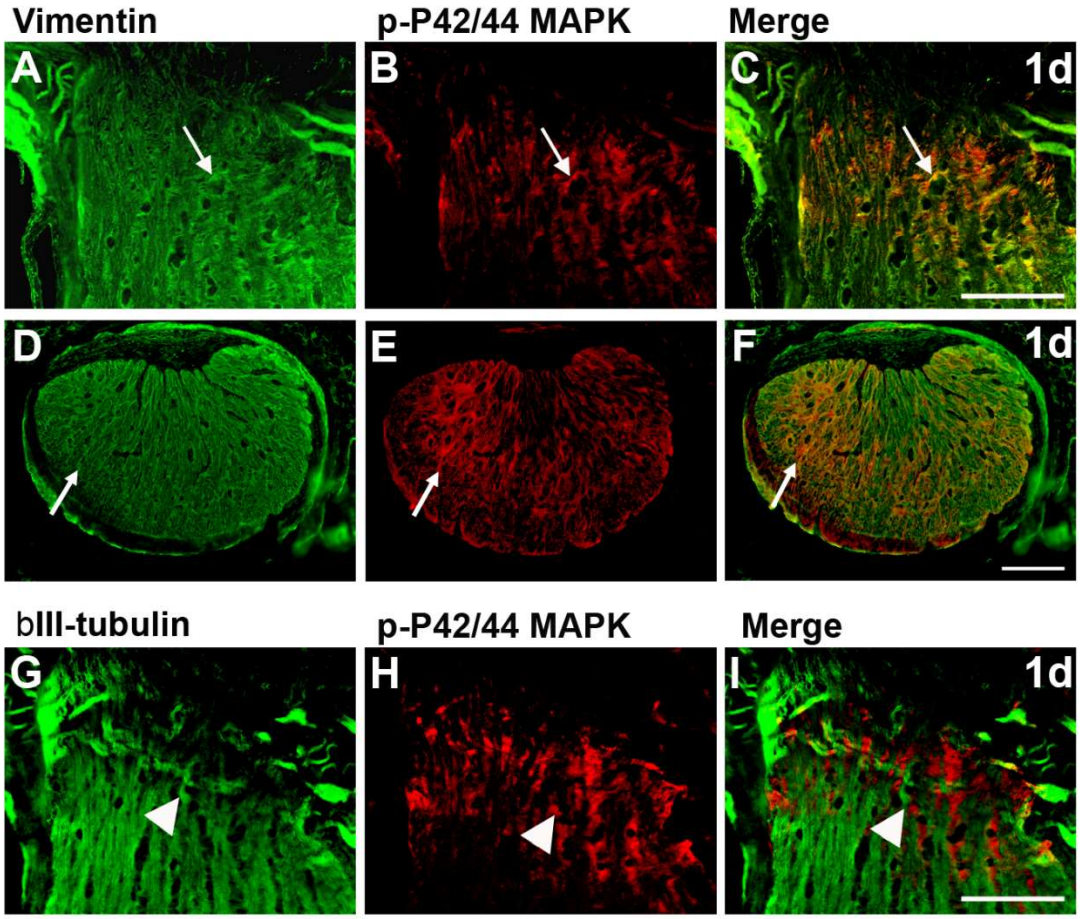

Figure 3. Double-fluorescent immunohistochemistry for p-P42/44 MAPK to ascertain the precise cellular labelling location in the ONH region delineated in Figure 2. All images show representative sections from animals subjected to elevated IOP for 1 day. Co-spatial labelling of both antibodies in each case is indicative of co-localisation (yellow/orange labelling) as indicated by the arrow. (A-C) Double-labelling with the intermediate protein, vimentin (green) clearly shows that p-P42/44 MAPK (red) is present in glial cells (arrows) in the ONH, as seen in longitudinally-orientated sections. Sections taken in the transverse orientation through the ONH region are also shown (D-F), further demarcating the location of p-P42/44 MAPK in glial elements. (G-I) Double-labelling with the axonal protein βIII-tubulin (green) shows no co-localisation with p-P42/44 MAPK (arrowhead). Scale bars, 50μm.

Immunolabelling in retina: Both P42/44 MAPK and p-P42/44 MAPK were present in control retinas. P42/44 MAPK was detectable at low levels throughout the retina, notably in putative Müller cell perikarya in the inner nuclear layer (Figure 4), while p-P42/44 MAPK was expressed within the perikarya and retinal-spanning radial processes of cells which were

identified as Müller cells by double labelling with S100 (Figure 4C, E-G). The patterns of expression of both the total (Figure 4B) and phosphorylated (Figure 4D) forms of P42/44 MAPK were unaffected in the retina following elevation of IOP.

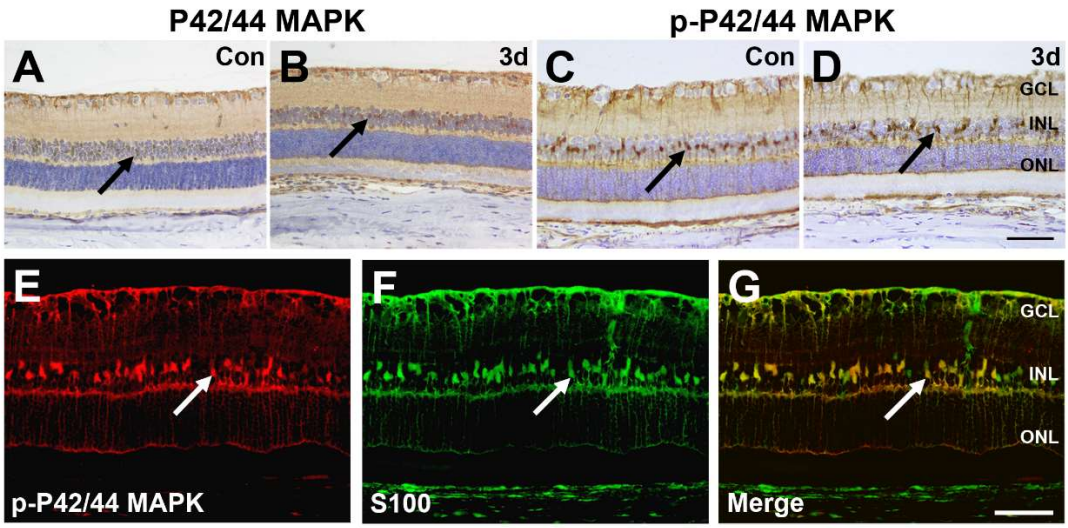

Figure 4. Immunohistochemical labelling of the retina for P42/44 MAPK and p-P42/44 MAPK. P42/44 MAPK was expressed in control retinas (A) and retinas subjected to 3 days of elevated IOP (B). Labelling was predominantly present in cell bodies in the inner nuclear layer (arrow) and there was no evident alteration as a result of IOP elevation. (C) p-P42/44 MAPK was present in control retinas in cells which had perikarya in the inner nuclear layer (arrow) and processes which radiated in both directions from these in the manner of Müller glia. There was no alteration in retinas subjected to 3 days of elevated IOP (D); this was the case for all time-points analysed. Double-immunofluorescent labelling with the retinal Müller cell marker S100 (green; E-G; labels cell bodies, processes and end-feet) confirmed that p-P42/44 MAPK (red) was located to these cells. Co-spatial labelling of both antibodies in each case was indicative of co-localisation (yellow/orange labelling) as indicated by the white arrow. Scale bars, 50µm. GCL, ganglion cell layer; INL, inner nuclear layer; ONL, outer nuclear layer.

Immunolabelling in optic nerve: In the myelinated, control optic nerve, total P42/44 MAPK was expressed by a specific population of small cell perikarya (Figure 5A); this pattern of expression was unaltered following sustained elevation of IOP (data not shown). Double labelling with OLIG2 identified the P42/44 MAPK-positive cells as a population of oligodendrocytes (Figure 5B-D). In contrast, phospho-P42/44 MAPK was barely detectable

in the control optic nerve (Figure 5E) or at 1 day after treatment (Figure 5F); at 3 days after elevation of IOP, however (Figure 5G), labelling had started appearing diffusely in a population of cells in this region, reaching an apparent maximum by 7 days (Figure 5H). Double-labelling with vimentin demarcated the location of p-P42/44 MAPK to be in astrocytes (Figure 5I-L). Unlike total P42/44 MAPK, no labelling of the activated, phosphorylated form was observed in OLIG2-positive oligodendrocytes (data not shown). Alterations in labelling for non-phosphorylated neurofilament 200 kD (npNFH; SMI32) were also determined on analogous sections, as shown previously (Chidlow et al. 2011b) in order to provide a context for the spatio-temporal pattern of activation for P42/44 MAPK in the post-laminar optic nerve. No alterations were seen for npNFH after 24 hours (Figure 5N), compared with control animals (Figure 5M), but limited changes such as axonal swelling and beading were visualised at 3 days after treatment (Figure 5O). By 7 days after treatment, npNFH changes were extensive (Figure 5P) and were detected throughout the optic nerves. Axonal changes, as denoted by npNFH-immunoreactivity, therefore, were spatio-temporally co-incident with activation of P42/44 MAPK in glial cells in the optic nerve.

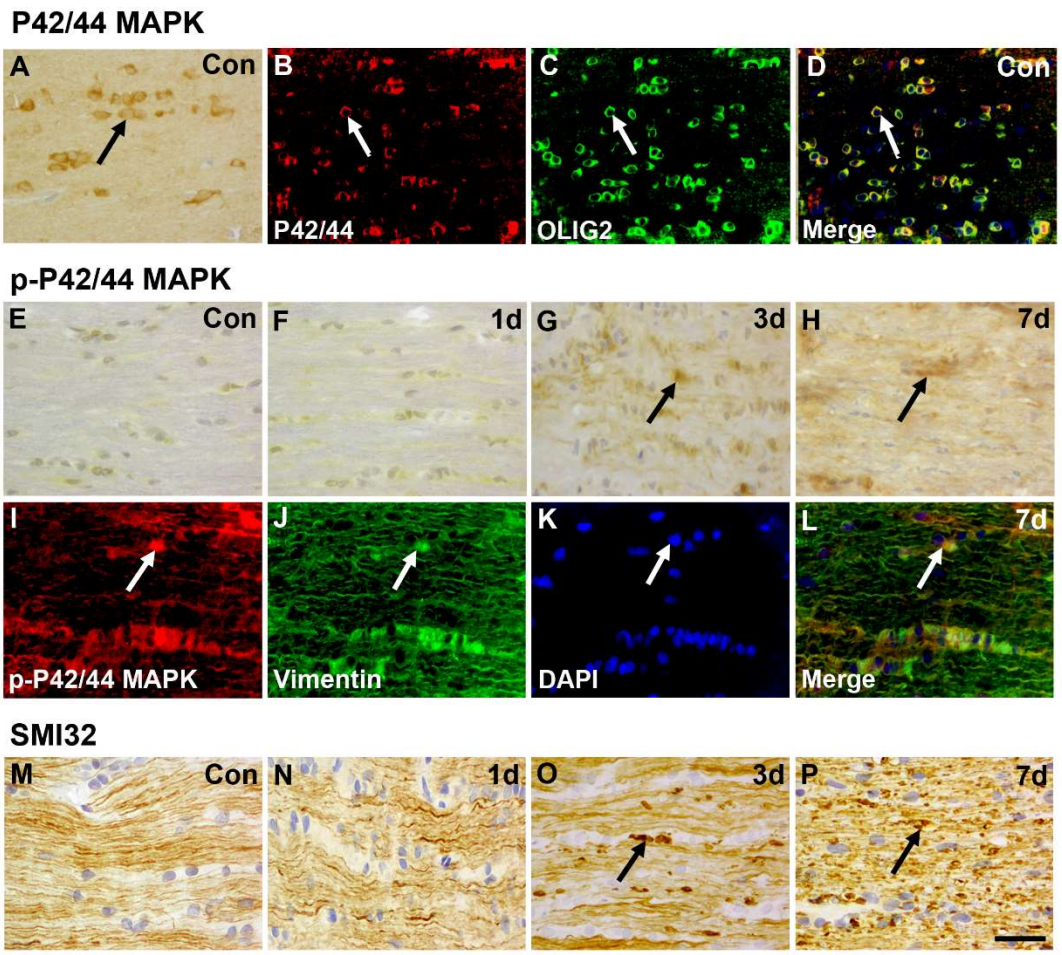

Figure 5. Immunohistochemical labelling of the optic nerve for P42/44 MAPK and p-P42/44 MAPK. P42/44 MAPK was diffusely labelled throughout the optic nerve, but was particularly prominent throughout the nerve in cells arranged parallel with the direction of the nerve sheath (A). Double-immunofluorescent labelling of P42/44 MAPK (red) with the oligodendrocyte marker, OLIG2 (green) indicated that the cells showing concentrated amounts of P42/44 MAPK were oligodendrocytes (D; control tissue). Immunoreactivity of p-P42/44 MAPK was not present in control nerves (E) or in nerves subjected to 1 day of elevated IOP (F). However, diffuse labelling was detected after 3 days (G) and 7 days (H) of pressure elevation. By 7 days, this pattern of labelling was similar to that of total P42/44 MAPK except that it was not present in concentrated amounts in oligodendrocytes. Instead, p-P42/44 MAPK (red) was particularly localised to a population of astrocytes (arrows), as shown by double-immunofluorescent co-labelling with vimentin (green) (I-L). (M-P) Time course of axonal degradation as shown by analysis of non-phosphorylated 200kD neurofilament (npNFH; using antibody clone SMI32) labelling, in order to define the spatio-temporal relationship of detrimental axonal changes with P42/44 MAPK activation in nerve glia. Axons appear unchanged relative to untreated eyes (M) at one day after elevation of pressure (N), but degradative changes (arrows) are noticeable by 3 days (O) and are widespread by 7 days (P). Thus, the appearance of phosphorylated P42/44 MAPK in optic nerve glia coincides with observable axonal degradative changes. Scale bars, 50µm. Direction of optic nerves shown: left to right is proximal to distal.

SAPK/JNK

Expression levels of SAPK/JNK mRNA and protein: Expression of SAPK/JNK was evaluated in ONH extracts by real-time RT-PCR and Western immunoblotting, respectively. SAPK/JNK comprises (at least) 10 separate isoenzymes derived from five mRNAs (JNK1α, JNK1β, JNK2α, JNK2β, JNK3), themselves derived from three genes, *MAPK8* (four isoforms of JNK1), *MAPK9* (four isoforms of JNK2) and *MAPK10* (two (or more) isoforms of JNK3) (Zeke et al. 2016). Primers were designed to recognise homologous regions of each of the possible mRNAs such that the end products of the PCR would not distinguish between the different isoforms of SAPK/JNK. Data showed that mRNA signals for SAPK/JNK were detected in all ONH extracts. No significant differences in expression were measured at any time point after induction of OHT, when compared with contralateral untreated samples (Figure 6A).

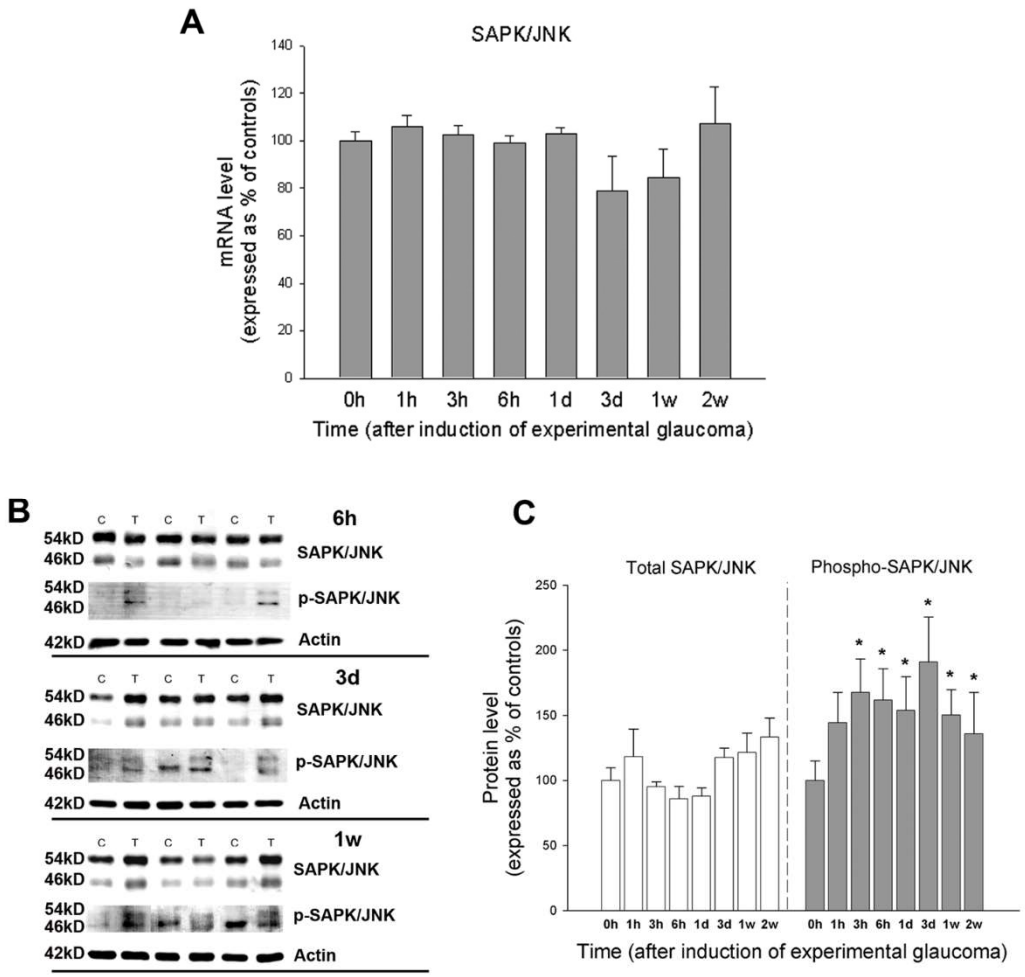

Figure 6. Expression of mRNA and protein products for SAPK/JNK at different times after induction of elevated IOP. (A) mRNA levels of SAPK/JNK, as determined by real-time RT-PCR, expressed as a percentage of the untreated, contralateral eye normalised to GAPDH in each case. Data are expressed as mean percentage values ± SEM (*n*=6 animals). (B) Western immunoblots shown for SAPK/JNK and p-SAPK/JNK for three representative animals (C, control eye; T, treated eye) for each of three time-points after induction of elevated IOP (6 hours, 3 days, 1 week). β-actin immunoblots are also shown for the same samples, as gel-loading controls. (C) Quantification of Western blot data, relative to levels of β-actin. For each animal, results were calculated as relative percentage levels of either total SAPK/JNK or phosphorylated p-SAPK/JNK in treated versus control eyes; data are expressed as mean ± SEM values in each case. **P* <0.05, when compared with sham, non-treated animals (time zero), by two sample paired t-test followed by a Bonferroni correction.

The antibodies used for detection of SAPK/JNK, and activated p-SAPK/JNK, were each able to detect all isoforms of this enzyme. Furthermore, each of the five mRNAs is processed to produce an equal quantity of two functionally identical, but different sized, final proteins of either 46 kD or 54 kD. Thus, protein products detected by these antibodies in ONH

samples had masses of either 46 kD or 54 kD (supplemental Figure 2B, Figure 6B). In each case, there was more of the long 54 kD form present than the short 46 kD form. Immunoblot analysis of ONH samples from eyes subjected to different times of elevated IOP showed that levels of total SAPK/JNK were statistically equivalent to those in contralateral, untreated eyes (Figure 6C). Levels of the activated p-SAPK/JNK, however, were significantly increased in eyes subjected to elevated IOP, relative to contralateral controls, at all times after 3 hours (Figure 6C).

Immunolabelling in ONH: Having identified that SAPK/JNK was present in ONH extracts and had been phosphorylated as a result of elevation of IOP, we undertook a spatial analysis of the activation of this enzyme. Activated p-SAPK/JNK was present in the ONH of control eyes in axons (Figure 7A, G). Following induction of OHT, no changes in p-SAPK/JNK within the ONH were seen after 1 hour (Figure 7B) but an increase was observed by 6 hours (Figure 7C) which peaked between 24 hours (Figure 7D, H) and 3 days (Figure 7E, I). By 7 days, a large amount of p-SAPK/JNK labelling was also confined to the prelaminar retinal nerve fibre layer (Figure 7F). The increase in p-SAPK/JNK-immunoreactivity in the ONH within 6-24 hours was mirrored by that of amyloid precursor protein (APP; Figures 7J-L) which is synthesised by RGCs and transported along their axons into the optic nerve (Morin et al. 1993). Double-labelling with the axon-based protein βIII-tubulin confirmed that p-SAPK/JNK was present and distributed throughout axons in the control ONH (Figure 8A-C). After 7 days, however, p-SAPK/JNK also co-labelled with βIII-tubulin in the adjacent retina, as well as in the ONH (Figure 8D-F). Double-labelling was also performed with an antibody to APP; cessation of anterograde axonal transport will cause its accumulation upstream of the site of blockade. Here, APP was seen to accumulate in the central retinal nerve fibre layer and in the ONH of eyes subjected to 3 days of elevated IOP (Figure 8G). This almost

completely co-labelled with p-SAPK/JNK (Figure 8H, I). To determine whether p-SAPK/JNK was accumulating at the ONH at the site of pathology specifically in response to elevated pressure, we also labelled this activated protein in the ONH/proximal optic nerve of eyes subjected to a traumatic model of optic nerve crush injury (Figure 8J, K). Here, again, clear axonal localisation of p-SAPK/JNK was present in control sections (Figure 8J) but there had been an accumulation of labelling proximal to the site of injury after induction of optic nerve crush (Figure 8K). The proximal accumulation of p-SAPK/JNK mirrored the pre-injury site accumulation of APP (Figure 8L). In the case of APP, however, accumulation of immunolabelling was also detected immediately distal to the region of crush.

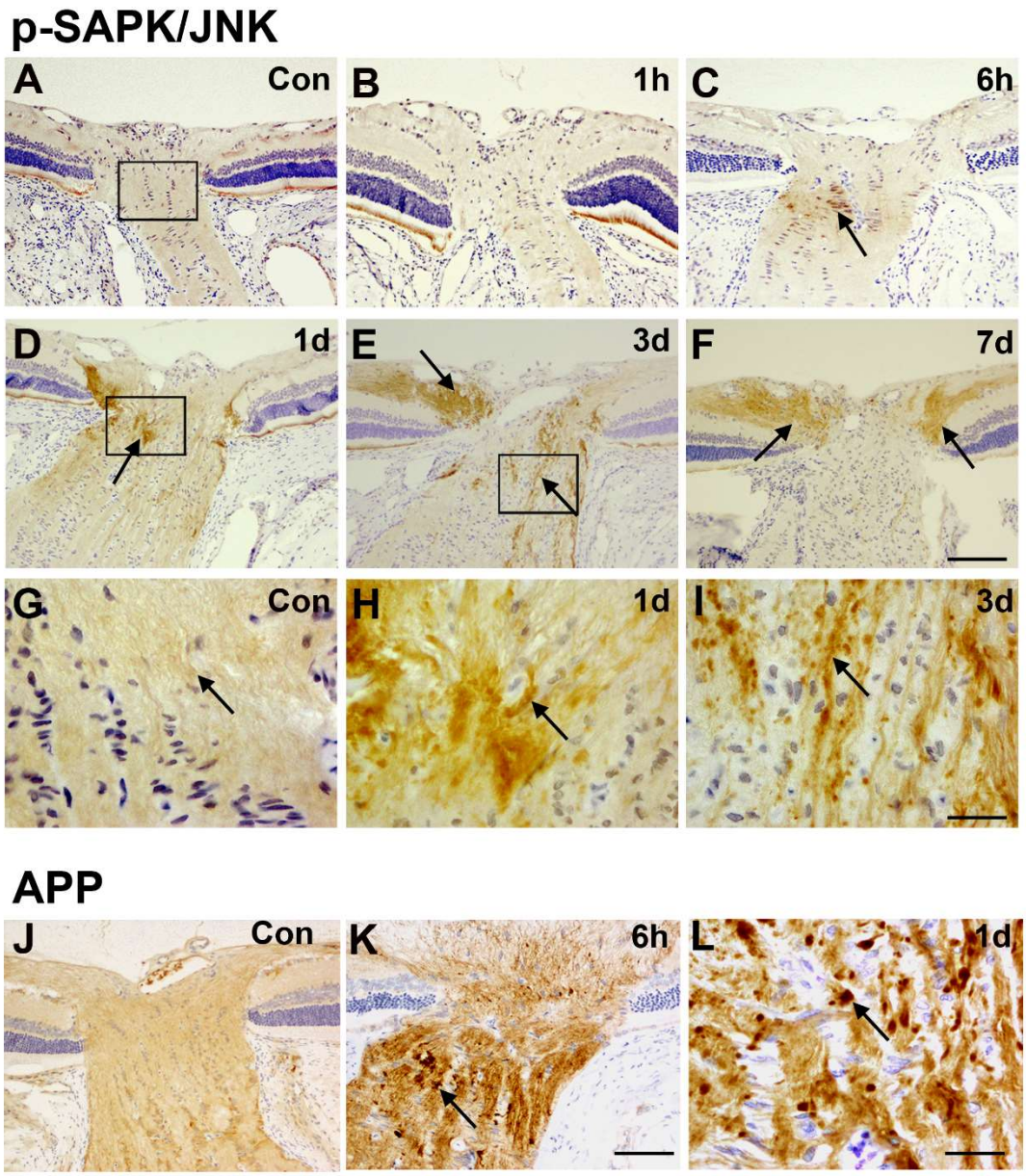

Figure 7. Immunohistochemical localisation of p-SAPK/JNK in the ONH of animals subjected to unilateral elevation of IOP. Localisation of p-SAPK/JNK in the ONH region in untreated eyes (A) and in eyes subjected to elevated IOP for 1 hour (B), 6 hours (C), 1 day (D), 3 days (E) or 7 days (F). More detailed images (x4 relative zoom) of demarcated, labelled regions from (A) control, (D) 1 day and (E) 3 day nerve heads are also shown in (G), (H) and (I), respectively. From 1-6 hours after induction of elevated IOP, there is an evident increase in p-SAPK/JNK-immunoreactivity in focal elements of the ONH (arrows). Increased labelling in the ONH region persists at 7 days, although from 3 days onwards the immunoreactivity is more diffuse and less focal. p-SAPK/JNK also markedly accumulates in adjacent, thickened regions of the retinal nerve fibre layer from 24 hours (D) and this labelling persists at 3 days (E) and 7 days (F) post-treatment. Localisation of amyloid precursor protein (APP; arrows) in the ONH region of control tissue (J), 6 hours (K) and 1 day (L) of raised IOP to illustrate increasing impairment of axonal transport. The accumulation of APP in the ONH region as a result of axon transport disruption mirrors the observed spatio-temporal changes in p-SAPK/JNK labelling. Scale bar, 100µm (A-F, J-K); 25µm (G-I, L).

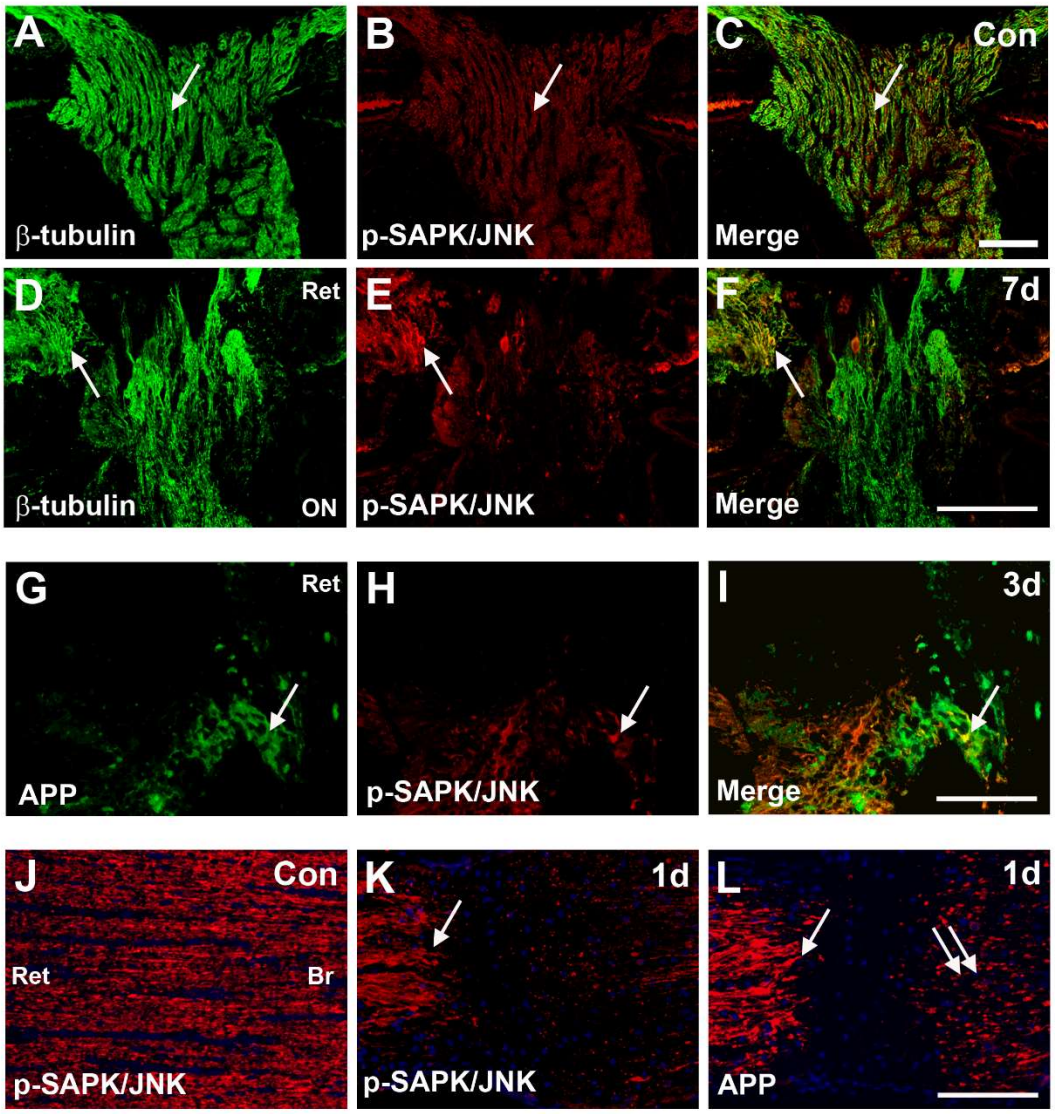

Figure 8. Double-fluorescent immunohistochemistry for p-SAPK/JNK to ascertain its precise cellular labelling location in the ONH region. Double-labelling of ONH sections with βIII-tubulin antibody (green) demarcated clear co-localisation of p-SAPK/JNK (red) in control animals (A-C) and animals subjected to elevated IOP for 7 days (D-F). At 7 days post-IOP elevation, βIII-tubulin was still associated with axons within the nerve head (D), but more of the p-SAPK/JNK labelling was confined to the retinal nerve fibre layer adjacent to this (E, F) and therefore mainly co-localised with the axonal protein in the latter region. (G-I) Labelling ONH-accumulated p-SAPK/JNK alongside the axon transport marker APP (green) showed a clear co-localisation of both antibodies at 3 days post-laser. (J-L) Analysis of the region immediately distal to the nerve head after induction of optic nerve crush. Immunolabelling of p-SAPK/JNK in control animals (J) and after 1 day of optic nerve crush (K) showed reduced labelling (K) in the affected area as a result of axonal damage. Labelling a consecutively cut section for APP (L) showed a similar effect. In both cases, there was a loss of labelling in the area of axonal crush (arrows) and a resultant accumulation of label proximal to this region; in the case of APP there was also an increase immediately distal to this region (double-arrow). Ret, retina; ON, optic nerve; Br, brain. Scale bar, 50μm.

Immunolabelling in retina: In control retinas, total SAPK/JNK was detected in the RGC layer by immunohistochemistry (Figure 9A). Co-localisation of SAPK/JNK with γ-synuclein confirmed its location in RGC perikarya (supplemental Figure 9B, C). Phospho-SAPK/JNK immunolabelling was present in control retinas in the nerve fibre layer (Figure 9D); co-localisation with βIII-tubulin confirmed that this was present in RGC axons but not somas (Figure 9E, F). Western blot analysis clearly showed that there were increases in levels of both SAPK/JNK and p-SAPK/JNK in retinal extracts after induction of elevated IOP. By 7 days post-treatment, the increases in both were statistically significant (Figure 9G).

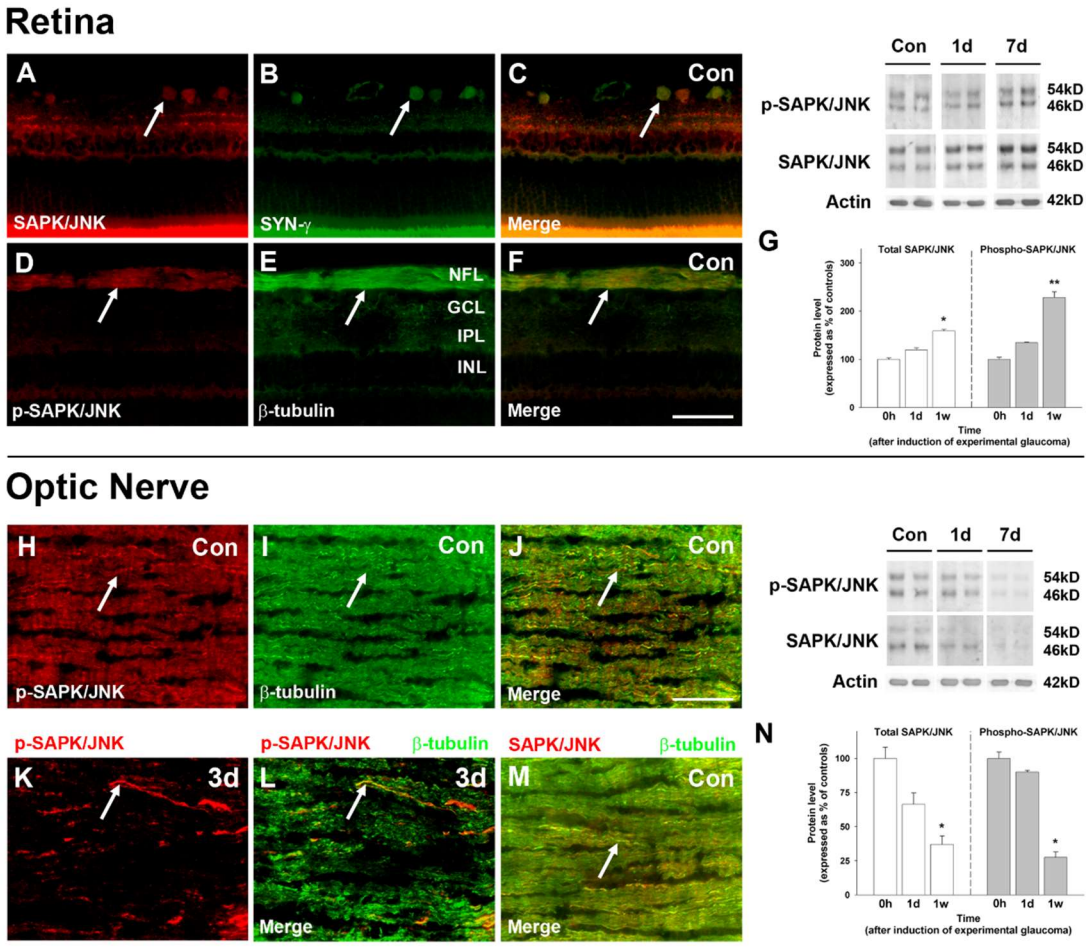

Figure 9. Responses of SAPK/JNK and p-SAPK/JNK in retina/optic nerve in response to induced OHT. (A-C) Co-labelling of SAPK (A; red) in control animals with γ-synuclein (B; green; arrows) in ganglion cell bodies (C). (D-F) p-SAPK/JNK (D; red) co-labelled with βIII-tubulin (E; green) in ganglion cell axons (F; arrow). (G) Western immunoblot for total retinal SAPK/JNK and p-SAPK/JNK shown for two representative samples from control animals or animals subjected to 1 or 7 days of elevated IOP. β-

actin was labelled in the same samples, as a gel-loading control. Also shown, quantification of blot data, relative to β-actin levels. For each animal, results were calculated as relative percentage levels of total SAPK/JNK or p-SAPK/JNK in treated versus control eyes; data are expressed as mean ± SEM values (n=6). (H-J) Labelling of p-SAPK/JNK (H) and βIII-tubulin (I) in control optic nerves showed clear co-localisation in axons (J). (K) In nerves subjected to elevated IOP for 3 days, p-SAPK/JNK was present (K) but considerably more sparse and discontinuous than βIII-tubulin (L). (M) Total SAPK/JNK, as expected, co-localised with βIII-tubulin in control optic nerves. (N) Western immunoblot for total optic nerve SAPK/JNK and p-SAPK/JNK for two representative samples from control animals and animals subjected to 1 or 7 days of elevated IOP. β-actin immunoblots are also shown for the same samples. Quantification was calculated as relative percentage levels of total SAPK/JNK or p-SAPK/JNK in treated versus control eyes (with respect to β-actin levels); data are expressed as mean ± SEM values (n=6).*P <0.05, **P <0.01, compared with non-treated animals (time zero) by two sample paired t-test followed by a Bonferroni correction. Scale bars, 50 μm. NFL, nerve fibre layer; GCL, ganglion cell layer; IPL, inner plexiform layer; INL, inner nuclear layer. Direction of optic nerves shown: left to right, proximal to distal.

Immunolabelling in optic nerve: Optic nerves were analysed immediately distal to the ONH for the presence of SAPK/JNK and its activated form, p-SAPK/JNK. In untreated eyes, total SAPK/JNK (Figure 9M) and p-SAPK/JNK (Figure 9H-J) were associated with axons within the optic nerve, as identified by co-labelling with βIII-tubulin. In nerves from eyes subjected to elevated pressure for 7 days labelling was greatly diminished compared with βIII-tubulin (Figure 9K, L). Quantification of levels of both total and phosphorylated MAPK in optic nerve extracts by Western immunoblot (Figure 9N) confirmed that both were decreased post-treatment, with these losses being statistically significant by 7 days (SAPK/JNK, 36.93 ± 6.35 % and p-SAPK/JNK, 27.60 ± 3.89 % of untreated, contralateral eye values by 7 days; P <0.05, by two sample paired t-test plus Bonferroni correction; n=6).

P38 MAPK

Expression levels of P38 MAPK mRNA and protein: These were evaluated in ONH extracts by real-time RT-PCR and Western immunoblotting, respectively. Four P38 MAPKs have

currently been identified (P38α, P38β, P38γ, P38δ), as the products of four respective genes (*MAPK14*, *MAPK11*, *MAPK12*, *MAPK13*) (Cargnello and Roux 2011) and the primers employed were designed to recognise homologous regions of each of the possible mRNAs such that the end product of the real-time RT-PCR reactions would consist of all mRNA combinations, all of which would be of indistinguishable size. Upon analysis, mRNA was detected for P38 MAPK in all ONH samples. Statistical tests indicated no significant difference between levels measured in samples at any time after elevation of IOP, when compared with contralateral untreated eyes (Figure 10A).

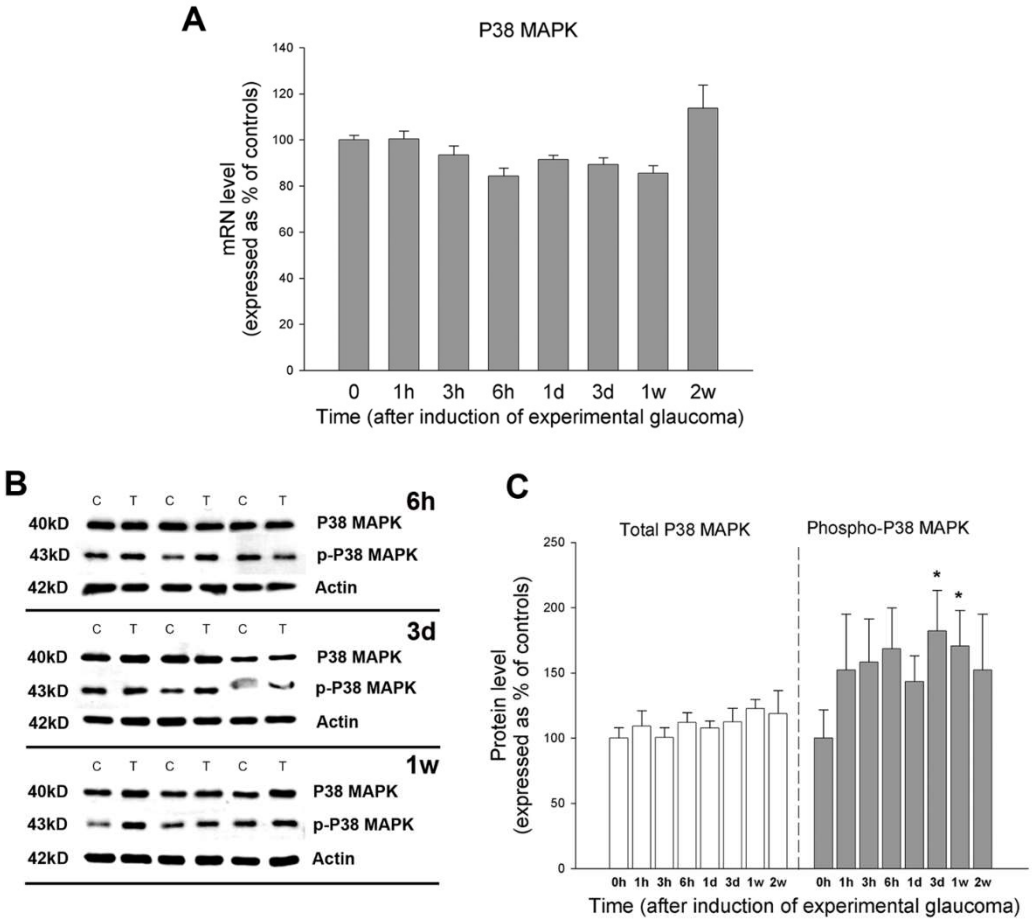

Figure 10. Expression of mRNA and protein products for P38 MAPK and p-P38 MAPK at different times after induction of elevated IOP. (A) mRNA levels of P38 MAPK, as determined by real-time RT-PCR, expressed as a percentage of the untreated, contralateral eye in each case. Data are expressed as mean percentage values ± SEM (n=6 animals) normalised to GAPDH. (B) Western immunoblots shown for P38 MAPK and p-P38 MAPK for three representative animals (C, control eye; T, treated

eye) for each of three time-points after induction of elevated IOP (6 hours, 3 days, 1 week). β-actin immunoblots are also shown for the same samples, as gel-loading controls. (C) Quantification of Western blot data, relative to levels of β-actin. For each animal, results were calculated as relative percentage levels of either total P38 MAPK or phospho-P38 MAPK in treated versus control eyes; data are expressed as mean ± SEM values in each case. *P <0.05, when compared with sham, non-treated animals (time zero), by two sample paired t-test followed by a Bonferroni correction.

The antibodies used for detection of P38 MAPK and activated, p-P38 MAPK were each able to detect all isoforms of this enzyme. Expected molecular masses for P38 MAPK and p-P38 MAPK by immunoblotting were 40 kD and 43 kD, respectively. These were indeed the masses which we detected in samples (see supplemental Figure 2C). Both P38 MAPK and p-P38 MAPK were detected in all ONH samples analysed, in the present study (Figure 10B). There were no significant changes in levels of P38 MAPK as a result of elevating IOP, when comparing with levels in contralateral untreated eyes (Figure 10B, C). Levels of p-P38 MAPK, however, were significantly increased in eyes subjected to OHT at 3 and 7 days post-treatment (Figure 10C; 170.7±27.3 %, 182.2±30.9 % of control values, respectively; P <0.05).

Immunolabelling in ONH: Immunohistochemical assessment of P38 MAPK labelling at the ONH (Figure 11A, B, E) denoted that this enzyme was expressed by a population of cells with small round somata and short processes (Figure 11C). Double-labelling immunofluorescence subsequently confirmed that P38 MAPK was present in approximately 50 % of Iba-positive microglia (Figure 11C-F). There was no obvious difference between numbers of P38 MAPK-positive cells in the ONH at 3 days post-treatment as compared with untreated controls (Figure 11 A, B). Activated p-P38 MAPK labelling was absent from the ONH of untreated eyes (Figure 11G) but was present in some small, round cells after 3 days (Figure 11H) and 7 days (Figure 11I) of IOP. Labelling was also confirmed to be present in a population of Iba1-positive microglia (Figure 11J-L).

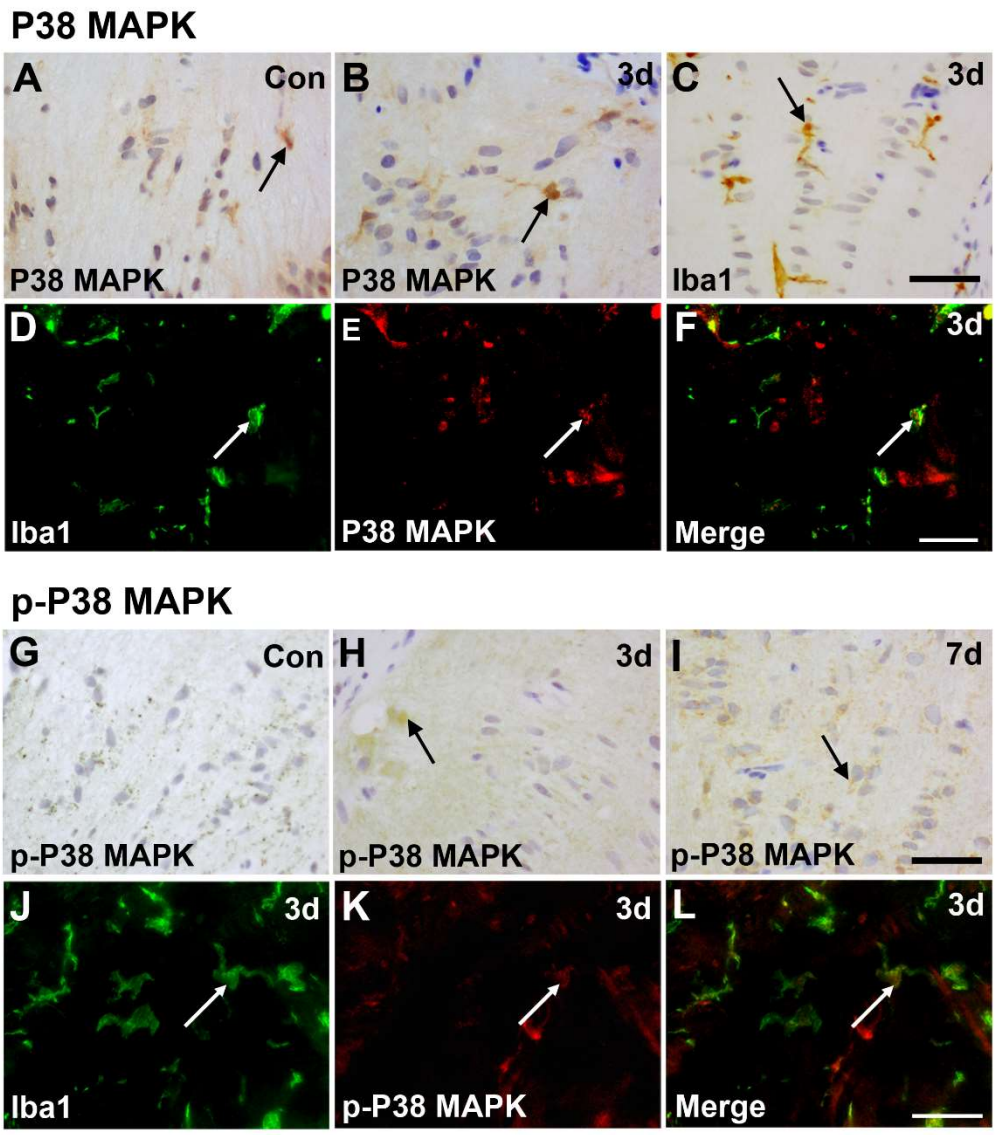

Figure 11. Immunohistochemical localisation of P38 MAPK and p-P38 MAPK in the ONH of animals subjected to unilateral elevation of IOP. The ONH region labelled for P38 MAPK in untreated eyes (A) and eyes subjected to elevated IOP for 3 days (B); small cells resembling microglia labelled positively in all nerve heads regardless of treatment (arrow). For comparative purposes, Iba1-positive microglia are also shown (C). (D-F) Double-fluorescent immunohistochemistry for P38 MAPK (red) confirmed co-spatial labelling with Iba1 (green) in microglia in the ONH (yellow, arrow). Immunohistochemical localisation for p-P38 MAPK was much more limited (G-I). Limited labelling was detected in control tissue (G) and tissues subjected to 3 days (H) or 7 days (I) of elevated IOP. Positively labelled cells appeared after 3 days and 7 days of elevated pressure (arrows). Double-fluorescent immunohistochemistry for p-P38 MAPK (K) again confirmed that p-P38 MAPK was predominantly co-localised with Iba1 (J) in some microglia (L). Scale bars, 50µm.

Immunolabelling in retina: P38 MAPK localised to a population of small, discrete cells within the untreated retina (Figure 12A). Double-immunofluorescent labelling identified

these cells as a population of Iba1-positive microglia (Figure 12E-G). Approximately 50 % of Iba1-immunoreactive microglia also labelled for P38 MAPK. In eyes subjected to elevated IOP, the numbers of P38 MAPK-positive microglia were significantly increased after 3 or more days (Figure 12B-D, H) relative to untreated contralateral retinas. P38 MAPK was also present in some soma in the RGC layer after 1 or more days of elevated IOP (Figure 12 B-D). Active p-P38 MAPK was largely absent from the untreated retina (Figure 12I) or 6 hours after treatment (Figure 12J). However, by 24 hours after induction of OHT, p-P38 MAPK labelling was detectable in the cytoplasm of some large cell somas in the ganglion cell layer (Figure 12K, L). These cells were identified as a population of RGCs by co-labelling with Brn3a (Figure 12M-P).

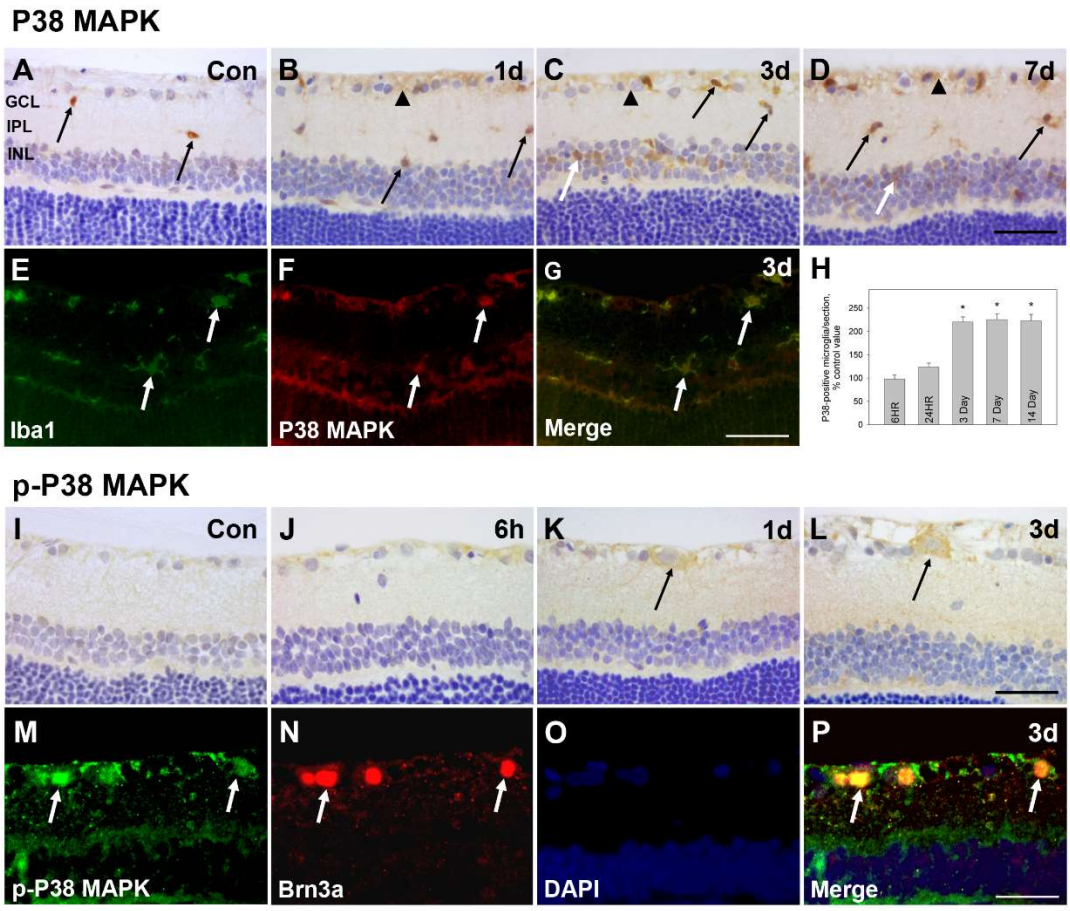

Figure 12. The effect of elevation of IOP on immunohistochemical localisation of P38 MAPK and its phosphorylated form in the rat retina. P38 was present in specific cells in the inner plexiform layer in untreated retinas (A; arrows). Similar cells were labelled in animals subjected to elevated IOP for 1 day (B), 3 days (C), and 7 days (D), except that such cells became significantly more numerous after 3 days (G, H). Some labelling was also present in the retinal nerve fibre layer or ganglion cell layer after 1 day (B-D; arrowheads). Double-labelling with the marker Iba1 in retinas from eyes treated for 3 days identified the labelled cells as microglia (E-G). In retinas from control eyes (I) or eyes subjected to 6 hours of elevated IOP (J), p-P38 MAPK could not be detected. By 24 hours (K) and 3 days (L) after elevating IOP, however, labelling for p-P38 MAPK could be detected in and around some cell bodies in the ganglion cell layer. Double-labelling with an antibody recognising the transcription factor Brn3a identified that p-P38 MAPK was present in ganglion cells (M-P). Scale bars, 50µm. GCL, ganglion cell layer; IPL, inner plexiform layer; INL, inner nuclear layer.

Immunolabelling in optic nerve: In the untreated optic nerve (Figure 13A, B), and in nerves from eyes subjected to elevated IOP (eg. for 7 days; C, D) P38 MAPK was localised to a population of small cells with the morphological appearance of microglia. Such cells were generally aligned parallel to the orientation of axon fibres and in untreated eyes, they had

small somata and thin processes. There were no obvious differences in either appearance or quantity of labelled cells in sections from either proximal (immediately adjacent to the ONH) or distal (immediately adjacent to the optic chiasm) optic nerve in untreated eyes. After 3 days of elevated IOP, however, there were significantly more labelled cells in the proximal as compared with the distal optic nerve (Figure 13 C-E). These labelled cells were more intensely labelled and had fewer processes. By 7 days of pressure elevation there were comparable numbers of P38 MAPK-immunoreactive cells in proximal and distal regions of the optic nerve (Figure 13 E). Double-labelling confirmed P38 MAPK-labelled cells represented a population of microglia (approximately 50 % of microglia; Figure 13F-H). Activated, p-P38 MAPK was not present in untreated optic nerves, but was present in a sparse population of microglia in nerves from eyes subjected to elevated pressure for 3 or more days (Figure 13I-K).

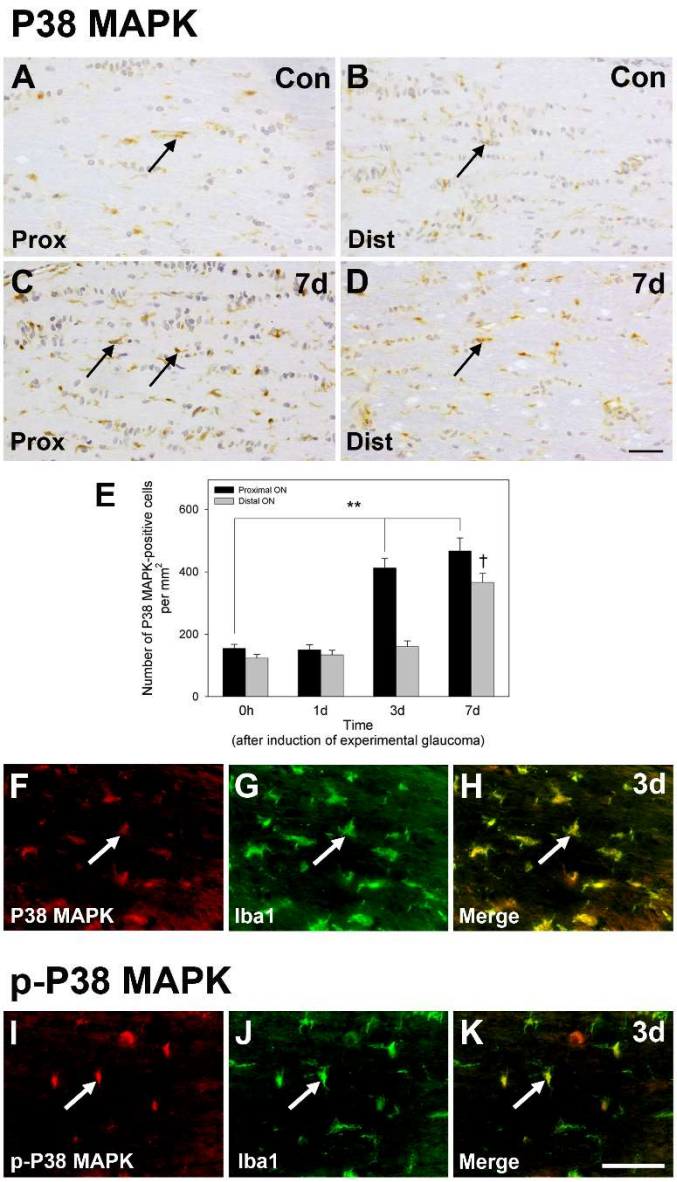

Figure 13. P38 MAPK localisation and activation in optic nerve. (A-D) Localisation of P38 MAPK in proximal (adjacent to the ONH; A) and distal (adjacent to the optic chiasm; B) optic nerve in control (Con), untreated eyes. Localisation of P38 MAPK in proximal (C) and distal (D) optic nerves from animals subjected to elevated IOP for 7 days. (E) Quantification of P38 MAPK-immunoreactive cells in proximal and distal areas of optic nerve in untreated eyes and in eyes subjected to elevated IOP for 1 day (1d), 3 days (3d) or 7 days (7d). (F-H) Double-fluorescent immunohistochemical labelling of P38 MAPK (F; red) in mid-section of optic nerve from eyes subjected to 1 day of elevated pressure, and identification of co-spatial localisation with Iba1 (G; green) present in microglial cells (H). (I-K) Obvious labelling of p-P38 MAPK (I; red) was also associated with clearly demarcated small, round cells, in nerves from eyes subjected to elevated IOP for 3 days or more (3d; arrow). Once again double-fluorescent labelling with Iba1 (J; green) identified such cells as a population of microglia (K). Scale bars, 50µm. Scale bar in (D) relates to (A-D) and scale bar in (K) relates to (F-K). Direction of optic nerves shown: left to right is proximal to distal.

DISCUSSION

Although the exact molecular processes governing the loss of RGCs in glaucoma are unknown, useful mechanistic hints can be gained by studying animal models such as the OHT model used here. For example, numerous studies have demonstrated that MAPK isoenzymes are activated in the experimentally stressed retina (Dapper et al. 2013, Fernandes et al. 2012, Kikuchi et al. 2000, Kim et al. 2016, Munemasa et al. 2005, Manabe and Lipton 2003, Nakazawa et al. 2002, Nitzan et al. 2006, Roth et al. 2003, Zhou et al. 2007). Furthermore, activation of this family of enzymes has been detected in retinas from human glaucoma patients (Tezel et al. 2003). All of these data implicate activation of MAPK signalling in retinal pathology. The role that MAPKs play in the development of ONH pathology, however, which is where the initial insult to ganglion cells is thought to arise in glaucoma (Chidlow et al. 2011a, Chidlow et al. 2011b, Howell et al. 2007), is currently unknown. The present study sought to address this.

P42/44 MAPK

In this study we found clear evidence that there was an increase in phosphorylation, and hence, activation, of both P42 and P44 MAPK isoforms, by 6 hours of IOP elevation in astrocytes in the ONH. In normal tissues, astrocytes provide functional and nutritive support to neurons (Constable and Lawrenson 2009, Liu et al. 1998), for example RGC axons in the ONH (Morrison et al. 1995). These cells respond rapidly to injury in the CNS, however, by becoming reactive contributing to the formation of a glial scar to seal the affected area (Lobsiger and Leveland 2007, Hernandez et al. 2008, Sofroniew and Vinters 2010). Reactive astrocytic changes are known to occur in the ONH in human (Hernandez et al. 2008, Morgan

2000) and experimental glaucoma (Chidlow et al. 2011b, Lye-Barthel et al. 2013). Reactive astrocytes can proliferate, dedifferentiate, or release factors which can directly impact surrounding cells (Sofroniew and Vinters 2010), and all of these actions have been associated with activation of P42/44 MAPK (Mandell and VandenBerg 1999, Tournier et al. 1994). Furthermore, P42/44 activation accompanies communication between astrocytes via gap junctions (Wang et al. 2013), enabling rapid dispersion of signals to neighbouring cells during situations of homeostatic disturbance (Giaume et al. 2010). For these reasons, Roth suggested that this enzyme plays a key role in induction and maintenance of the activated glial state (Mandell and VandenBerg 1999, Roth et al. 2003).

Astrocytes also respond to mechanical stresses such as pressure or stretch (Sofroniew and Vinters 2010). This is particularly pertinent in the ONH, where these cells (Morrison et al. 1995) are exposed to all perturbations in IOP (Hernandez et al. 2008, Morgan 2000). In response to increased pressure in vivo, astrocytes in the ONH express markers of activation such as tenascin and GFAP, and release factors such as transforming growth factor β (Hernandez et al. 2008, Morgan 2000). ONH astrocytes also respond in a similar manner to elevated hydrostatic pressure in vitro (Hashimoto et al. 2005, Hernandez 2000, Johnson et al. 2000, Salvador-Silva et al. 2004, Yang et al. 2004). Furthermore, not only is P42/44 MAPK itself stimulated in astrocytes in monkey (Hashimoto et al. 2005) or human glaucoma (Tezel et al. 2003) but it is also activated in cultured brain astrocytes in response to stretch injury (Neary et al. 2003). The early activation of P42/44 MAPK in the ONH in our model suggests that astrocytes do respond rapidly to raised IOP. Indeed, it has been suggested that astrocytes and, by implication, their response to elevated IOP, represent the primary source of pathology in glaucoma (Hernandez et al. 2008, Morgan 2000). Data herein, however, show that RGC axon transport abnormalities are also detectable within hours of pressure

elevation in the ONH and, indeed, precede P42/44 MAPK activation in astrocytes in the optic nerve. It is likely, therefore, that astrocyte activation occurs as a result of axonal pathology and, thus, does not give rise to it. What is clear from this study, though, is that early activation of P42/44 MAPK in astrocytes likely plays a key role in the response of these cells to stress. Finally, the reason for the expression of P42/44 MAPK in optic nerve oligodendrocytes is unclear, but the fact that even in eyes subjected to elevated IOP it is not activated suggests that it is not a mediator of pathological change in these cells.

Activated P42/44 MAPK was also demonstrated in Müller glial cells in retinas from both untreated eyes and eyes subjected to IOP elevation. There was no difference between the labelling before or at any time after elevation of IOP, however. Such data led us to conclude that this enzyme did not significantly contribute to any direct retinal pathology in our model. Although our data agree with previous work describing the presence of active P42/44 MAPK in the human glaucomatous retina (Tezel et al. 2003) and in the rodent retina in a variety of experimental situations (Liu et al. 1998, Munemasa et al. 2005, Nitzan et al. 2006, Roth et al. 2003, Takeda and Ichijo 2002, Ye et al. 2012), a significant discrepancy lies in the fact that we also detected the active form of this enzyme by immunohistochemistry in untreated eyes (Ye et al. 2012, Munemasa et al. 2005, Roth et al. 2003, Nitzan et al. 2006, Tezel et al. 2003, Liu et al. 1998). This difference likely lies in our use of Davidson's fixative, which we selected for consistency of labelling. Davidson's fixative is useful for ocular studies because it both offers good preservation of morphological integrity and limits retinal detachment (Latendresse et al. 2002). Moreover, Davidson's is now know to offer similar antigen preservation to formalin in many cases (Chidlow et al. 2011a, McKay et al. 2009, Casson et al. 2016).

SAPK/JNK

Total SAPK/JNK was present in all samples and was unaffected by chronic OHT. Although neither PCR primers nor antibodies could distinguish between the different SAPK/JNK isoforms, Western immunoblot identified that both short (46 kD) and long forms (54 kD) were expressed. In all cases, the long form was of greater relative abundance. Since the functional difference between each form is unclear (Zeke et al. 2016) then the significance of this finding is unknown.

Activated p-SAPK/JNK was present in untreated eyes, and localised to RGC axons in the retina, ONH and optic nerve. Although p-SAPK/JNK has been detected in optic nerve extracts from control eyes (Fernandes et al. 2014, Watkins et al. 2013, Huntwork-Rodriguez et al. 2013), it has not been specifically localised to RGC axons. As with p-P42/44 MAPK, the use of Davidson's instead of formalin to fix eyes herein is likely the reason for this difference in immunolabelling sensitivity (Fernandes et al. 2012, Fernandes et al. 2014). Nonetheless, what must be concluded from the present data is that since SAPK/JNK is constitutively active in RGCs from untreated eyes, then it must play a defined role in the physiological functioning of these cells. SAPK/JNK is known to have physiological actions in neurons: roles have been described in microtubular stability and axon transport (Chang et al. 2003), regulation of dendritic architecture (Bjorkblom et al. 2005) and maintenance of synaptic function and plasticity (Kim et al. 2007).

Activated p-SAPK/JNK was significantly elevated in ONH extracts after 3 or more hours of elevated IOP. Additionally, immunohistochemistry revealed that p-SAPK/JNK labelling was no longer evenly distributed throughout axons but had amassed within the ONH region relative to the optic nerve by 6 hours of raised IOP. Previous work described axon transport failure at the ONH in our model within hours of pressure elevation, as

detected by observing accumulation of fast-transported proteins such as APP (Chidlow et al. 2011b, Chidlow et al. 2012). This finding was reinforced in the present study. Further, the increased labelling for p-SAPK/JNK mimicked that of APP, suggesting not only that it was also transported in RGC axons, but that axon transport failure resulted in its accumulation at the ONH, proximal to the region of damage. This finding was paralleled by data showing that levels of p-SAPK/JNK decreased in optic nerves and increased in retinal extracts. In contrast to this, labelling for the structural protein, βIII-tubulin, which co-localised with p-SAPK/JNK in control axons, was not decreased as a result of transport dysfunction, but only by subsequent axonal degradation (Chidlow et al. 2011b). Fernandes and colleagues (Fernandes et al. 2012, Fernandes et al. 2013, Fernandes et al. 2014), localised p-SAPK/JNK in ONH axons after nerve crush, but since they did not see it in untreated eyes they described it as an activation of this enzyme and not an accumulation. Additionally, the build-up of p-SAPK/JNK proximal to the ONH in the present study was not a specific response to elevated pressure since this also occurred after optic nerve crush (Figure 8), which has no effect on IOP. Like APP, the accumulation of this enzyme was therefore likely to be in response to axonal injury generally (Chidlow et al. 2011b). The fact that in either situation, p-SAPK/JNK accumulated proximal to the injury site confirmed that transport of this activated protein was in the anterograde direction, unlike APP, which accumulated on both sides of the crush injury site, indicating its known bidirectional transport (Fu and Holzbaur 2013).

Studies have identified that SAPK/JNK is activated in RGCs in response to different forms of stress (Kwong and Caprioli 2006, Kim et al. 2016, Roth et al. 2003, Produit-Zengaffinen et al. 2016, Munemasa et al. 2005, Osborne et al. 2015, Li et al. 2013, Fernandes et al. 2012). This enzyme is also activated in RGCs in human glaucoma patients (Tezel et al.

2003). Additionally, several researchers have reported that inhibition or knockdown of specific isoforms of SAPK/JNK can abrogate RGC death induced by acute (Kim et al. 2016) or chronic IOP elevation (Sun et al. 2011), as well as optic nerve crush (Tezel et al. 2004, Fernandes et al. 2012). It is therefore likely in the present study that the increased levels of p-SAPK/JNK detected in retinal extracts and at the ONH represent both an accumulation of axon transported enzymes and the additional activation of one of more JNK isoforms in RGCs as a direct response to injury. Interestingly, dual leucine zipper kinase, an enzyme involved in RGC loss in glaucoma (Welsbie et al. 2013) was shown to activate SAPK/JNK in injured RGC somata but not axons (Watkins et al. 2013). Further, knock-out of dual leucine zipper kinase prevented RGC soma loss but not axon degeneration, implying that SAPK/JNK is only activated in cell bodies and not axons in response to injury (Fernandes et al. 2014). These data together imply distinct compartmentalisation of SAPK/JNK isoforms in RGCs, relating to physiological functioning of either axon-based and or soma-based, relating to an RGC injury response.

P38 MAPK

P38 MAPK is involved in the microglial response to tissue insult or disease, playing a part in processes such as cell activation and cytokine release (Bu et al. 2007, Koistinaho and Koistinaho 2002, Bachstetter et al. 2013, Liu et al. 2014) as well as phagocytosis of degenerating axons (Hosmane et al. 2012). P38 MAPK has been localised to rat retinal microglia in a model of diabetes (Ibrahim et al. 2010, Ibrahim et al. 2011), after lipopolysaccharide treatment (Xu et al. 2012, Ahmad et al. 2014), and in response to optic nerve trauma (Katome et al. 2013) but not in eyes subjected to IOP elevation.

Here we show that P38 MAPK is physiologically expressed by approximately 50 % of the Iba1-positive microglia in the retina, ONH and optic nerve. Further, there is a significant increase in P38 MAPK-positive microglia (Ebneter et al. 2010) after IOP elevation. These data suggest a role for P38 MAPK in microglial functioning in glaucoma. Since P38 MAPK was not expressed by all microglia, however, then it cannot be a component of a generic microglial stress response. It is possible that P38 MAPK is expressed by a subset of retinal microglia which have a specific purpose. It is known in the diabetic retina, for example, that P38 MAPK controls release of TNFα only from a sub-population of microglia (Ibrahim et al. 2011), whereas it can regulate TNFα, Il-6 and IL-1β release, and prostaglandin signalling in brain and spinal cord microglia (Bachstetter et al. 2013; Ji and Suter 2007).

Despite the physiological presence of P38 MAPK in microglia, and the increase in numbers of these cells after IOP elevation, activation of this enzyme only occurred in microglia localised to the ONH and optic nerve. Clearly, since microglia are also activated in the retina as well as the ONH and optic nerve in this model (Ebneter et al. 2010), then P38 MAPK cannot form a generic component of this activation process. In the ONH/optic nerve, phosphorylation of P38 MAPK was only detected in microglia after 3 or more days of elevated IOP, whereas microglial activation itself occurs within hours of pressure elevation (Ebneter et al. 2010). After 3 days, however, neurofilament abnormalities are evident in the ONH, likely as a result of axonal breakdown (Chidlow et al. 2011b, Ebneter et al. 2010). This is co-incident not only with the activation of P38 MAPK, but also with the appearance of the phagocytic microglial marker, ED1 (Ebneter et al. 2010). Taking into account the fact that P38 MAPK is known to play a key role in microglial phagocytosis (Hosmane et al. 2012), then it is possible that its activation here is related to removal of damaged axon tissue.

Interestingly, activation of P38 MAPK did occur in the retina, but in RGCs rather than microglia. This effect has been described in other studies: P38 MAPK has been reported to be activated in RGCs in numerous retinal (Dapper et al. 2013, Foxton et al. 2016, Manabe and Lipton 2003, Munemasa et al. 2005, Roth et al. 2003) and optic nerve injury models (Nitzan et al. 2006, Kikuchi et al. 2000) as well as in retinas from human glaucoma patients (Tezel et al. 2003). In most cases, however, P38 MAPK activation was seen within 6 hours of induction of retinal pathology, clearly indicating its part in the somal injury response to axonal stress. Due to the fact that retinal activation of P38 MAPK in the present study occurs from 24 hours after IOP elevation, it is unlikely that this is an initiator of the stress response in RGC somata. However, P38 MAPK activation certainly contributes to RGC neurodegeneration, as seen in studies where pharmacological inhibition of this enzyme abrogated the death of these cells induced by N-methyl-D-aspartate (Munemasa et al. 2005, Manabe and Lipton 2003), retinal ischemia (Roth et al. 2003), optic nerve transection (Kikuchi et al. 2000) and acute experimental elevation of IOP (Dapper et al. 2013).

CONCLUSIONS

In summary we have shown that each of the three classes of MAPK: P42/44 MAPK, SAPK/JNK and P38 MAPK are expressed in the retina/ONH and that they are differentially influenced by elevation of IOP, as induced by laser treatment of the trabecular meshwork. P42/44 MAPK is present in retinal Müller glia and oligodendrocytes within the optic nerve, but it is rapidly activated in ONH astrocytes as a result of elevated IOP. SAPK/JNK is present in its active form throughout RGC axons but quickly accumulates at the ONH as a result of pressure-induced axon transport failure. P38 MAPK is expressed by microglia throughout

the retina and optic nerve. It is only activated in microglia in the ONH and optic nerve, as a result of elevation of IOP, however; in the retina P38 MAPK is induced and activated in RGC somas. The expression and activation of these MAPKs in the retina/ONH/optic nerve as a result of IOP elevation suggest that these enzymes play a role in the developing pathology in our model, and, by implication, in the pathogenesis of glaucomatous RGC loss. Selective manipulation of the activities of the individual MAPKs, therefore, may prove useful as a therapeutic strategy to combat glaucoma.

DECLARATION

Ethics approval

This study was approved by the Animal Ethics Committee of SA Pathology/Central Adelaide Local Health Network. The study conformed to the ARRIVE Guidelines and both the Australian Code of Practice for the Care and Use of Animals for Scientific Purposes (2013) and to the Association for Research in Vision and Ophthalmology Statement for The Use Of Animals In Ophthalmic And Vision Research.

Availability of data and materials

The datasets used and/or analysed during the current study are available from the corresponding author on reasonable request.

Conflict of interests

The authors declare that they have no conflict of interests.

Funding

The financial support of the BrightFocus Foundation (grant #G2013135), the Ophthalmic Research Institute of Australia and the National Health and Medical Research Council of Australia (Project Grant #565202) are gratefully acknowledged. The Bodies who provided funding for this work had no other role in the study.

Author contribution

Teresa Mammone: Experimental work, manuscript preparation.

Glyn Chidlow: Conception of study, manuscript editing.

Robert Casson: Provision of laboratory space and equipment, manuscript editing.

John Wood: Conception and design of study, manuscript preparation.

Acknowledgments

The technical assistance of Mr Mark Daymon is gratefully acknowledged.

REFERENCES

AHMAD S, ELSHERBINY NM, BHATIA K, ELSHERBINI AM, FULZELE S AND LIOU GI. 2014. Inhibition of adenosine kinase attenuates inflammation and neurotoxicity in traumatic optic neuropathy. J Neuroimmunol 277: 96-104.

BACHSTETTER AD, ROWE RK, KANEKO M, GOULDING D, LIFSHITZ J AND VAN ELDIK LJ. 2013. The p38 alpha MAPK regulates microglial responsiveness to diffuse traumatic brain injury. J Neurosci 33: 6143-6153.

BJORKBLOM B, OSTMAN N, HONGISTO V, KOMAROVSKI V, FILEN JJ, NYMAN TA, KALLUNKI T, COURTNEY MJ AND COFFEY ET. 2005. Constitutively active cytoplasmic c-Jun N-terminal kinase 1 is a dominant regulator of dendritic architecture: Role of microtubule-associated protein 2 as an effector. J Neurosci 25: 6350-6361.

BU XN, HUANG P, QI ZF, ZHANG N, HAN S, FANG L AND LI JF. 2007. Cell type-specific activation of p38 MAPK in the brain regions of hypoxic preconditioned mice. Neurochem Int 51: 459-466.

BURGOYNE CF. 2011. A biomechanical paradigm for axonal insult within the optic nerve head in aging and glaucoma. Exp Eye Res 93: 120-132.

CARGNELLO M AND ROUX PP. 2011. Activation and function of the MAPKs and their substrates, the MAPK-activated protein Kinases. Microbiol Mol Biol Rev 75: 50-83.

CASSON RJ, CHIDLOW G, WOOD JP, CROWSTON JG AND GOLDBERG I. 2012. Definition of glaucoma: clinical and experimental concepts. Clin Experiment Ophthalmol 40: 341-349.

CASSON RJ, WOOD JPM, HAN GG, KITTIPASSORN T, PEET DJ AND CHIDLOW G. 2016. M-type pyruvate kinase isoforms and lactate dehydrogenase A in the mammalian retina: metabolic implications. Invest Ophthalmol Vis Sci 57: 66-80.

CHANG LF, JONES Y, ELLISMAN MH, GOLDSTEIN LSB AND KARIN M. 2003. JNK1 is required for maintenance of neuronal microtubules and controls phosphorylation of microtubule-associated proteins. Dev Cell 4: 521-533.

CHIDLOW G, DAYMON M, WOOD JPM AND CASSON RJ. 2011a. Localization of a wide-ranging panel of antigens in the rat retina by immunohistochemistry: comparison of davidson's solution and formalin as fixatives. J Histochem Cytochem 59: 884-898.

CHIDLOW G, EBNETER A, WOOD JPM AND CASSON RJ. 2011b. The optic nerve head is the site of axonal transport disruption, axonal cytoskeleton damage and putative axonal regeneration failure in a rat model of glaucoma. Acta Neuropathol 121: 737-751.

CHIDLOW G, WOOD JPM AND CASSON RJ. 2007. Pharmacological neuroprotection for glaucoma. Drugs 67: 725-759.

CHIDLOW G, WOOD JPM, EBNETER A AND CASSON RJ. 2012. Interleukin-6 is an efficacious marker of axonal transport disruption during experimental glaucoma and stimulates neuritogenesis in cultured retinal ganglion cells. Neurobiol Dis 48: 568-581.

CHIDLOW G, WOOD JPM, MANAVIS J, OSBORNE NN AND CASSON RJ. 2008. Expression of osteopontin in the rat retina: Effects of excitotoxic and ischemic injuries. Invest Ophthalmol Vis Sci 49: 762-771.

CONSTABLE PA AND LAWRENSON JG. 2009. Glial cell factors and the outer blood retinal barrier. Ophthalmic Physiol Opt 29: 557-564.

COWAN KJ AND STOREY KB. 2003. Mitogen-activated protein kinases: new signaling pathways functioning in cellular responses to environmental stress. J Exp Biol 206: 1107-1115.

CUENDA A AND ROUSSEAU S. 2007. P38 MAP-Kinases pathway regulation, function and role in human diseases. Biochimica Et Biophysica Acta-Molecular Cell Research 1773: 1358-1375.

DAPPER JD, CRISH SD, PANG IH AND CALKINS DJ. 2013. Proximal inhibition of p38 MAPK stress signaling prevents distal axonopathy. Neurobiol Dis 59: 26-37.

DAVIDSON B, KONSTANTINOVSKY S, KLEINBERG L, NGUYEN MTP, BASSAROVA A, KVALHEIM G, NESLAND JM AND REICH R. 2006. The mitogen-activated protein kinases (MAPK) p38 and JNK are markers of tumor progression in breast carcinoma. Gynecol Oncol 102: 453-461.

EBNETER A, CASSON RJ, WOOD JP AND CHIDLOW G. 2010. Microglial activation in the visual pathway in experimental glaucoma: spatiotemporal characterization and correlation with axonal injury. Invest Ophthalmol Vis Sci 51: 6448-6460.

EBNETER A, CASSON RJ, WOOD JP AND CHIDLOW G. 2012. Estimation of axon counts in a rat model of glaucoma: comparison of fixed-pattern sampling with targeted sampling. Clin Exp Ophthalmol 40: 626-633.

EBNETER A, CHIDLOW G, WOOD JPM AND CASSON RJ. 2011. Protection of retinal ganglion cells and the optic nerve during short-term hyperglycemia in experimental glaucoma. Arch Ophthalmol 129: 1337-1344.

FERNANDES KA, HARDER JM, FORNAROLA LB, FREEMAN RS, CLARK AF, PANG IH, JOHN SWM AND LIBBY RT. 2012. JNK2 and JNK3 are major regulators of axonal injury-induced retinal ganglion cell death. Neurobiol Dis 46: 393-401.

FERNANDES KA, HARDER JM, JOHN SW, SHRAGER P AND LIBBY RT. 2014. DLK-dependent signaling is important for somal but not axonal degeneration of retinal ganglion cells following axonal injury. Neurobiol Dis 69: 108-116.

FERNANDES KA, HARDER JM, KIM J AND LIBBY RT. 2013. JUN regulates early transcriptional responses to axonal injury in retinal ganglion cells. Exp Eye Res 112: 106-117.

FLAMMER J, HAEFLIGER IO, ORGUL S AND RESINK T. 1999. Vascular dysregulation: A principal risk factor for glaucomatous damage? J Glaucoma 8: 212-219.

FLOOD DG, FINN JP, WALTON KM, DIONNE CA, CONTRERAS PC, MILLER MS AND BHAT RV. 1998. Immunolocalization of the mitogen-activated protein kinases p42(MAPK) and JNK1, and their regulatory kinases MEK1 and MEK4, in adult rat central nervous system. J Comp Neurol 398: 373-392.

FOXTON R, OSBORNE A, MARTIN KR, NG YS AND SHIMA DT. 2016. Distal retinal ganglion cell axon transport loss and activation of p38 MAPK stress pathway following VEGF-A antagonism. Cell Death Dis 7: e2212.

FU MM AND HOLZBAUR ELF. 2013. JIP1 regulates the directionality of APP axonal transport by coordinating kinesin and dynein motors. J Cell Biol 202: 495-508.

GIAUME C, KOULAKOFF A, ROUX L, HOLCMAN D AND ROUACH N. 2010. Astroglial networks: a step further in neuroglial and gliovascular interactions. Nature Reviews Neuroscience 11: 87-99.

GREWAL SS, YORK RD AND STORK PJS. 1999. Extracellular-signal-regulated kinase signalling in neurons. Curr Opin Neurobiol 9: 544-553.

HASHIMOTO K, PARKER A, MALONE P, GABELT BT, RASMUSSEN C, KAUFMAN PS AND HERNANDEZ MR. 2005. Long-term activation of c-Fos and c-Jun in optic nerve head astrocytes in experimental ocular hypertension in monkeys and after exposure to elevated pressure in vitro. Brain Res 1054: 103-115.

HERNANDEZ MR. 2000. The optic nerve head in glaucoma; Role of astrocytes in tissue remodeling. Prog Retin Eye Res 19: 297.

HERNANDEZ MR, MIAO HX AND LUKAS T 2008. Astrocytes in glaucomatous optic neuropathy. In*:* NUCCI, C, CERULLI, L, OSBORNE, NN AND BAGETTA, G (Eds.) Glaucoma: An Open Window to Neurodegeneration and Neuroprotection, Amsterdam: Elsevier Science Bv, p. 353-373.

HETMAN M AND GOZDZ A. 2004. Role of extracellular signal regulated kinases 1 and 2 in neuronal survival. Eur J Biochem 271: 2050-2055.

HOSMANE S, TEGENGE MA, RAJBHANDARI L, UAPINYOYING P, KUMAR NG, THAKOR N AND VENKATESAN A. 2012. Toll/Interleukin-1 receptor domain-containing adapter inducing interferon-beta mediates microglial phagocytosis of degenerating axons. J Neurosci 32: 7745-7757.

HOWELL GR ET AL. 2007. Axons of retinal ganglion cells are insulted in the optic nerve early in DBA/2J glaucoma. J Cell Biol 179: 1523-1537.

HUNTWORK-RODRIGUEZ S, WANG B, WATKINS T, GHOSH AS, POZNIAK CD, BUSTOS D, NEWTON K, KIRKPATRICK DS AND LEWCOCK JW. 2013. JNK-mediated phosphorylation of DLK suppresses its ubiquitination to promote neuronal apoptosis. J Cell Biol 202: 747-763.

IBRAHIM AS, EL-REMESSY AB, MATRAGOON S, ZHANG WB, PATEL Y, KHAN S, AL-GAYYAR MM, EL-SHISHTAWY MM AND LIOU GI. 2011. Retinal microglial activation and inflammation induced by amadori-glycated albumin in a rat model of diabetes. Diabetes 60: 1122-1133.

IBRAHIM AS, EL-SHISHTAWY MM, PENA A AND LIOU GI. 2010. Genistein attenuates retinal inflammation associated with diabetes by targeting of microglial activation. Mol Vis 16: 2033-2042.

JI RR AND SUTER MR. 2007. p38 MAPK, microglial signaling, and neuropathic pain. Mol Pain 3: 9.

JOHNSON EC, DEPPMEIER LMH, WENTZIEN SKF, HSU I AND MORRISON JC. 2000. Chronology of optic nerve head and retinal responses to elevated intraocular pressure. Invest Ophthalmol Vis Sci 41: 431-442.

JOHNSON GL AND LAPADAT R. 2002. Mitogen-activated protein kinase pathways mediated by ERK, JNK and p38 protein kinases. Science 298: 1911-1912.

KATOME T ET AL. 2013. Inhibition of ASK1-p38 pathway prevents neural cell death following optic nerve injury. Cell Death Differ 20: 270-280.

KIKUCHI M, TENNETI L AND LIPTON SA. 2000. Role of p38 mitogen-activated protein kinase in axotomy-induced apoptosis of rat retinal ganglion cells. J Neurosci 20: 5037-5044.

KIM B-J, SILVERMAN SM, LIU Y, WORDINGER RJ, PANG I-H AND CLARK AF. 2016. In vitro and in vivo neuroprotective effects of cJun N-terminal kinase inhibitors on retinal ganglion cells. Mol Neurodegener 11.

KIM EK AND CHOI EJ. 2010. Pathological roles of MAPK signaling pathways in human diseases. Biochim Biophys Acta 1802: 396-405.

KIM MJ, FUTAI K, JO J, HAYASHI Y, CHO K AND SHENG M. 2007. Synaptic accumulation of PSD-95 and synaptic function regulated by phosphorylation of serine-295 of PSD-95. Neuron 56: 488-502.

KOISTINAHO M AND KOISTINAHO J. 2002. Role of p38 and p44/42 mitogen-activated protein kinases in microglia. Glia 40: 175-183.

KWONG JMK AND CAPRIOLI J. 2006. Expression of phosphorylated c-Jun N-terminal protein kinase (JNK) in experimental glaucoma in rats. Exp Eye Res 82: 576-582.

LATENDRESSE JR, WARBRITTION AR, JONASSEN H AND CREASY DM. 2002. Fixation of testes and eyes using a modified Davidson's fluid: Comparison with Bouin's fluid and conventional Davidson's fluid. Toxicol Pathol 30: 524-533.

LEVKOVITCH-VERBIN H, QUIGLEY HA, MARTIN KRG, VALENTA D, BAUMRIND LA AND PEASE ME. 2002. Translimbal laser photocoagulation to the trabecular meshwork as a model of glaucoma in rats. Invest Ophthalmol Vis Sci 43: 402-410.

LI HY, LIANG YX, CHIU K, YUAN QJ, LIN B, CHANG RCC AND SO KF. 2013. Lycium barbarum (Wolfberry) reduces secondary degeneration and oxidative stress, and inhibits JNK pathway in retina after partial optic nerve transection. PLoS One 8: 13.

LIU CD, PENG M, LATIES AM AND WEN R. 1998. Preconditioning with bright light evokes a protective response against light damage in the rat retina. J Neurosci 18: 1337-1344.

LIU L, DORAN S, XU Y, MANWANI B, RITZEL R, BENASHSKI S, MCCULLOUGH L AND LI J. 2014. Inhibition of mitogen-activated protein kinase phosphatase-1 (MKP-1) increases experimental stroke injury. Exp Neurol 261: 404-411.

LOBSIGER CS AND LEVELAND DW. 2007. Glial cells as intrinsic components of non-cell-autonomous neurodegenerative disease. Nat Neurosci 10: 1355-1360.

LYE-BARTHEL M, SUN D AND JAKOBS TC. 2013. Morphology of astrocytes in a glaucomatous optic nerve. Invest Ophthalmol Vis Sci 54: 909-917.

MANABE S AND LIPTON SA. 2003. Divergent NMDA signals leading to proapoptotic and antiapoptotic pathways in the rat retina. Invest Ophthalmol Vis Sci 44: 385-392.

MANDELL JW AND VANDENBERG SR. 1999. ERK/MAP kinase is chronically activated in human reactive astrocytes. Neuroreport 10: 3567-3572.

MCKAY JS, STEELE SJ, AHMED G, JOHNSON E AND RATCLIFFE K. 2009. An antibody panel for immunohistochemical analysis of the retina in Davidson's-fixed, paraffin-embedded eyes of rats. Exp Toxicol Pathol 61: 91-100.

MEHAN S, MEENA H, SHARMA D AND SANKHLA R. 2011. JNK: A stress-activated protein kinase therapeutic strategies and involvement in alzheimer's and various neurodegenerative abnormalities. J Mol Neurosci 43: 376-390.

MORGAN JE. 2000. Optic nerve head structure in glaucoma: astrocytes as mediators of axonal damage. Eye 14: 437-444.

MORIN PJ, ABRAHAM CR, AMARATUNGA A, JOHNSON RJ, HUBER G, SANDELL JH AND FINE RE. 1993. Amyloid precursor protein is synthesized by retinal ganglion-cells, rapidly trasported to the optic-nerve plasma-membrane and nerve-terminals, and metabolized. J Neurochem 61: 464-473.

MORRISON J, FARRELL S, JOHNSON E, DEPPMEIER L, MOORE CG AND GROSSMANN E. 1995. Structure and composition of the rodent lamina cribrosa. Exp Eye Res 60: 127-135.

MUNEMASA Y ET AL. 2005. Contribution of mitogen-activated protein kinases to NMDA-induced neurotoxicity in the rat retina. Brain Res 1044: 227-240.

NAKAZAWA T, TAMAI M AND MORI N. 2002. Brain-derived neurotrophic factor prevents axotomized retinal ganglion cell death through MAPK and PI3K signaling pathways. Invest Ophthalmol Vis Sci 43: 3319-3326.

NEARY JT, KANG Y, WILLOUGHBY KA AND ELLIS EF. 2003. Activation of extracellular signal-regulated kinase by stretch-induced injury in astrocytes involves extracellular ATP and P2 purinergic receptors. J Neurosci 23: 2348-2356.

NITZAN A, KERMER P, SHIRVAN A, BAHR M, BARZILAI A AND SOLOMON AS. 2006. Examination of cellular and molecular events associated with optic nerve axotomy. Glia 54: 545-556.

OSBORNE A, ALDARWESH A, RHODES JD, BROADWAY DC, EVERITT C AND SANDERSON J. 2015. Hydrostatic pressure does not cause detectable changes in survival of human retinal ganglion cells. PLoS One 10: e0115591.

OSBORNE NN, WOOD JPM, CHIDLOW G, BAE JH, MELENA J AND NASH MS. 1999. Ganglion cell death in glaucoma: what do we really know? Br J Ophthalmol 83: 980-986.

OZAWA H, SHIODA S, DOHI K, MATSUMOTO H, MIZUSHIMA H, ZHOU CJ, FUNAHASHI H, NAKAI Y, NAKAJO S AND MATSUMOTO K. 1999. Delayed neuronal cell death in the rat hippocampus is mediated by the mitogen-activated protein kinase signal transduction pathway. Neurosci Lett 262: 57-60.

PRODUIT-ZENGAFFINEN N, FAVEZ T, POURNARAS CJ AND SCHORDERET DF 2016. JNK inhibition reduced retinal ganglion cell death after ischemia/reperfusion in vivo and after hypoxia in vitro. In*:* RICKMAN, CB, LAVAIL, MM, ANDERSON, RE, GRIMM, C, HOLLYFIELD, J AND ASH, J (Eds.) Retinal Degenerative Diseases: Mechanisms and Experimental Therapy, Cham: Springer Int Publishing Ag, p. 677-683.

QUIGLEY HA AND BROMAN AT. 2006. The number of people with glaucoma worldwide in 2010 and 2020. Br J Ophthalmol 90: 262-267.

ROSKOSKI R. 2012. ERK1/2 MAP kinases: Structure, function, and regulation. Pharmacol Res 66: 105-143.

ROTH S, SHAIKH AR, HENNELLY MM, LI Q, BINDOKAS V AND GRAHAM CE. 2003. Mitogen-activated protein kinases and retinal ischemia. Invest Ophthalmol Vis Sci 44: 5383-5395.

SALVADOR-SILVA M, AOI S, PARKER A, YANG P, PECEN P AND HERNANDEZ MR. 2004. Responses and signaling pathways in human optic nerve head astrocytes exposed to hydrostatic pressure in vitro. Glia 45: 364-377.

SHACKELFORD DA AND YEH RY. 2006. Modulation of ERK and JNK activity by transient forebrain ischemia in rats. J Neurosci Res 83: 476-488.

SOFRONIEW MV AND VINTERS HV. 2010. Astrocytes: biology and pathology. Acta Neuropathol 119: 7-35.

SUGINO T, NOZAKI K, TAKAGI Y, HATTORI I, HASHIMOTO N, MORIGUCHI T AND NISHIDA E. 2000. Activation of mitogen-activated protein kinases after transient forebrain ischemia in gerbil hippocampus. J Neurosci 20: 4506-4514.

SUN H, WANG Y, PANG IH, SHEN JQ, TANG X, LI Y, LIU CY AND LI B. 2011. Protective effect of a JNK inhibitor against retinal ganglion cell loss induced by acute moderate ocular hypertension. Mol Vis 17: 864-875.

TAKEDA K AND ICHIJO H. 2002. Neuronal p38 MAPK signalling: an emerging regulator of cell fate and function in the nervous system. Genes Cells 7: 1099-1111.

TEZEL G, CHAUBAN BC, LEBLANC RP AND WAX MB. 2003. Immunohistochemical assessment of glial mitogen-activated protein kinase (MAPK) activation in glaucoma. Invest Ophthalmol Vis Sci 7: 3025-3033.

TEZEL G, YANG XJ, YANG JJ AND WAX MB. 2004. Role of tumor necrosis factor receptor-1 in the death of retinal ganglion cells following optic nerve crush injury in mice. Brain Res 996: 202-212.

TOURNIER C, POMERANCE M, GAVARET JM AND PIERRE M. 1994. MAP Kinase cascade in astrocytes. Glia 10: 81-88.

WANG L, COSSETTE SM, RARICK KR, GERSHAN J, DWINELL MB, HARDER DR AND RAMCHANDRAN R. 2013. Astrocytes directly influence tumor cell invasion and metastasis in vivo. PLoS One 8: 13.

WATKINS TA, WANG B, HUNTWORK-RODRIGUEZ S, YANG J, JIANG ZY, EASTHAM-ANDERSON J, MODRUSAN Z, KAMINKER JS, TESSIER-LAVIGNE M AND LEWCOCK JW. 2013. DLK initiates a transcriptional program that couples apoptotic and regenerative responses to axonal injury. Proc Natl Acad Sci U S A 110: 4039-4044.

WELSBIE DS ET AL. 2013. Functional genomic screening identifies dual leucine zipper kinase as a key mediator of retinal ganglion cell death. Proc Natl Acad Sci U S A 110: 4045-4050.

XU YF, FU LL, JIANG CH, QIN YW, NI YQ AND FAN JW. 2012. Naloxone inhibition of lipopolysaccharide-induced activation of retinal microglia is partly mediated via the p38 mitogen activated protein kinase signalling pathway. J Int Med Res 40: 1438-1448.

YANG J-C, JI X-Q, LI C-L, LIN J-H AND LIU X-G. 2004. Impact of early-stage hepatic ischemia-reperfusion injury on other organs of rats. Di 1 jun yi da xue xue bao = Academic journal of the first medical college of PLA 24: 1019-1022.

YE X, REN H, ZHANG M, SUN Z, JIANG AC AND XU G. 2012. ERK1/2 signaling pathway in the release of VEGF from Muller cells in diabetes. Invest Ophthalmol Vis Sci 53: 3481-3489.

ZEKE A, MISHEVA M, REMENYI A AND BOGOYEVITCH MA. 2016. JNK signaling: Regulation and functions based on complex protein-protein partnerships. Microbiol Mol Biol Rev 80: 793-835.

ZHOU RH, YAN H, WANG BR, KUANG F, DUAN XL AND XU Z. 2007. Role of extracellular signal-regulated kinase in glutamate-stimulated apoptosis of rat retinal ganglion cells. Curr Eye Res 32: 233-239.

SUPPLIMENTAL FIGURES

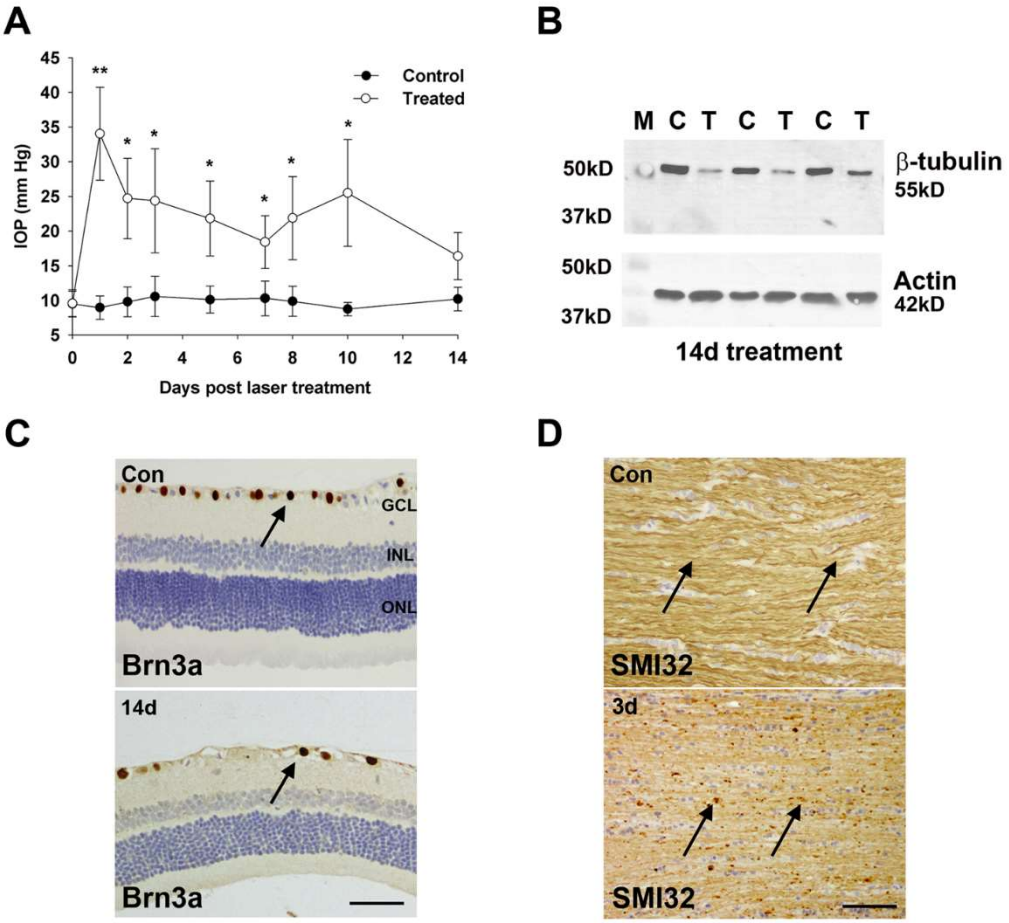

Supplemental Figure 1. Validation of the model used in the study. Data are shown which agree with previously-reported data in order to prove the efficacy of the model used. (A) IOP profiles for treated (open circles) and non-treated (closed circles) eyes after induction of OHT. Data are shown as mean IOP ± SD values and are taken from the cumulative total of animals treated throughout the study. Thus, *n* varies between 15 and 25, depending on the frequency of analysing each time-point. (B) Analysis of βIII-tubulin levels in whole optic nerve extracts by Western immunoblot after chronic IOP elevation for 14 days, β-actin immunoblots are also shown for the same samples, as gel-loading controls (M, molecular weight marker C, control eye; T, treated eye). βIII-tubulin was clearly decreased in treated nerve extracts when compared to those from contralateral, control nerves. (C) Following IOP elevation for 14 days, immunohistochemical labelling of Brn3a-labelled RGC clearly indicated a significant and specific loss of these cells. (D) Analysis of non-phosphorylated 200 kD neurofilament with SMI32 labelling in the mid-optic nerve after 3 days of elevated pressure. Damaged axons displayed neurofilament discontinuity and swellings throughout the length of the nerve. Scale bars: C, 50µm; D, 25µm. GCL, ganglion cell layer; INL, inner nuclear layer; ONL, outer nuclear layer. Direction of optic nerves shown: left to right is apical to distal.

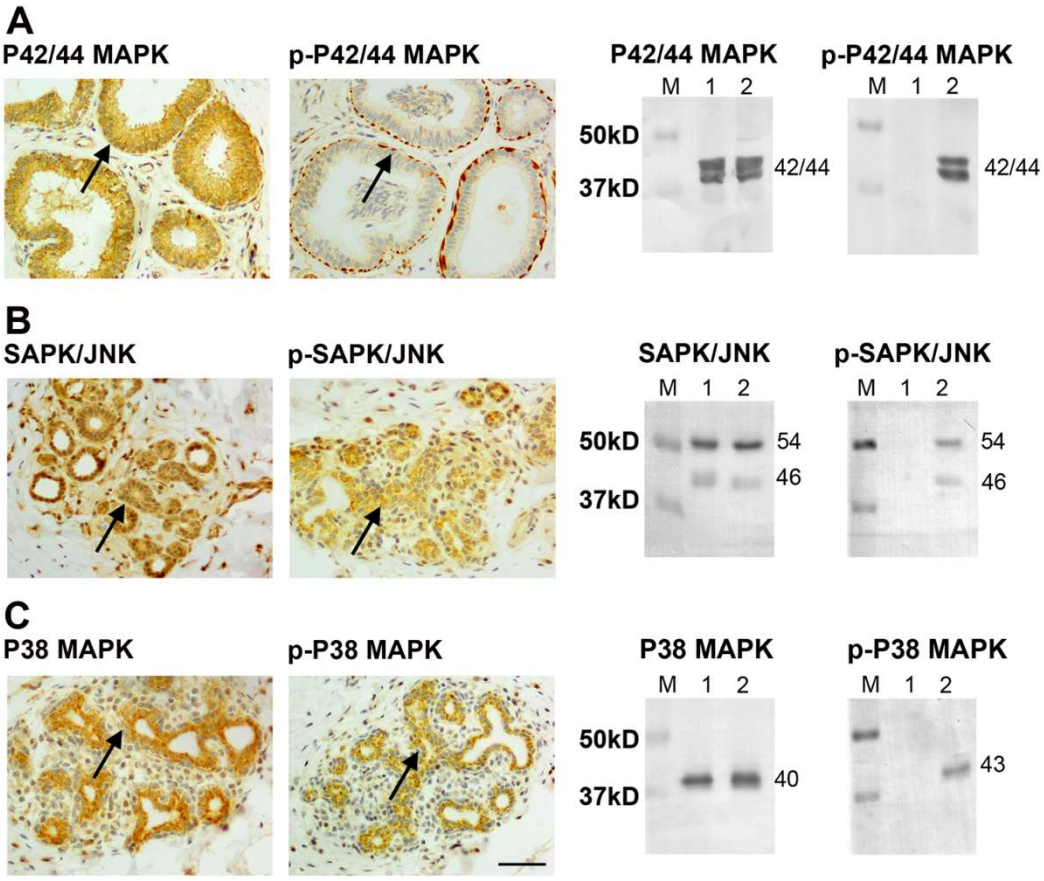

Supplemental Figure 2. Validation of antibodies used in the study. Identification of positive labelling in sections of ductal breast carcinoma tissue agreed with previous findings (see text) and served as an antibody labelling control in each case (A-C). Further, commercially-obtained cell extracts which were positive for total or phosphorylated forms of each of the MAPKs under investigation showed that proteins with the correct mass were detected by each. (A) P42/44 MAPK is localised in myoepithelium as well as in hyperplastic ductal epithelial cells, while active, p-P42/44 MAPK is restricted to the ductal myoepithelium. Furthermore, both P42/44 MAPK and p-P42/44 MAPK form are detectable in U0126 (MEK1/2 inhibitor)-stimulated total Jurkat cell extract, but only the former was present in a comparable unstimulated extract. M, molecular weight markers; lane 1, unstimulated Jurkat cell extract; lane 2, stimulated Jurkat cell extract. (B) Detection of SAPK/JNK and p-SAPK/JNK in breast carcinoma ductal epithelial cells. Both SAPK/JNK and p-SAPK/JNK are present in HEK 293 cell extracts stimulated with UV light, but only the former is present in a comparable unstimulated extract. M, molecular weight markers; lane 1, unstimulated HEK 293 cell extract; lane 2, stimulated HEK 293 cell extract. (C) P38 MAPK and p-P38 MAPK are present in breast carcinoma ductal epithelial cells. Both P38 MAPK and p-P38 MAPK were present in C-6 glioma cell extracts stimulated with anisomycin, but only the former was present in a comparable unstimulated extract M, molecular weight markers; lane 1, unstimulated C-6 glioma cell extract; lane 2, stimulated C-6 glioma cell extract. Scale bar, 50µm.

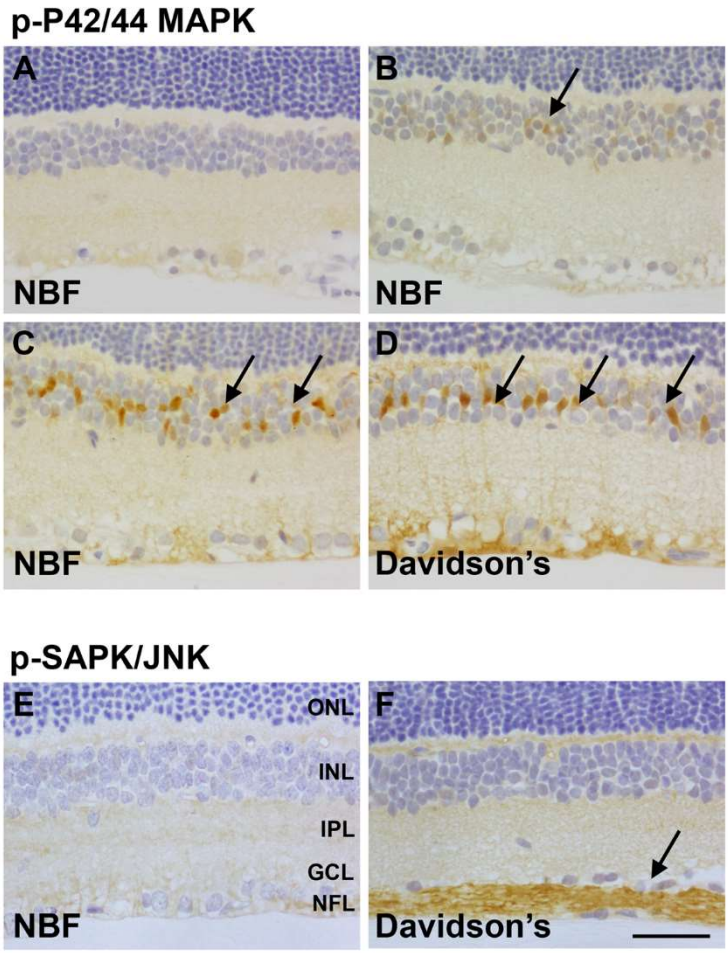

Supplemental Figure 3. Choice of fixative and outcome of immunohistochemical labelling for p-P42/44 MAPK (A-D) and p-SAPK/JNK (E, F) in untreated rat retinas. Neutral buffered formalin (NBF; containing 4% formaldehyde) was used to fix some eyes; subsequent immunohistochemistry revealed substantial variations in labelling for p-P42/44 MAPK that fell into three groups: no labelling (A), faint labelling detected in the inner plexiform layer (B; arrow) and clear putative Müller Cell labelling (C; arrows). In contrast, the use of Davidson's fixative for fixation (see Methods section) gave clear and consistent labelling for p-P42/44 MAPK in putative Müller Cells in untreated retinas (D; arrows). In the case of p-SAPK/JNK, use of NBF fixative meant that no labelling was detected in sections (E), whereas fixation with Davidson's revealed clear binding of the antibody in the retinal nerve fibre layer (F; arrow). Based on these tests, Davidson's fixative was selected for use throughout this study. ONL, outer nuclear layer; INL, inner nuclear layer; IPL, inner plexiform layer; GCL, ganglion cell layer; NFL, nerve fibre layer. Scale bar, 50μm.

CHAPTER 2 PRELUDE

Is that the end of MAPK in the ONH?

Results in the previous chapter showed that there was an activation of different classes of MAPKs in the ONH in our rodent model of chronic OHT. Results obtained by immunohistochemistry, however, although always clearly indicative of MAPK activation, were subject to a degree of variability. The reasons for this were unknown but could have represented a true variation in the activation of the enzymes themselves. This could be because either the MAPKs were in low abundance, such that small alterations in the level of activation between different samples could manifest as large detectable differences, or because small variations in IOP elevations between experimental animals could have profound effects on activation of the enzymes themselves. There was, however, a third possibility, that the variation in detectable levels of phosphorylated MAPKs alterations were the result of methodological considerations. For example, during tissue collection for immunohistochemistry, cellular processes still occur until fixation is absolute. Variability in the time taken for complete fixative penetration to occur could subject the tissue to external environmental factors such as body temperature changes, oxygen availability alterations or depletion of available cellular nutrients. All of these factors could conceivably alter cellular signalling during fixation, and this could influence the degree of phosphorylation or, particularly, dephosphorylation of previously activated MAPKs.

With this in mind, it was decided to investigate an improved method for procuring sections for immunohistochemical detection of phosphorylated MAPKs and to see whether use of this method was able to reduce the variability in detected labelling.

CHAPTER 2

Statement of Authorship

Title of Paper:	Improved immunohistochemical detection of phosphorylated map kinases in the injured rat ONH
Publication Status:	Unpublished and unsubmitted work written in manuscript style
Publication Details:	Provisions for Journal of Histochemistry and Cytochemistry

Principal Author

Name of Principle Author (candidate):	Teresa Mammone
Contribution to the Paper:	Experimental work, manuscript preparation
Overall percentage (%):	85%
Certification:	This paper reports on original research I conducted during the period of my Higher Degree by Research candidature and is not subject to any obligations or contractual agreements with a third party that would constrain its inclusion in this thesis. I am the primary author of this paper.

Signature:

Date: 09-08-17

Co-Author Contributions

By signing the Statement of Authorship, each author certifies that:

i. the candidate's stated contribution to the publication is accurate (as detailed above);
ii. permission is granted for the candidate in include the publication in the thesis; and
iii. the sum of all co-author contributions is equal to 100% less the candidate's stated contribution.

Name of Co-Author:	John Wood
Contribution to the paper:	Conception and design of study, manuscript preparation

Signature:

Date: 09-08-17

Name of Co-Author:	Glyn Chidlow
Contribution to the paper:	Conception of study, manuscript editing

Signature:

Date: 09-08-17

Name of Co-Author:	Robert Casson
Contribution to the paper:	Provision of laboratory space and equipment, manuscript editing
Signature:	
Date:	09-08-17

IMPROVED IMMUNOHISTOCHEMICAL DETECTION OF PHOSPHORYLATED MAP KINASES IN THE INJURED RAT ONH

Teresa Mammone [a,b], Glyn Chidlow [a,b], Robert J. Casson [a,b], John P. M. Wood [a,b]

[a]Ophthalmic Research Laboratories, Central Adelaide Local Health Network, Level 7 Adelaide Health & Medical Sciences Building, University of Adelaide, Adelaide, South Australia, Australia

[b]Department of Ophthalmology and Visual Sciences, University of Adelaide, Adelaide, South Australia, Australia

Corresponding author: John P. M. Wood

Email: john.wood2@sa.gov.au

'Tel: +61 8 82223092

'Fax: +61 8 82223392

Other authors: teresa.mammone@sa.gov.au

glyn.chidlow@sa.gov.au

robert.casson@adelaide.edu.au

ABSTRACT

MAPKs constitute a closely related family of isoenzymes which play a key role in many cellular and pathological processes. MAPKs are activated by phosphorylation and this process is therefore of key interest to researchers attempting to understand the physiological and pathological roles of this enzyme family. Many factors can affect MAPK phosphorylation and dephosphorylation, which are carried out by kinase and phosphatase enzymes, respectively. Because of this, even the procurement of experimental samples for analysis, which exposes tissues to anoxia/hypoxia, hypothermia and tissue homeostatic failure, produces conditions in which intracellular signalling changes can affect MAPK phosphorylation status. This is obviously a problem if an experiment is designed to determine MAPK phosphorylation at a given end-point. We therefore attempted to improve the preservation of end-point MAPK phosphorylation levels by perfusing experimental tissues with normal saline plus a cocktail of phosphatase inhibitors (PIs) before fixation, preventing MAPK dephosphorylation and enabling true determination of the activation status of members of this enzyme family at given times after experimental treatment.

Experimentally, a rat model of OHT was employed in which pressure-induced ONH stress leads to a gradual death of RGC, and individual MAPK isoforms are activated in distinct spatio-temporal patterns. Due to the nature of the model, the extent of resultant tissue damage, upon which the degree of detected MAPK phosphorylation depends, can vary significantly. This is especially the case when tissue damage is not particularly extensive. Experimental animals were perfused at the appropriate times with saline plus PIs (PPIs) or saline minus PIs (MPIs) and ocular tissues assessed immunohistochemically for relative levels of damage and MAPK isozyme activation. Immunohistochemical labelling for MAPKs in control animals was unaffected by the presence or absence of PIs in the perfusate. This

was also the case for animals where tissue damage was extensive (“high damage” group) and MAPK isoenzyme changes were clear, as reported previously (Mammone et al. 2017). In animals where tissue damage was less extensive, however (“low damage” group), the degree of detectable MAPK phosphorylation varied significantly. The presence of PIs in the perfusate reduced this variability in MAPK phosphorylation and enabled clear changes to be detected which paralleled those seen in the “high damage” group.

In conclusion, we found that the addition of PIs to the perfusate when preparing ocular tissues for immunohistochemistry enabled a greater consistency in labelling for phosphorylated MAPKs and should be considered when studying MAPK activation by this technique, especially in ocular tissues.

Keywords: Mitogen-activated protein kinase (MAPK), phosphorylation, immunohistochemistry, phosphatase inhibitor

INTRODUCTION

MAPKs constitute a eukaryote-specific enzyme family which responds to a diverse array of stimuli and which controls key cellular processes such as proliferation, differentiation, mitosis, gene expression and cell survival and death (Kim and Choi 2010, Roskoski 2012). The MAPK family is broadly separated into three groups: the extracellular signal-regulated kinases (ERK; P42/44 MAPK), the stress-activated protein kinase/c-Jun N-terminal kinases (SAPK/JNK) and the P38 MAPKs (Johnson and Lapadat 2002). MAPK signalling pathways are highly regulated under physiological conditions and, thus, alterations in the function of these enzymes, or their regulators, can contribute to many diseases, for example, AD, Parkinson's disease, or some forms of cancer (Kim and Choi 2010, Mehan et al. 2011). MAPKs and their pathways therefore represent valid and well-researched therapeutic targets for disease treatment.

In general, to become fully activated, MAPKs are phosphorylated at one or more residues in their activation loops by MAPK-kinases (Pearson et al. 2001). Moreover, MAPKs are physiologically dephosphorylated and hence, deactivated, by MAPK phosphatases or dual-specificity phosphatases (Davidson et al. 2006). Thus, assessment of their phosphorylation status for individual family members in a given situation, allows a researcher to know their activation status. The availability of antibodies which not only recognise specific MAPKs but also recognise whether, and at which residues individual isoforms have been phosphorylated, has therefore proven vital in associating (activation of) individual family members with different physiological and pathological processes (Cuevas et al. 2007).

Non-physiological processes such as vascular compromise, hypothermia or general loss of cellular homeostasis will all have an immediate effect on cellular signalling and, likely,

therefore, on activation (ie phosphorylation) status of MAPKs (Mueller et al. 2011). This is of particular concern during tissue harvesting from experimental samples. Unless correct preservation of end-point phosphoprotein levels is rapidly undertaken prior to tissue procurement, irregular or incorrect data may result when analysing the degree of MAPK isoform phosphorylation. This may be particularly pertinent in experimental models where signalling alterations are being investigated. For this reason, it is critical to stabilise phosphoproteins such as phosphorylated MAPKs at the exact point at which data are required.

Previous studies have described various methods to preserve phosphoprotein status at the time of tissue procurement. Snap-freezing in liquid nitrogen is useful, but often impractical, and other means of freezing can cause tissue damage via ice crystal formation (Bova et al. 2005). Formalin-fixation combined with paraffin-embedding is a common means to procure experimental tissue but is less than ideal for analysis of phosphorylated proteins because even when tissue is perfused with fixative prior to removal (in the case of experimental animals, for example), fixation is relatively slow and therefore still allows for cellular signalling alterations which can affect results (Burns et al. 2009, Chidlow et al. 2011a, Groelz et al. 2013, Latendresse et al. 2002). In recent studies, researchers have described immersion of fresh tissues in buffers containing protein phosphatase or kinase inhibitors as well as fixative; this approach appears to be successful at preserving phosphoprotein levels in clinical specimens (Espina et al. 2008, Gundisch et al. 2012, Mueller et al. 2011).

The present study describes a similar technique for researchers who wish to preserve and analyse levels of phosphorylated MAPKs by immunohistochemistry in non-human research tissue: the addition of a cocktail of PIs to the physiological perfusate. We investigated this technique with rodent eyes that had been subjected to experimental OHT.

Although MAPK isoform phosphorylation has previously been detected in this model (Mammone et al. 2017), there is marked variability which relates to the degree of damage variability. We found that the present methodological alteration produced a greater consistency in immunohistochemical labelling. We believe that our method could equally be applied to any research tissue from small experimental animals.

MATERIALS AND METHODS

Materials

All chemicals were purchased from Sigma-Aldrich (Castle Hill, New South Wales, Australia), unless otherwise stated. A full list of antibodies used in the study is listed in Table 1. Antibodies specific to each of P42/44 MAPK, SAPK/JNK and P38 MAPK, or their phosphorylated forms, were reactive with all isoforms associated with that respective MAPK group (supplemental Figure 3): anti-P42/44 MAPK recognised P42 MAPK (ERK2) and P44 MAPK (ERK1) and therefore detected proteins of masses 42 and 44 kD; anti-SAPK/JNK recognised all ten separate isoforms - derived as either 46 or 54 kD forms from each of five mRNAs (JNK1α, JNK1β, JNK2α, JNK2β, JNK3) and therefore positively labelled two separate groups of protein species on Western immunoblots (46 kD and 54 kD); anti-P38 MAPK recognised the four isoforms of this enzyme (P38α, P38β, P38γ, P38δ) and therefore detected targets as a single protein band of approximately 40 kD. Results of Western immunoblotting and immunohistochemistry for phospho-MAPKs were confirmed with alternate antibodies (not shown; Cell Signaling Technology; phospho-P38 MAPK, cat #4511; phospho-P42/44 MAPK, cat #9106; phospho-SAPK/JNK, cat #9255). We have previously validated the anti-MAPK antibodies used here for immunohistochemistry in formalin-fixed, paraffin-embedded in situ ductal breast carcinoma sections (Mammone et al. 2017) which displayed positive labelling for these enzymes (Davidson et al. 2006).

Table. 1 Antibodies used in the study

Name	Cat No./ Clone	Host	Company	Dilution IHC	Dilution IF	Dilution WB
Amyloid Precursor Protein	clone 22C11	Mouse	Gift C. Masters		1:250*	
β-Tubulin III	MAB1637	Mouse	Millipore		1:400*	
Brn3a	SC-31984	Goat	Santa Cruz		1:500*	
Calretinin	MAB1568	Mouse	Millipore		1:250*	
Glial Fibrillary Acidic Protein	Z0334	Rabbit	Dako	1:40000		
Growth associated protein 43	G9264	Mouse	Sigma-Aldrich		1:3000*	
Iba1	019-19741	Rabbit	Wako	1:40000		
Iba1	Ab107159	Goat	Abcam		1:500*	
npNFH	SMI32	Mouse	Labome	1:15000		
P38 MAPK	8690	Rabbit	CST	1:3000	1:3000	1:500
P44/42 MAPK	9102	Rabbit	CST	1:2000	1:1000	1:1000
Phospho-P38 MAPK	4631	Rabbit	CST	1:250	1:250	1:250
Phospho-P44/42 MAPK	4376	Rabbit	CST	1:2000	1:1500	1:1000
Phospho-SAPK/JNK	9251	Rabbit	CST	1:250	1:250	1:250
S100	MAB079-1	Mouse	Millipore		1:1000*	

SAPK/ JNK	9258	Rabbit	CST	1:250	1:250	1:250
γ-synuclein	CPTC-SNCG-1	Mouse	DSHB		1:40*	

Abcam, Cambridge, UK; BioLengend, San Diego, CA; CST, Cell Signalling Technology, Danvers, MA; Dako, Sydney, NSW, Australia; DSHB-Developmental Studies Hybridoma Bank, University of Iowa, Iowa, United States; Labome, Borehamwood, UK; Millipore, North Ryde, NSW, Australia; Santa Cruz Biotechnology, Santa Cruz, CA; Sigma-Aldrich, Sydney, NSW, Australia; Wako Chemicals, Osaka, Japan.

* denotes concentration at a 2 step

Rat model of chronic OHT

This study was approved by the Animal Ethics Committee of SA Pathology/Central Adelaide Local Health Network and conformed to both the Australian Code of Practice for the Care and Use of Animals for Scientific Purposes (2013) and to the Association for Research in Vision and Ophthalmology Statement for The Use Of Animals In Ophthalmic And Vision Research. Adult female Sprague-Dawley rats (approximately 250 g) were housed in a temperature- and humidity-controlled room, with a 12 h light, 12 h dark cycle, and were provided with food and water ad libitum. All procedures were performed under anesthesia (100 mg/kg ketamine / 10 mg/kg xylazine), and all efforts were made to minimize suffering as per the tenets of the Codes under which experiments were conducted.

To establish the model of experimental glaucoma, raised IOP was induced in the right eye of each animal by laser photocoagulation of the trabecular meshwork using a modification of a published method (Levkovitch-Verbin 2004). Specifically, a continuous wave, frequency-doubled neodymium:yttrium-aluminium garnet (Nd:YAG) 532 nm laser supplied by Ellex R&D Pty Ltd (Adelaide, South Australia, Australia) with the following settings: 300 mW, 0.6 s duration, 50 µm spot diameter, was directed at approximately 80 % of the radial trabecular meshwork as viewed through a slit lamp. In addition, three of the four episcleral veins were also targeted using the following settings: 260 mW; 0.6 s duration; 100 µm spot diameter. Prior to induction of OHT, the IOP was recorded to obtain a baseline reading using a hand held, rebound tonometer (TonoLab; Icare Finland, Espoo, Finland). IOP measurements were recorded once daily for the 3 day duration of the experiment. All animals demonstrated an IOP elevation (minimum increase in IOP in treated versus control eye) of at least 10 mmHg for the duration of the experiment.

Tissue collection and processing for paraffin embedding

All rats were killed by transcardial perfusion under deep anesthesia. Two different perfusates were prepared: the first consisted of sterile physiological saline (0.9 %, w/v) with no additives (MPIs); the second comprised sterile physiological saline containing 1 % (v/v) phosphatase inhibitor cocktail 2 (contains sodium orthovanadate, sodium molybdate, sodium tartrate, imidazole; Sigma-Aldrich, Castle Hill, NSW, Australia), and 0.01 M sodium fluoride (PPIs). Animals were perfused with either saline PPIs or saline MPIs. Subsequently, eyes were enucleated, marked to ensure that exact orientation could be identified during and subsequent to embedding, and fixed for 24 hours in Davidson's fixative (2 parts formaldehyde, 3 parts absolute ethanol, 1 part glacial acetic acid, and 3 parts water) followed by 70 % ethanol. Globes were then processed for routine paraffin-embedded sections, oriented sagittaly, and 5 μm serial sections cut using a rotary microtome.

Immunohistochemistry

Tissue sections were deparaffinised in xylene followed by 100 % (v/v) ethanol before being treated for 25 min with 0.5 % (v/v) H_2O_2 to block endogenous peroxidise activity. For antigen retrieval, sections were immersed in sodium citrate buffer (10 mM; pH 6.0) which was heated until boiling before being microwaved for 10 min. Tissue sections were then blocked in PBS, (137 mM NaCl, 5.4 mM KCl, 1.28 mM NaH_2PO_4, 7 mM Na_2HPO_4; pH 7.4) containing 3 % normal horse serum (PBS-NHS), followed by incubation overnight at room temperature in primary antibody diluted in 3 % PBS-NHS (see Table 1). Subsequent incubations were carried out sequentially with the appropriate biotinylated secondary antibody (Vector, California, United

States) at a dilution of 1:250 in 3 % PBS-NHS for 30 min, followed by streptavidin-horseradish peroxidase conjugate (Pierce, Illinois, United States) at a dilution of 1:1000 in 3 % PBS-NHS for 1 h. Colour development was achieved using 3',3'-diaminobenzidine for 5 min at which time the reaction was stopped by submersion in water. Sections were counterstained with Lillie-Mayer's haematoxylin, dehydrated and cleared in histolene before mounting with DPX.

Fluorescent double-label immunohistochemistry was used to determine co-localisation of antibody labelling with known cell-specific markers. Visualisation of one antigen was achieved using a 3-step procedure (appropriate primary antibody, biotinylated secondary antibody, streptavidin-conjugated AlexaFluor 488 or 594), while the second antigen was concurrently labelled by a 2-step procedure (primary antibody, secondary antibody conjugated to AlexaFluor 488 or 594 - the opposite fluorophore to the first antigen). In brief, sections were prepared as above then incubated overnight at room temperature with the two relevant primary antibodies (see Table 1). On the following day, sections were incubated with the appropriate biotinylated secondary antibody (Vector; 1:250; 30 min) for the 3-step procedure plus the correct secondary antibody conjugated to AlexaFluor 488 or 594 (Molecular Probes, Thermo Fisher Scientific, Massachusetts, United States; 1:250; 30 min) for the 2-step procedure, followed by streptavidin-conjugated AlexaFluor 488 or 594 (Molecular Probes; 1:500; 1 h). Nuclear labelling was carried out for 5 min with 500 ng/ml 4',6-diamidino-2-phenylindole (DAPI) in PBS. Sections were then mounted with fluorescence-preserving mounting medium (Dako, Sydney, New South Wales, Australia) and examined with a confocal fluorescence microscope.

Evaluation of Immunohistochemistry

Immunolabelling of sections for all samples being directly compared was always performed in a single batch. Sections were semi-quantitatively assessed to define the extent of labelling for each antibody in all cases, as described below.

Degree of tissue damage: Tissue was evaluated for relative damage level by immunohistochemical assessment of non-phosphorylated 200kD neurofilament (npNFH; SMI32), glial fibrillary acidic protein (GFAP) and Iba1: three antigens known to be significantly altered after three days of elevated IOP in the optic nerve, retina, ONH and in tissues, respectively (Ebneter et al. 2010). Ocular sections from each animal were separately immunohistochemically labelled with the three antibodies and changes were semi-quantitatively graded according to an integer scale of 0-3, where 0 referred to no labelling change, 1 referred to minimal labelling change, 2 referred to clear labelling changes and 3 referred to extensive labelling changes (supplemental Figure 1). Antigen reactivity assessment was conducted in a blind manner by 2 independent reviewers. Scores for each animal were recorded and averaged. A mean "labelling value" was determined by averaging the three separate mean antibody scores for each animal. Experimental animals were then split into two broad groups: low damage (LD) or high damage (HD), where the former was defined by an overall labelling score of less than 1.5 (the median original score value) and the latter by a score greater than or equal to 1.5. Data and category definitions for the samples analysed in the study are shown in Table 2. To determine whether there was a correlation between damage category and IOP, the mean IOP elevation value, averaged over the three days of the experiment was also plotted against mean damage score value for each animal (supplemental Figure 2).

Table 2. Damage assessment and categorisation of the animals involved in the study

Animal	+/- PIs (Y/N)	Mean SMI Grade	Mean GFAP Grade	Mean Iba1 Grade	Total Mean Grade	High/Low
1	N	1.5	2.5	2.5	2.16	H
2	Y	1.5	2.5	1.5	1.83	H
3	N	2	2.5	1.5	2	H
4	Y	1.5	2.5	2	2	H
5	N	1	1.5	1.5	1.33	L
6	N	0.5	2	1.5	1.33	L
7	N	0.5	1.5	1.5	1.16	L
8	N	0.5	1.5	2	1.33	L
9	Y	1	2	1.5	1.5	H
10	Y	0.5	2.5	2.5	1.83	H
11	N	2	2.5	2.5	2.33	H
12	Y	1.5	1.5	2.5	1.83	H
13	N	1.5	2.5	3	2.33	H
14	Y	2.5	2.5	2.5	2.5	H
15	N	3	2.5	2.5	2.66	H
16	Y	1.5	3	2.5	2.33	H
17	Y	1.5	2.5	3	2.33	H
18	N	2	2.5	3	2.5	H
19	Y	1.5	3	3	2.5	H
20	N	3	2.5	1.5	2.33	H
21	Y	2.5	3	3	2.83	H
22	N	1.5	3	3	2.5	H
23	Y	2.5	3	2.5	2.66	H
24	N	2	3	2.5	2.5	H
25	Y	0.5	0.5	0.5	0.5	L
26	Y	0.5	0.5	1.5	0.83	L
27	N	1.5	0.5	0.5	0.83	L
28	N	1.5	0.5	1.5	1.16	L

29	Y	0	0.5	0.5	0.33	L
30	Y	0	0.5	1.5	0.66	L
31	Y	0	1.5	0.5	0.66	L
32	N	0	1.5	1.5	1	L
33	N	0	0.5	0	0.16	L
34	Y	0.5	0	0	0.16	L
35	N	0.5	0	0.5	0.33	L
36	Y	0.5	0.5	0.5	0.5	L

Assessment of MAPK isoform labelling alterations: We have previously demonstrated that MAPK isoforms are altered in the eye, ONH and optic nerve in our laser-induced model of OHT (Mammone et al. 2017). This study only included animals with sustained IOP elevations of 10 mmHg or greater for the duration of the study at each time point. By the definitions described above, each of these animals were in the HD category. In the present study, we also included animals in the LD category, and we anticipated there being either no detectable MAPK changes or less robust changes in some animals. Analysis of MAPK antigen labelling was conducted in a blind manner by 2 independent observers. For each antibody tested, a semi-quantitative grading scheme was used to evaluate the ONH immunostaining when perfused with either saline MPI or saline PPI: 0 no change, + minimal specific labelling; ++ weak specific labelling; +++ intense specific labelling. Data were shown in stacked bar graphs but due to the nature of this analysis no statistical calculations were performed.

Western Immunoblotting

For preparation of tissues for electrophoresis/immunoblotting, ONH protein samples were prepared from TRI-reagent (Sigma-Aldrich) according to manufactures method and as previously described (Mammone et al. 2017). In brief eyes were immediately enucleated and ONH samples were prepared by removing the anterior portion, vitreous and lens from each eye. The remaining eye-cup was subsequently dissected into a flattened whole-mount and a biopsy punch of 2 mm in diameter (Stiefel Laboratories, Brentford, United Kingdom, cat # BIOPSY-5918) was then utilized to separate the ONH containing 1 mm of optic nerve length from the remaining ocular tissue. Purified protein were sonicated in homogenisation buffer (20 mM Tris-HCl, pH 7.4; containing 2 mM EDTA, 0.5 mM EGTA, 1 mM dithiothreitol, 50 μg/ml leupeptin, 50 μg/ml pepstatin A, 50 μg/ml aprotinin, and 0.1 mM phenylmethylsulfonyl fluoride). Protein determination for equalisation of samples was carried out by the bicinchoninic acid assay (Sigma-Aldrich) after which an equal volume of sample buffer (62.5 mM Tris-HCl, pH 7.4, containing 4 % SDS, 10 % glycerol, 10 % beta-mercaptoethanol, and 0.002 % bromophenol blue) was added and samples denatured by heating to 80^{o}C for 5 min. Electrophoresis was performed using 10 % denaturing polyacrylamide gels for protein separation. After separation, proteins were transferred, overnight, to polyvinylidine fluoride membranes (Bio-Rad, Sydney, New South Wales, Australia). Membranes were blocked in tris-buffered saline (10 mM Tris, 140 mM NaCl) containing 5 % non-fat dried skimmed milk powder (TBST-NDSM) before being incubated with the appropriate antibody (see Table 1), diluted in TBST-NDSM, for 3 h at room temperature. Relevant biotinylated secondary antibodies (Vector; 1:1,000; 30 min) were applied followed by streptavidin horseradish peroxidase conjugate (Pierce; 1:1,000; 1 h). Chromogenic detection of antibody labelling was achieved using 3-amino-9-ethylcarbazole and hydrogen peroxide. Reaction was stopped by submersion of

membranes in 0.1 % sodium azide solution. Membranes were subsequently scanned to determine correct band size and evaluation of the antibodies.

Experimental design

Animals were split into two equally-sized groups, of which half were perfused with saline PPI and half with saline MPI (n=18 per group). All animals were treated only in their right eye, with the left eye serving as an internal control. Eyes subjected to OHT were assessed for their relative degrees of overall tissue damage and categorised as previously defined as LD or HD (see table 2). Phosphorylated MAPK isoform labelling was then carried out for each eye and correlated with damage category for that animal and with the type of perfusate used.

RESULTS

Evaluation of damage profiles

In control retinal sections, GFAP labelling was associated with glial astrocytes in the innermost part of this tissue in the region of the inner limiting membrane and the nerve fibre layer. This labelling had increased to include trans-retinal Müller glial cell processes after three days of elevated IOP (supplemental Figure 1A). The pro-inflammatory marker Iba1 was labelled in the ONH region to determine the sensitivity and infiltration of microglia. Minimal Iba1-labelled microglia were present in control ONHs; after three days of elevated pressure the number of labelling cells had increased throughout this region and these cells had more visibly swollen somas (supplemental Figure 1B). Immunohistochemical labelling for SMI32 was present in axons in the RGC layer and the optic nerve. After three days of elevated IOP, SMI32 labelling in the proximal optic nerve revealed axonal abnormalities including swellings and discontinuities (supplemental Figure 1C), as described previously (Chidlow et al. 2011b). Variation in the degree of observed changes in labelling for each of these three antibodies following IOP elevation for three days allowed a relative damage grade to be defined for each animal, as described in the methods section (supplemental Figure 1). Assessment of immunolabelling changes defined 20 animals in the HD and 16 animals in the LD groups (Table 2). Of the animals in the LD category, 9 each had been perfused PPIs and MPIs. Of the HD animals, 11 were PPI and 7 were MPI.

Intuitively, observed overall damage grade correlated well with mean IOP elevation over the three days of the experiment ($r=0.669$; $P<0.0001$; supplemental Figure 2). It was clear that the greater the IOP elevation, the greater the degree of damage. This was further true for

the specific defined damage grade categories: LD was correlated with relatively lower increases in IOP and HD with more significant increases.

Verification of antibody detection of MAPK species by Western immunoblot

Western immunoblot was used to confirm the correct reactivity of antibodies with the requisite MAPK isoforms. Protein samples of control and treated ONH subjected to three days of OHT were prepared and treated for both total and phosphorylated forms of P42/44 MAPK, SAPK/JNK and P38 MAPK (supplemental Figure 3). Each target was verified according to correct labelling of a protein species at their respective predicted molecular weight.

Immunolabelling of MAPK subtypes

The immunohistochemical labelling of both total and phosphorylated forms of each of the sub-groups of MAPKs under investigation (P42/44 MAPK, SAPK/JNK and P38 MAPK) were compared in animals perfused with either saline MPI or PPI.

P42/44 MAPK

In animals perfused with normal saline (MPI), immunolabelling of total P42/44 MAPK revealed the presence of this enzyme within the ONH of control animals (Figure 1A). The signal was mainly associated with cells situated between axon bundles throughout the lamina region. No difference was detected in the expression of total P42/44 MAPK when comparing control and treated ONH sections, whether the damage level was defined as LD (Figure 1B) or HD (Figure 1C). Furthermore, perfusion with saline PPIs had no effect on improving labelling in control

tissue (Figure 1D) or tissue subjected to elevated IOP and defined as having LD (Figure 1E) or HD (Figure 1F).

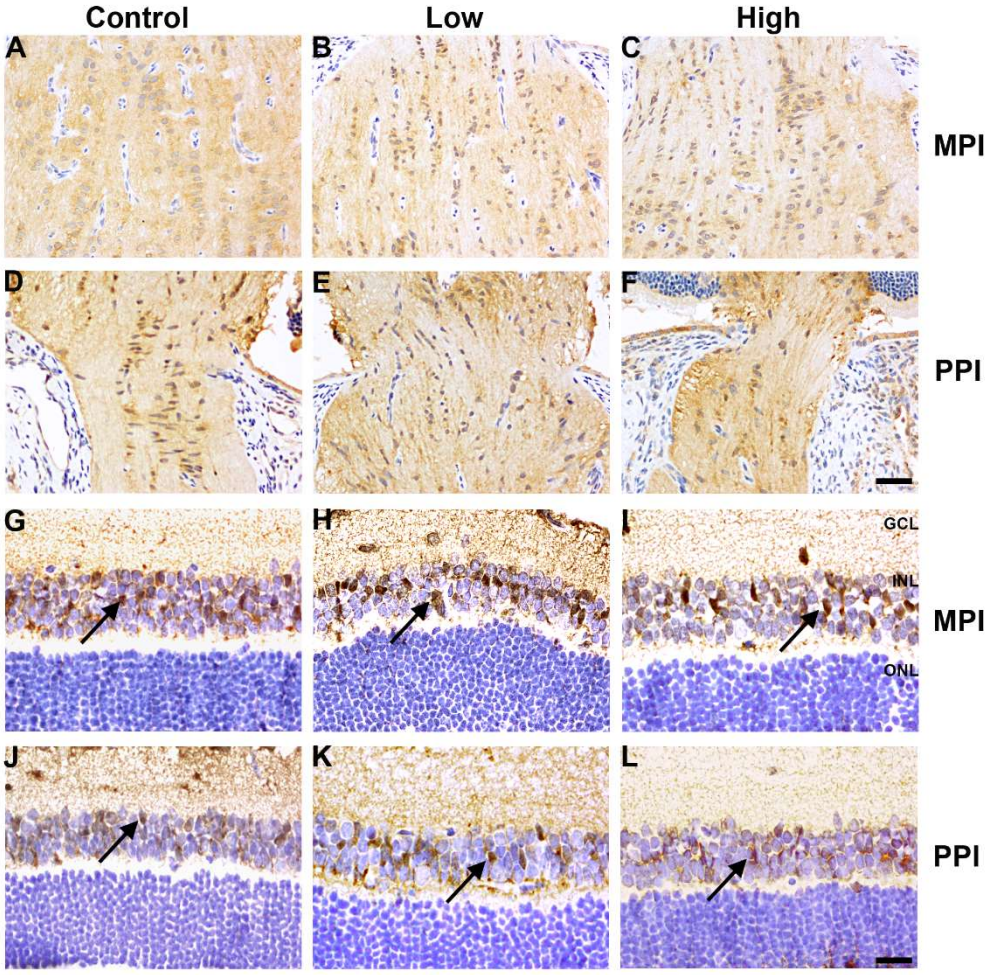

Figure 1. Immunohistochemical labelling of total P42/44 MAPK in the ONH (ONH; A-F) and retina (G-L) of control animals and treated animals which had been categorised as being of either low damage (LD) or high damage (HD) after induction of OHT for three days. In each case, images are shown of animals perfused with either saline alone (ie. minus phosphatase inhibitors; MPI) or saline with added phosphatase inhibitors (ie. plus phosphatase inhibitors; PPI). Saline MPI-perfused ONHs of control (A), LD (B) and HD (C) animals. There were no obvious changes when comparing P42/44 MAPK immunoreactivity in the ONH of either LD or HD animals to controls. Saline PPI-perfused ONHs of control (D), LD (E) and HD (F) animals. There were also no obvious changes when comparing P42/44 MAPK immunoreactivity in the ONH of either LD or HD animals with controls when perfusion was carried out with saline PPI. Comparison of immunoreactivity for P42/44 MAPK in the retina in control animals (G) and animals subjected to OHT and categorised as either LD (H) or HD (I), demonstrated labelling of Müller glial cells in the inner nuclear layer (arrow); no changes were observed when saline MPI was used for perfusion. This was also the case when animals were perfused with saline PPI in control animals (J) compared with animals subjected to OHT for three days and classified as LD (K) or HD (L). GCL, ganglion cell layer; INL, inner nuclear layer; ONL, outer nuclear layer. Direction of ONH is top to bottom, retina to brain. Scale bar (A-F) 100µm, (G-L) 50µm.

Total P42/44 MAPK was also clearly detectable in a population of cells in inner nuclear layer in the untreated retina when perfused with saline alone (MPIs; Figure 1G). These cells were demonstrated to be glial cells, likely both Müller cells and astrocytes, as they co-localised with the antigen, S100 (supplemental Figure 4A-C). Again, there were no detectable changes in total P42/44 MAPK localisation in the retina after elevation of IOP for three days, whether the tissue had been classified as LD (Figure 1H) or HD (Figure 1I). Perfusion with saline PPIs had no observable effect on detection of total P42/44 MAPK localisation (Figure 1J-L). This clearly indicates that the addition of PIs to saline during perfusion has no effect on labelling of total P42/44 MAPK.

Little signal for phospho-P42/44 MAPK (p-P42/44 MAPK) was detected in the ONH of either control animals or in animals subjected to elevated pressure and categorised in the LD group (Figure 2A, B). In comparison, a pronounced signal for p-P42/44 MAPK was detected in cells in the ONH of animals defined in the HD group (Figure 2C); labelling was determined to be confined to astrocytes in this region, as shown by co-labelling with the glial protein S100 (supplemental Figure 4G-I). Inclusion of PPI in the perfusate did not increase the detected signal of p-P42/44 MAPK in the ONH of control animals or experimental animals in the HD category (Figure 2D, F). However, a significantly increased signal was detected in animals from the LD category (Figure 2E). In fact, the presence of PPIs in the perfusate increased the detected signal in the experimental LD animals to the level seen in the HD group.

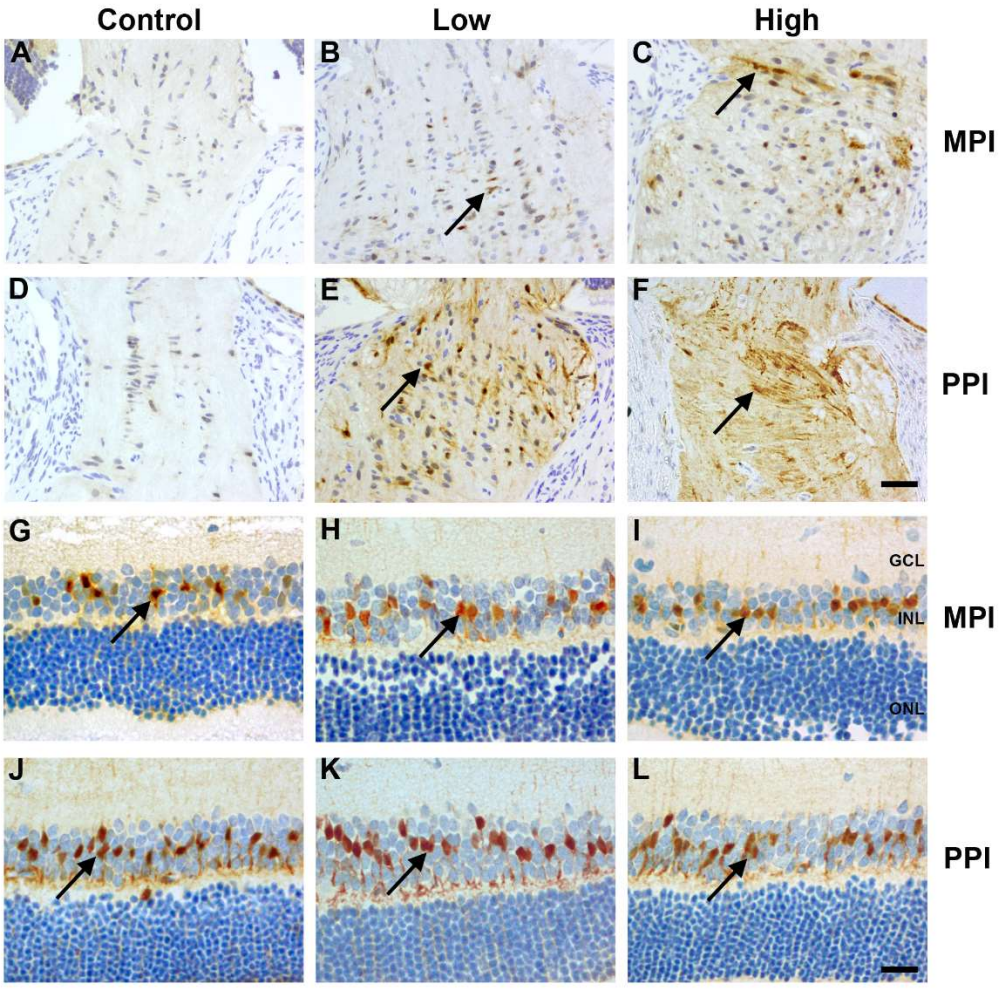

Figure 2. Immunohistochemical labelling of phospho-P42/44 MAPK (p-P42/44 MAPK) in the ONH (ONH; A-F) and retina (G-L) of control animals and treated animals which had been categorised as being of either low damage (LD) or high damage (HD) after induction of OHT for three days. In each case, images are shown from animals perfused with either saline alone (ie. minus phosphatase inhibitors; MPI) or saline with added phosphatase inhibitors (ie. plus phosphatase inhibitors; PPI). Saline MPI-perfused ONHs of control (A), LD (B) and HD (C) animals; saline PPI-perfused ONHs of control (D), LD (E) and HD (F) animals. There were obvious changes when comparing p-P42/44 MAPK immunoreactivity in the ONH (arrow) of HD but not LD animals compared to controls. Addition of phosphatase inhibitors to the perfusate had no effect on control (D) or HD animals (F), but significantly increased labelling for p-P42/44 MAPK immunoreactivity in the ONH (arrow) of LD animals (E). Comparison of immunoreactivity for p-P42/44 MAPK in the retina in control animals (G) and animals subjected to OHT and categorised as either LD (H) or HD (I) grades, when perfused with saline MPI; control animals (J), LD animals (K), HD animals (L) when perfused with saline PPI. GCL, ganglion cell layer; INL, inner nuclear layer; ONL, outer nuclear layer. Direction of ONH is top to bottom, retina to brain. Scale bar (A-F) 100µm, (G-L) 50µm.

Labelling of p-P42/44 MAPK was identified in a population of cells in the inner nuclear layer of the retina (Figure 2G). Co-localisation with S100 confirmed that these cells were glial:

likely Müller cells and astrocytes (supplemental Figure 4D-F). There were no changes in retinal labelling for p-P42/44 MAPK in any animals subjected to elevated IOP, regardless of the defined damage category (LD, Figure 2H; HD, Figure 2I). Furthermore, unlike in the ONH, the presence of PI in the saline perfusate did not improve or in any other way alter quantity or location of p-P42/44 MAPK signal within the retina (Figure 2J-L).

Each ONH was graded for total and phosphorylated P42/44 MAPK reactivity and bar graphs plotted based on the relative levels of labelling in each defined category (Figure 3) of immuoreactivity. Figure 3A demonstrates that that there was no grade change for immunolabelling of total P42/44 MAPK for control, LD or HD group animals perfused with saline MPIs or PPIs. When semi-quantifying the immuoreactivity of p-P42/44 MAPK (Figure 3B) within each MAPK labelling category of the control, LD and HD groups, however, although no clear changes were obvious in the control or HD groups, a significant increase in the amount and intensity of specific staining was seen in the saline PPI perfused animals compared with the saline MPI perfused animals in the LD group. Here, although grading categories remained the same, there was a significant increase in cellular labelling with intense MAPK immunoreactivity (+++) when perfusion was carried out with saline PPIs. Overall it was clear that the presence of PIs in the perfusate increased the quantity and intensity of immunoreactivity for p-P42/44 MAPK.

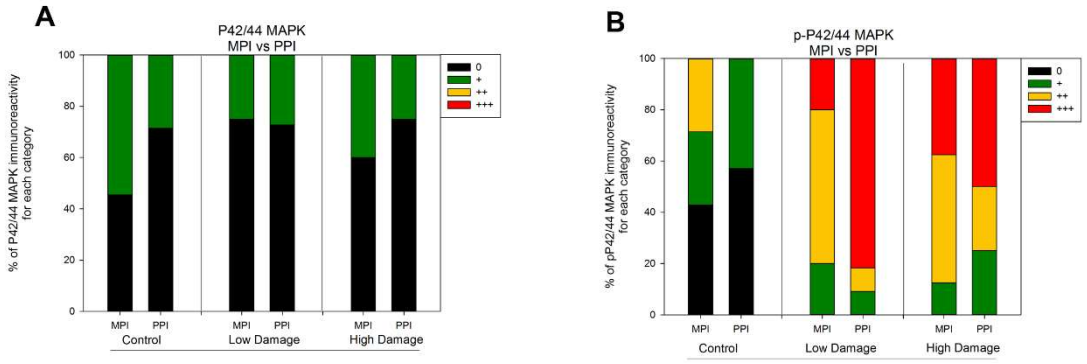

Figure 3. Separation of P42/44 MAPK (A) and phospho-P42/44 MAPK (p-P42/44 MAPK; B) immunoreactivity in the ONH into a range of intensity grades in order to assess potential improvements in labelling after addition of phosphatase inhibitors to saline perfusate (ie. plus phosphatase inhibitors; PPI), as compared with perfusing with saline alone (ie. minus phosphatase inhibitors; MPI). There is no notable change in labelling comparing control, LD or HD animals when either saline MPI or saline PPI was used for perfusion when labelling with P42/44 MAPK. In the case of p-P42/44 MAPK (B), labelling was slightly variable but remained minimal in control animals perfused with saline PPIs. In HD animals, there were no changes in overall labelling grades, however, in LD animals there was a marked increase in staining intensity when perfusing with saline PPI. Each bar on the graph is split into different categories, according to the numbers of animals labelling in each grade; scale refers to as the following (as described in Methods Section): 0 no change; + minimal specific labelling; ++ weak specific labelling; +++ intense specific labelling. The total number of specimens that were graded for P42/44 MAPK: saline MPI, *n*=25; saline PPI, *n*=29 and for p-P42/44 MAPK: saline MPI, *n*=27; saline PPI; *n*=29.

SAPK/JNK

Total SAPK/JNK labelled uniformly in control sections of ONH (Figure 4A). Labelling was unaffected by elevation of IOP (Figure 3B, C). Moreover, no changes in SAPK/JNK labelling were observed when PIs were included in the perfusate (Figure 4D-F). In the untreated retina perfused with normal saline, expression of SAPK/JNK was present in ganglion cell bodies and axons (Figure 4G), as defined by co-labelling with Brn3a (supplemental Figure 5A-C) and γ-synuclein (supplemental Figure 5G-I) respectively, as well as two strata of synaptic terminals in the inner plexiform layer (Figure 3G), which showed partial co-localisation with calretinin (supplemental Figure 5D-F). Labelling of SAPK/JNK was not affected by elevation of IOP (Figure 4H, I) and the addition of PIs to the perfusate also had no effect on immunolocalisation of this enzyme (Figure 4J-L).

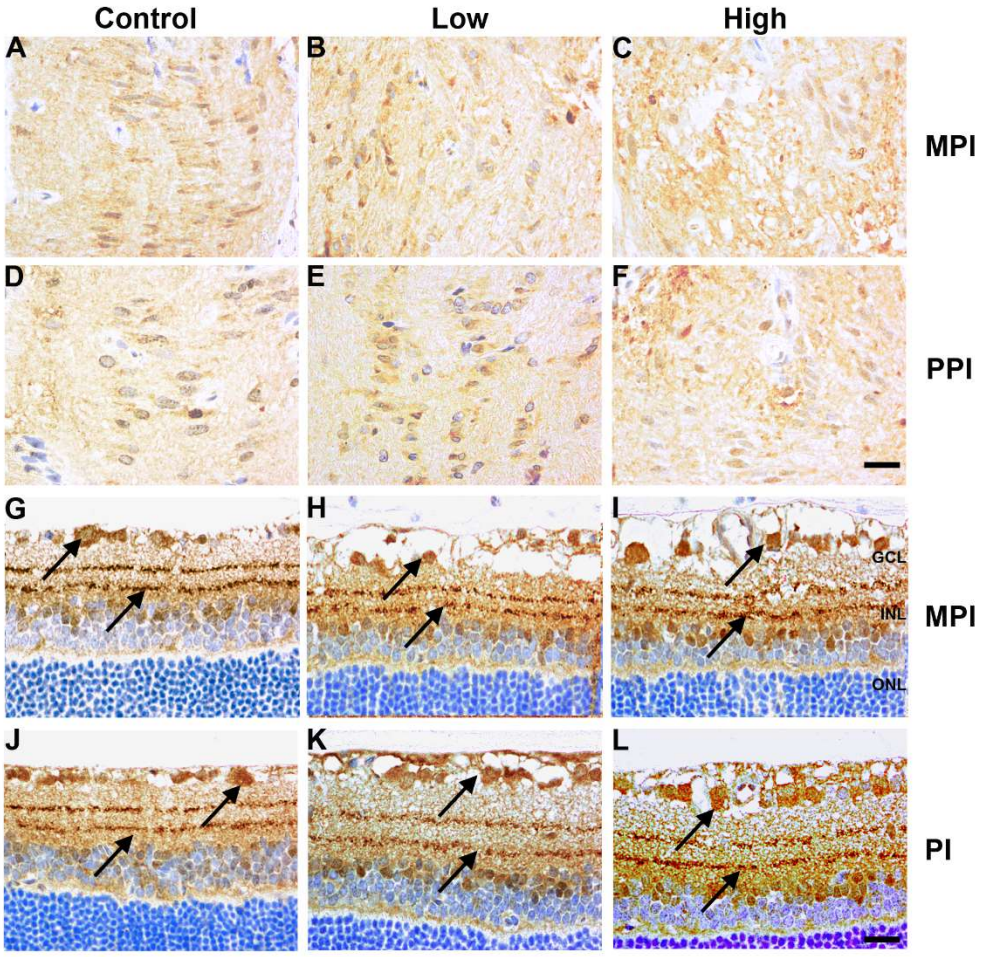

Figure 4. Immunohistochemical labelling of total SAPK/JNK in the ONH (ONH; A-F) and retina (G-L) of control animals and treated animals which had been categorised as being of either low damage (LD) or high damage (HD) after induction of OHT for three days. In each case, images are shown of animals perfused with either saline alone (ie. minus phosphatase inhibitors; MPI) or saline with added phosphatase inhibitors (ie. plus phosphatase inhibitors; PPI). Saline MPI-perfused ONHs of control (A), LD (B) and HD (C) animals. There were no obvious changes when comparing SAPK/JNK immunoreactivity in the ONH of either LD or HD animals to controls. Saline PPI-perfused ONHs of control (D), LD (E) and HD (F) animals. Addition of phosphatase inhibitors had no obvious effect on SAPK/JNK immunoreactivity in the ONH for any of control, LD or HD animals. Immunoreactivity for SAPK/JNK in the retina of control animals (G) and animals subjected to OHT and categorised as either LD (H) or HD (I), when saline alone was used as perfusate. Immunoreactivity was present in ganglion cells (arrow) and ganglion cell terminals within the inner nuclear layer (arrow head). No alterations were seen in labelling after phosphatase inhibitors were added to the perfusate in control (J), LD (K) or HD (L) animals. GCL, ganglion cell layer; INL, inner nuclear layer; ONL, outer nuclear layer. Direction of ONH is top to bottom, retina to brain. Scale bar (A-F) 75µm, (G-L) 50µm.

Some phospho-SAPK/JNK (p-SAPK/JNK) could be detected in axons in the ONH of control animals perfused with saline alone (Figure 5A), as reported previously (Mammone et

al. 2017). After elevation of IOP for three days, there was no obvious change in immunolabelling of p-SAPK/JNK in the ONH of animals classified as being in the LD category (Figure 5B), but a significant increase in labelling for the phosphorylated form of this enzyme was detected in the ONH of animals in the HD category (Figure 5C). As shown in supplemental Figure 5A-C, this increased labelling co-localised with APP in damaged axons. In animals perfused with saline containing PIs, however, although there was no additional labelling in control ONH sections (Figure 5D), p-SAPK/JNK was clearly detected in damaged axons in the treated LD group (Figure 5E). The labelling was of a similar pattern to that seen in HD category animals (Figure 5C), which themselves were not affected by the presence of PIs in the perfusate (Figure 5F).

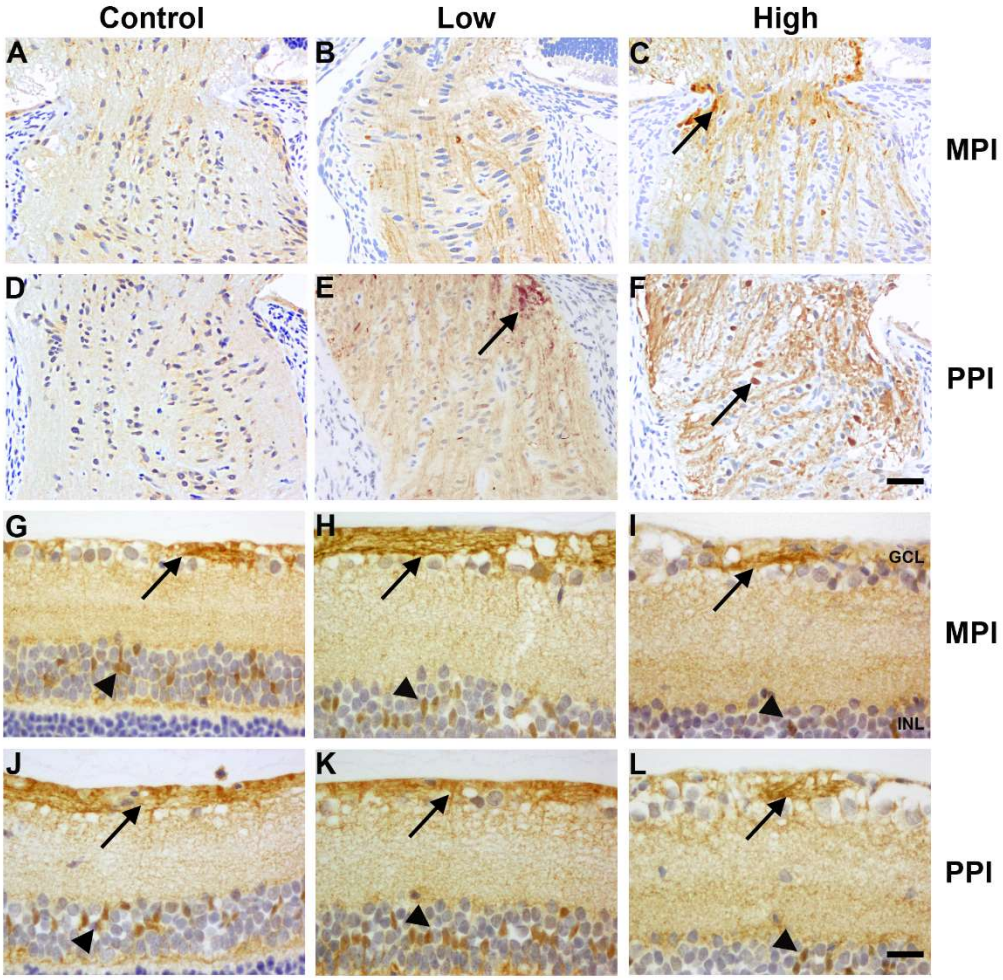

Figure 5. Immunohistochemical labelling of phospho-SAPK/JNK (p-SAPK/JNK) in the ONH (ONH; A-F) and retina (G-L) of control animals and treated animals which had been categorised as being of either low damage (LD) or high damage (HD) after induction of OHT for three days. In each case, images are shown of animals perfused with either saline alone (ie. minus phosphatase inhibitors; MPI) or saline with added phosphatase inhibitors (ie. plus phosphatase inhibitors; PPI). MPI perfused ONHs of control (A), LD (B) and HD (C) animals. There were obvious changes when comparing p-SAPK/JNK immunoreactivity, localised in the ONH (arrow) of HD animals compared to control and LD animals. Saline PPI-perfused ONHs of control (D), LD (E) and HD (F) animals. In the presence of phosphatase inhibitors, no changes were seen to p-SAPK/JNK immunoreactivity in control (D) or HD group animals (F), however, there was increased labelling for animals in the LD group (E). Comparison of immunoreactivity for p-SAPK/JNK in the saline-perfused retina in control animals (G) and animals subjected to OHT and categorised as either LD (H) or HD (I). Immunoreactivity was detected in axons (arrow) within the ganglion cell layer and cell perikarya in the inner nuclear layer (arrow head) in all samples. Perfusion with saline PPI had no effect on control (J), LD (K) or HD (L) animals. GCL, ganglion cell layer; INL, inner nuclear layer; ONL, outer nuclear layer. Direction of ONH is top to bottom, retina to brain. Scale bar (A-F) 100µm, (G-L) 25µm.

In the retina, p-SAPK/JNK was present in ganglion cells and their axons in control untreated eyes (Figure 5G), as shown by co-labelling with β-tubulin (supplemental Figure 6D-F) and γ-synuclein (supplemental Figure 6G-I). This immunolocalisation was not altered by elevation of IOP for three days, in either LD category animals (Figure 5H) or HD category animals (Figure 5I). The presence of PI in the perfusate also had no discernible effect on the detected signal for p-SAPK/JNK in the retina.

Each ONH was graded for total and phosphorylated SAPK/JNK reactivity and bar graphs plotted based on the relative levels of labelling in each defined category (Figure 6) of immunoreactivity. Figure 6A demonstrates that that there was no grade change for immunolabelling of total SAPK/JNK for control, LD or HD group animals whether perfused with saline MPIs or PPIs. When semi-quantifying the immunoreactivity of p-SAPK/JNK (Figure 6B) within each MAPK labelling category of the control, LD and HD groups, however, a clear increase in the amount and intensity of specific staining was seen in the saline PPI perfused animals compared with the saline MPI perfused animals. This was the case in the control, LD and HD groups (Figure 6B). For example, in the LD category group, grading was restricted to no, minimal and weak specific labelling of p-SAPK/JNK when perfusion was carried out with saline MPIs. The inclusion of PIs in the saline perfusate, however, increased labelling to include some animals with intense labelling. Overall it was clear that the presence of PIs in the perfusate increased the clarity, quantity and intensity of immunoreactivity for p-SAPK/JNK.

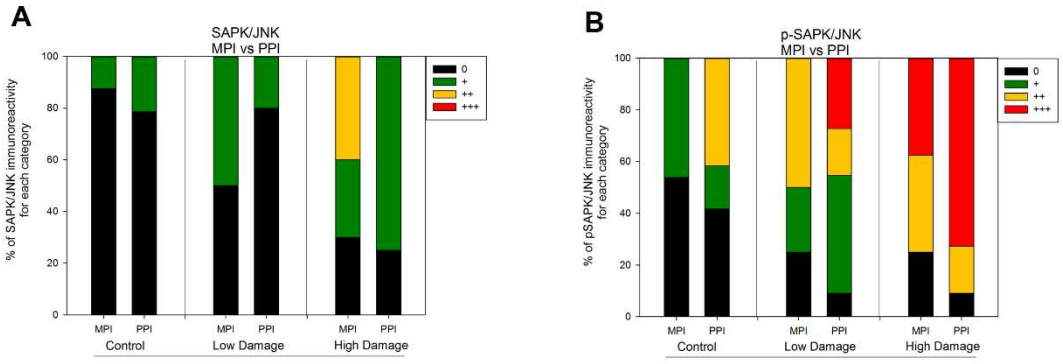

Figure 6. Separation of SAPK/JNK (A) and phospho-SAPK/JNK (p-SAPK/JNK; B) immunoreactivity in the ONH into a range of intensity grades in order to assess potential improvements in labelling after addition of phosphatase inhibitors to saline perfusate (ie. plus phosphatase inhibitors; PPI), as compared with using saline alone (ie. minus phosphatase inhibitors; MPI). There is no notable change in labelling comparing control, LD or HD animals when either saline MPI or saline PPI was used for perfusion when labelling with SAPK/JNK. In the case of p-SAPK/JNK (B), addition of phosphatase inhibitors to the perfusate increased intensity of labelling in control, HD and LD animals. Each bar on the graph is split into different categories, according to the numbers of animals labelling in each grade; scale refers to as the following (as described in Methods Section): 0 no change; + minimal specific labelling; ++ weak specific labelling; +++ intense specific labelling. The total number of specimens that were graded for SAPK/JNK: saline MPI, *n*=30; saline PPI, *n*=28 and for p-SAPK/JNK: saline MPI, *n*=29; saline PPI; *n*=34.

P38 MAPK

Total P38 MAPK was detected in a population of cells evenly distributed throughout the ONH in control animals (Figure 7A), which were proven to be microglia by co-labelling with Iba1 (supplemental Figure 7A-C). There was no labelling change in the ONH after experimental glaucoma, whether the overall category was LD (Figure 7B) or HD (Figure 7C). Furthermore, the presence of PIs in the perfusate had no effect on detection of P38 MAPK in control (Figure 7D) or experimental LD (Figure 7E) or HD (Figure 7F) animals. In the untreated retina (Figure 7G), P38 MAPK was localised to small, round cells with extended processes, which were co-labelled with Iba1 and therefore identified as microglia (supplemental Figure 7D-F). Some cell perikarya in the inner nuclear layer were also labelled for this enzyme (Figure 7G); these cells were identified as Müller glial cells by double-labelling (supplemental Figure 7D-F). There were

no changes in type or quantity of labelling cells after elevation of IOP for three days, whether damage was graded as LD (Figure 7H) or HD (Figure 7I). The presence of PIs in the saline perfusate also had no effect on the labelling (Figure 7J-L).

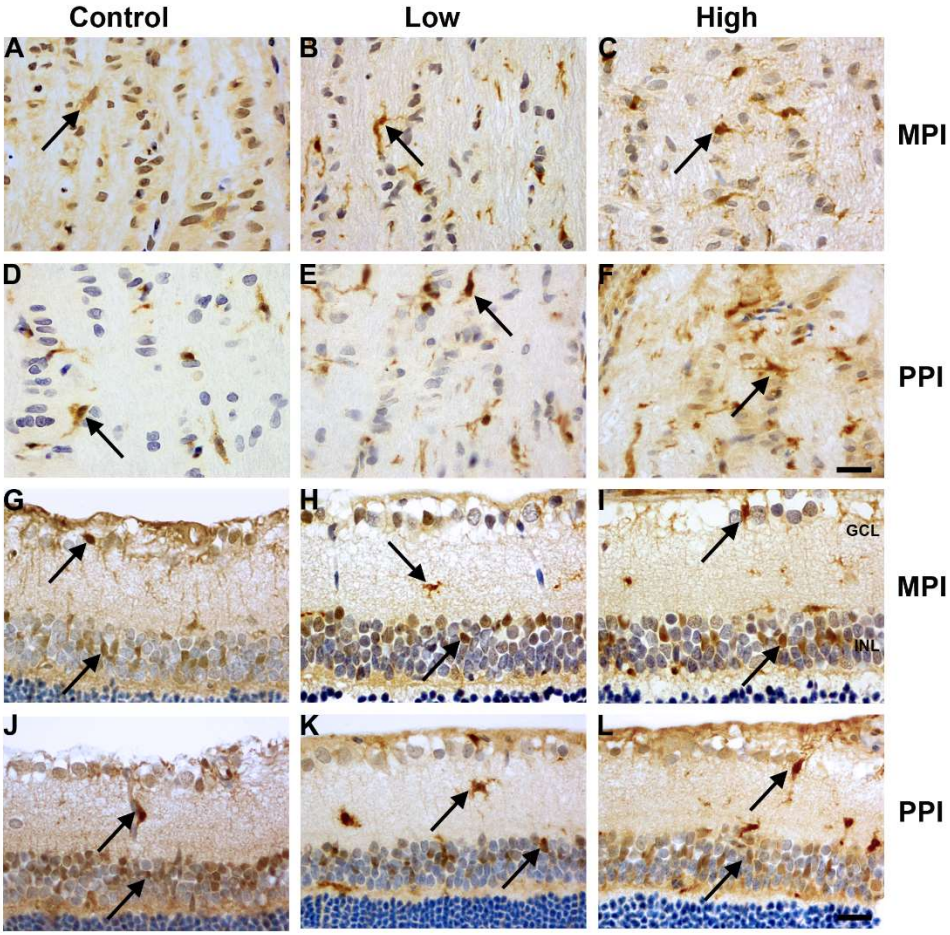

Figure 7. Immunohistochemical labelling of total P38 MAPK in the ONH (ONH; A-F) and retina (G-L) of control animals and treated animals which had been categorised as being of either low damage (LD) or high damage (HD) after induction of OHT for three days. In each case, images are shown of animals perfused with either saline alone (ie. minus phosphatase inhibitors; MPI) or saline with added phosphatase inhibitors (ie. plus phosphatase inhibitors; PPI). Saline MPI-perfused ONHs of control (A), LD (B) and HD (C) animals. Immunoreactivity was present in control and both treated groups but there were no obvious differences between each category. Saline PPI-perfused ONHs of control (D), LD (E) and HD (F) animals; saline PPI made no difference to labelling. Immunoreactivity localised in putative microglia (arrow) present in the ONH. Comparison of immunoreactivity for P38 MAPK in the retina of control animals (G) and animals subjected to OHT and categorised as either LD (H) or HD (I), when saline MPI was used as perfusate. Immunoreactivity was present in microglia (arrow) and Müller glial cells (arrow head). No obvious differences were seen between control and treated eyes. When perfusion of tissue was undertaken with saline PPIs, there were no differences in control animals (J) or animals in LD (K) or HD (L) groups. GCL, ganglion cell layer; INL, inner nuclear layer. Direction of ONH is top to bottom, retina to brain. Scale bar (A-F) 50µm, (G-L) 25µm.

Phospho-P38 MAPK (p-P38 MAPK) could not be detected in the ONH in control, untreated animals where normal saline MPI was used to perfuse tissue (Figure 8A). However, in the corresponding ONH of animals where IOP had been elevated for three days, labelled cells could be detected. In the case of the LD category animals, a very sparse selection of cells labelled for p-P38 MAPK (Figure 8B), whereas in the case of the HD animals, a much greater number of cells were positive (Figure 8C). When PIs were included in the perfusate, there were still no cells labelling for p-P38 MAPK in the untreated ONH (Figure 8D), but there was a significant increase in the amount of cells detected in the ONH of LD category animals (Figure 8E). There was no change in the labelling seen in the ONH of experimental HD category animals, when PIs were present in the perfusate (Figure 8F).

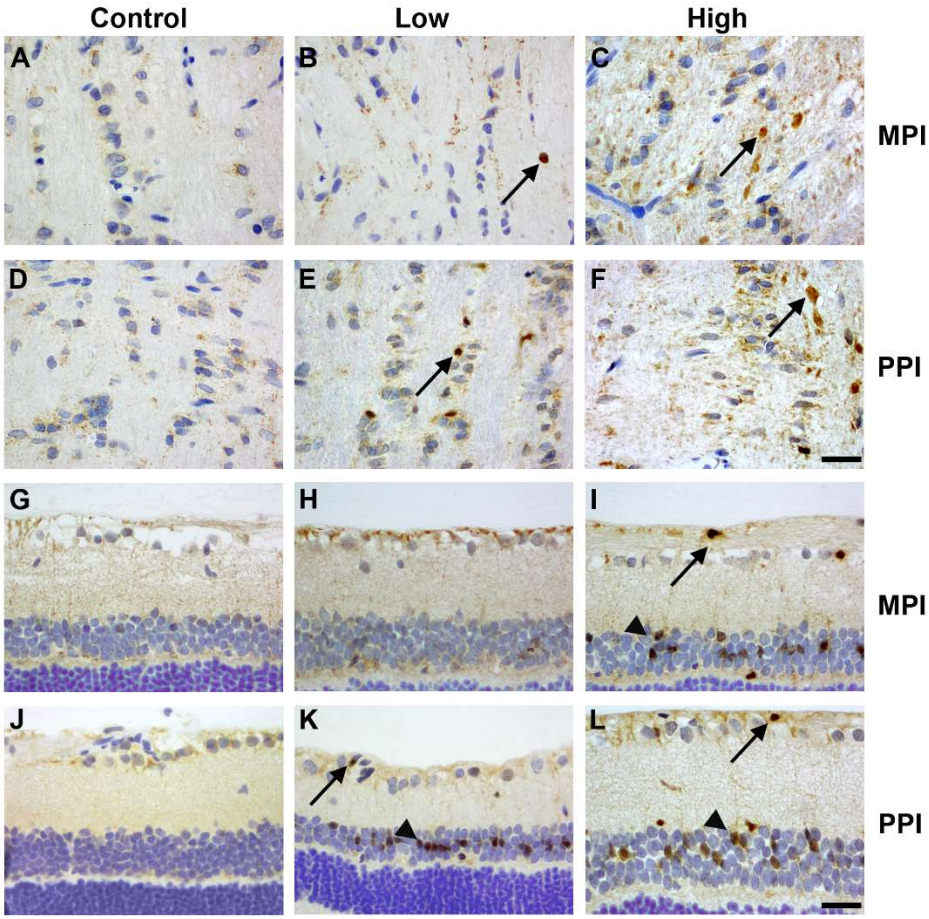

Figure 8. Immunohistochemical labelling of phospho-P38 MAPK (p-P38 MAPK) in the ONH (ONH; A-F) and retina (G-L) of control animals and treated animals which had been categorised as being of either low damage (LD) or high damage (HD) after induction of OHT for three days. In each case, images are shown of animals perfused with either saline alone (ie. minus phosphatase inhibitors; MPI) or saline with added phosphatase inhibitors (ie. plus phosphatase inhibitors; PPI). Saline MPI-perfused ONHs of control (A), LD (B) and HD (C) animals. There were obvious changes when comparing p-P38 MAPK immunoreactivity (arrow) in HD animals and to a lesser extent, LD animals, to controls. Saline PPI-perfused ONHs of control (D), LD (E) and HD (F) animals. When saline PPI was used, no changes were seen to p-P38 MAPK immunoreactivity in control (D) or HD group animals (F), however, there was increased labelling for animals in the LD group (E). Comparison of immunoreactivity for p-P38 MAPK in the retina in control animals (G) and animals subjected to OHT and categorised as either LD (H) or HD (I). No immunoreactivity was detected in control retinas (G) but labelling was present in HD group animals in the ganglion cell layer (arrow) and the inner nuclear layer (arrow head). The presence of phosphatase inhibitors in the perfusate had no effect on control (J) or HD group animals (L), but significantly increased the labelling intensity of LD group animal retinas (K). Selected staining was present in ganglion cell layer (arrow) and perikarya (arrow head) within the inner nuclear layer. GCL, ganglion cell layer; INL, inner nuclear layer; ONL, outer nuclear layer. Direction of ONH is top to bottom, retina to brain. Scale bar (A-F) 100µm, (G-L) 25µm.

There was no immunolabelling present for p-P38 MAPK in the control retina whether saline MPIs (Figure 8G) or saline PPIs (Figure 8J) were used for perfusion. However, labelling for p-P38 MAPK was present in cell perikayra in the ganglion cell layer and in the inner nuclear layer in experimental HD category animals (Figure 8I), which was unaffected by PIs in the perfusate (Figure 8L). For animals in the LD category, no labelling for p-P38 MAPK was present when PIs were not included in the perfusate (Figure 8H), but their presence enabled improved detection of the active form of this enzyme (Figure 8K). Indeed, after perfusion with saline PPIs, labelling resembled that of the HD; ie additional labelling was present in cell bodies in the ganglion cell layer and inner nuclear layer (Figure 8L). Detected cells were identified as ganglion cells and Müller glial cells by double-labelling with Brn3a and S100, respectively (supplemental Figure 8A-C, D-F).

In attempting to quantify P38 MAPK immunolabelling changes after perfusion with saline PPIs, graphs were plotted based on the relative levels of labelling in each defined category (Figure 9) of immunoreactivity. Figure 9A demonstrates that that there was no grade change for immunolabelling of total P38 MAPK for control, LD or HD group animals whether perfused with saline MPIs or saline PPIs. Semi-quantification of p-P38 MAPK immunoreactivity (Figure 9B), however, revealed that although no labelling changes were observed in control animals perfused with or without addition of PIs, a clear increase in the amount of specific staining in the saline PPI perfused animals compared with the saline MPI perfused animals was seen in both the LD and HD groups (Figure 9B). In the LD category group, grading was confined to minimal labelling of p-P38 MAPK when perfusion was carried out in saline MPIs, but addition of PIs to the saline perfusate revealed a marked increase in quantity and intensity in visible labelling. Additionally, specific p-P38 MAPK labelling for animals in the HD group was clearly

improved to the highest grades (++, +++) in the presence of PIs in the perfusate compared to the animals in the HD group perfused with saline MPIs.

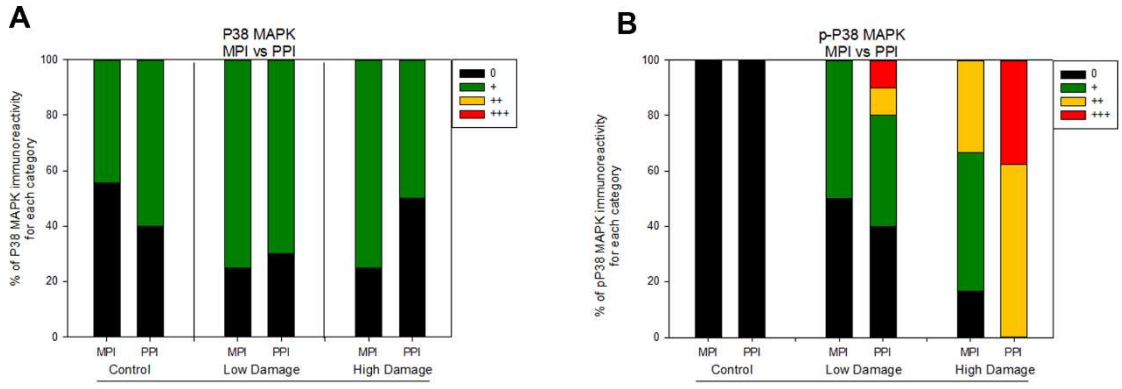

Figure 9. Separation of P38 MAPK (A) and phospho-P38 MAPK (p-P38 MAPK; B) immunoreactivity in the ONH into a range of intensity grades in order to assess potential improvements in labelling after addition of phosphatase inhibitors to saline perfusate (ie. plus phosphatase inhibitors; PPI), as compared with using saline alone (ie. minus phosphatase inhibitors; MPI). There is no notable change in labelling comparing control, LD or HD animals when either saline MPI or saline PPI was used for perfusion when labelling with total P38 MAPK. In the case of p-P38 MAPK (B), saline PPI-perfusate did not alter labelling in controls but allowed clear intensity increases of labelling in both LD and HD group animals. Each bar on the graph is split into different categories, according to the numbers of animals labelling in each grade; scale refers to as the following (as described in Methods Section): 0 no change; + minimal specific labelling; ++ weak specific labelling; +++ intense specific labelling. The total number of specimens that were graded for P38 MAPK: saline MPI, *n*=17; saline PPI, *n*=28 and for p-P38 MAPK: saline MPI, *n*=19; saline PPI; *n*=30.

DISCUSSION

The MAPK family, which includes the P42/44 MAPK, SAPK/JNK and P38 MAPK sub-groups, is known to have crucial roles in the control and functioning of many cellular processes (Cargnello and Roux 2011, Pearson et al. 2001). The importance of this enzyme family in physiological processes suggests that MAPKs will also likely be involved in initiation or development of tissue pathology. As a result, changes in MAPK activity have been implicated in neurological diseases such as Parkinson's and AD as well as in different forms of cancer (Kim and Choi 2010, Mehan et al. 2011). Recent studies have also suggested MAPKs to have a role in retinal pathology in disease models and in human glaucoma (Dapper et al. 2013, Fernandes et al. 2012, Tezel et al. 2003).

Individual MAPK isoenzymes are activated and deactivated by phosphorylation and dephosphorylation, respectively. These actions are stimulated by upstream signalling pathways which are very tightly regulated by changes in the intracellular environment (Cargnello and Roux 2011). One way in which MAPK stimulation can be studied is to investigate spatio-temporal changes in tissue by immunohistochemistry, with antibodies specifically targeted to phosphorylated MAPK isoforms. This method therefore specifically detects the activated versions of each MAPK isoenzyme. When analysing phosphorylated proteins by immunohistochemistry, however, tissue preparation is critical. This is because tissue is effectively alive even after death of an experimental subject. As tissue ceases to function, in the process of death, the blood supply and other physiological functions fail and cellular events such as hypothermia, nutrient starvation and anoxia result. These processes disturb cellular homeostatic mechanisms and signalling, and will have significant effects upon levels and stability of phosphorylated proteins (Espina et al. 2008), since protein phosphorylation and dephosphorylation will become unchecked. This will occur up until all tissues and cells can be

completely fixed. Minimising time restraints between cessation of vital biological functions in an experimental subject and procurement of tissue for analysis, therefore, is key to the accurate dissemination of the end-point phosphoprotein status of a cell. Snap-freezing of tissue in liquid nitrogen has been suggested as a useful method for preserving tissue phosphoprotein levels (Lim et al. 2011), however this not only causes ice crystal formation and damage to a tissue, but the time taken for procurement before freezing still remains a problem. A recent study described the preservation of phosphoprotein levels by immersing excised tissue into a "novel one-step biomarker and tissue preservative" (BHP), which contained phosphatase and kinase inhibitors, a fixative, reversible cross-linkers and a permeation enhancer (Mueller et al. 2011). This still required the tissue to be excised, however, taking time and allowing the possibility of altered phosphoprotein status before actual fixation. We circumvented this problem by adding a cocktail of PIs, which prevent dephosphorylation of phosphoproteins (Mueller et al. 2011), to saline perfusate, which we routinely administer prior to fixation and tissue harvesting. We are therefore providing tissues with compounds which will inhibit phosphatase action *at the point of death* and which will prevent dephosphorylation of proteins, such as the MAPKs, which would be stimulated by changes in cellular homeostasis as a result of animal termination.

We have established a model of elevated OHT in rats, which we have used to provide insights into events that may be occurring in the eye in glaucoma (Chidlow et al. 2008, Chidlow et al. 2011b, Ebneter et al. 2010, Ebneter et al. 2011). This model involves laser-cauterisation of the trabecular meshwork in the anterior portion of the rodent eye, which causes aqueous humour accumulation and consequent elevation of IOP (Levkovitch-Verbin et al. 2002). The level of tissue damage in this model is clearly correlated with the overall increase in IOP (as shown in present study; Ebneter et al. 2010). However, the magnitude of the IOP elevation can

vary dramatically. In our previous studies, therefore, we have excluded animals with pressure increases of less than 10 mmHg, as measured over the three days following treatment. This necessarily means that the tissue damage responses in our studies have been relatively high and the cellular effects we have described have been profound and unambiguous (Chidlow et al. 2008, Chidlow et al. 2011b, Ebneter et al. 2010, Ebneter et al. 2011). We have previously reported robust MAPK changes in this model: within 6 hours of IOP elevation, P42/44 MAPK was activated in ONH astrocytes, p-SAPK/JNK had accumulated at the ONH in damaged axons, and after 24-72 hours, P38 MAPK was phosphorylated in RGC perikarya and ONH microglia (Mammone et al. 2017).

By assessing three antigenic markers used extensively to clarify retinal tissue damage in experimental models: Iba1 for microglia, GFAP for astrogliosis/Müller cell activation and SMI32 (npNFH) to determine breakdown of neurofilaments in axons (Chidlow et al. 2011b, Ebneter et al. 2010, Holman et al. 2010), we established a damage scale against which all animals in the study could be graded. From these data we defined a “high damage” (HD) group and a “low damage” (LD) group (see supplemental Figure 2). For the present study, we were particularly interested in the LD animals where IOP was significantly elevated, but generally at a magnitude of less than 10mmHg over the first three days. In these LD animals, we did see MAPK changes, but in contrast to the HD group, these were variable and, in some cases, difficult to detect. We were therefore interested in examining whether the addition of PIs to the saline perfusate improved detection of phosphorylated MAPKs, particularly in animals in the LD category (Mammone et al. 2017).

In the HD animals from the present study, there were clear changes in phosphorylated MAPK immunohistochemical labelling with relation to controls: p-P42/44 MAPK was induced in ONH astrocytes, p-SAPK/JNK was shown to accumulate in putatively damaged axons, and p-

P38 MAPK was demonstrated in RGC perikarya and ONH microglia. These data were exactly as reported previously (Mammone et al. 2017). Importantly, immunohistochemical localisation of each isoenzyme group of phospho-MAPKs was unchanged in control animals or in treated, HD animals, whether PIs were present in the perfusate or not. Clearly, then, when the pressure elevation in our model was relatively high, damage was robust and there were distinct and consistent alterations to phospho-MAPKs. Furthermore, such activation of MAPK isoenzymes must have been stable because there were no observed changes after application of phosphatase inhibitors to the system.

For animals in the LD category, the situation was more complicated. When analysing MAPK isoenzyme activation status in LD group animals, effects varied from non-existent to mild, when compared with clear changes associated with the HD group. In this case, comparison of phospho-MAPK isoenzyme labelling in LD animals perfused with saline PPIs compared to saline MPIs showed clear differences. In the case of each MAPK isoenzyme class, non-existent or mild labelling was reported when PIs were not present, but when they were, clear and distinct labelling of the same order of magnitude as the corresponding HD group was seen. Thus, in the case of the animals where tissue pathology was of a lower magnitude (i.e. the LD group), the presence of PIs in the perfusate proved extremely useful for stabilising the phospho-MAPKs and enabling their detection. This, then, was in agreement with similar attempts to abrogate phosphatase action as a means to stabilise tissue phosphoprotein species as reported in previous studies (Espina et al. 2008, Mueller et al. 2011).

What are the implication of these findings in relation to our model of OHT? Clearly, phosphorylation, and hence, activation of MAPKs, in the HD group animals is either more stable, more heavily stimulated or more reinforced than in the LD group because the magnitude of this effect does not change when phosphatases are inhibited. It is also possible

that phosphatases which can dephosphorylate MAPKs, such as MAPK phosphatases or dual-specificity phosphatases, (Davidson et al. 2006) have been damaged, deactivated or down-regulated as part of the pathology associated with the OHT in the HD animals. In this case there would be lower levels of phosphatase enzymes to be affected by the application of the PIs. In agreement with a loss of phosphatase activity being associated with neurodegeneration, a reduction in protein phosphatase 2A mRNA and protein levels have been reported in AD (Sontag et al. 2004, Vogelsberg-Ragaglia et al. 2001)

In the LD group animals, conversely, MAPK phosphorylation may have been more temporary, less reinforced, in a state of dynamic equilibrium, or at a reduced level than in the HD group. In this case, since the presence of PIs in the perfusate gave rise to a greater detectable degree of MAPK phosphorylation, then it is clear that the relevant MAPK phosphatases were still active in the tissue at the point of death. Thus, if we hypothesise that MAPK isoenzyme phosphorylation contributes in some manner to ocular pathology in our model of OHT, as has been described previously for other experimental paradigms in the retina (Dapper et al. 2013, Fernandes et al. 2012, Tezel et al. 2003), then activation of phosphatases could provide a rational means of reducing tissue pathology.

Another interesting hypothesis to draw from these studies concerns the relationship between MAPK phosphorylation and the degree of pathology. What was not clear from the original study (Mammone et al. 2017) was whether the magnitudes of the MAPK isoform activation that were observed were directly proportional to the degree of tissue damage or whether they occurred as an all-or-nothing response at a particular level of tissue stress (here, resulting from elevated IOP). That is, once IOP was of a sufficient magnitude, was all available MAPK phosphorylated, or was it phosphorylated in degrees according to the actual level of IOP increase? In the present study, addition of PIs to the perfusate in the LD group animals revealed

that the actual MAPK isoenzyme phosphorylation status at the exact time that the experiment was ceased was comparable to that observed in the HD group eyes. This proves that the same actual level of MAPK phosphorylation had occurred at this time point in both sets of animals, even if this phosphorylation was less stable in the LD animals. It is therefore most likely that the induction of phosphorylation of MAPK isoenzymes occurred as an all-or-nothing response at a given IOP level. Variation in observed labelling, in the absence of PIs, likely solely reflected a relatively greater activity level of endogenous MAPK phosphatases. It must therefore be considered, again, that increasing the activity of MAPK phosphatases may prove a useful therapeutic avenue to explore in relation to abrogating retinal pathology in (experimental) glaucoma.

In terms of the actual model used in this study, because the pattern of activation for each MAPK isoform was specific to a particular tissue element and was induced relatively rapidly, then data do not only reflect the effects of chronic IOP elevation on these enzymes themselves, but they also give hints as to the location where the initiation of pathology occurred. It can thus be deduced that in the ONH, where damage initiation is believed to occur (Burgoyne 2011, Chidlow et al. 2011b, Hernandez 2000) both astrocytes and RGCs are rapidly affected. Moreover, since ganglion cell perikarya are affected (24 hours) after their axons (6 hours), then these data support the notion of pathology being initiated in the ONH rather than in the retina.

CONCLUSION

In conclusion, MAPK phosphorylation has been associated with various neurodegenerative disorders and experimental models in both the brain (Culbert et al. 2006, Irving and Bamford 2002, Johnson 2003, Qi et al. 2016) and the retina (Ibrahim et al. 2011,

Roth et al. 2003). It is therefore likely to be the case that identification of spatio-temporal phosphorylation of each MAPK isoenzyme could prove crucial in determining the course of pathology development in the present, and other related models. It is imperative that for this reason an improved and clear detection system for MAPK phosphorylation be developed. This paper describes the use of an improved method for performing immunohistochemical detection of activated MAPKs in ocular tissue after experimental pathology. The addition of PIs to a perfusate used at the end of the experiment effectively stabilises any existing MAPK phosphorylation at that time, and allows a true picture of cellular events at that juncture to be seen. We would recommend the use of PIs in a perfusate for any small animal experiments, especially when phosphorylation of MAPKs is being investigated. Whether this technique is applicable to all phosphoproteins also warrants further investigation.

DECLARATION

Ethics approval

This study was approved by the Animal Ethics Committee of SA Pathology/Central Adelaide Local Health Network. The study conformed to the ARRIVE Guidelines and both the Australian Code of Practice for the Care and Use of Animals for Scientific Purposes (2013) and to the Association for Research in Vision and Ophthalmology Statement for The Use Of Animals In Ophthalmic And Vision Research.

Availability of data and materials

The datasets used and/or analysed during the current study are available from the corresponding author on reasonable request.

Conflict of interests

The authors declare that they have no conflict of interests.

Funding

The financial support of the BrightFocus Foundation (grant #G2013135), the Ophthalmic Research Institute of Australia and the National Health and Medical Research Council of Australia (Project Grant #565202) are gratefully acknowledged. The Bodies who provided funding for this work had no other role in the study.

Author contribution

Teresa Mammone: Experimental work, manuscript preparation.

Glyn Chidlow: Conception of study, manuscript editing.

Robert Casson: Provision of laboratory space and equipment, manuscript editing.

John Wood: Conception and design of study, manuscript preparation.

Acknowledgments

The technical assistance of Mr Mark Daymon is gratefully acknowledged.

REFERENCES

BOVA GS, ELTOUM IA, KIERNAN JA, SIEGAL GP, FROST AR, BEST CJM, GILLESPIE JW, SU GH AND EMMERT-BUCK MR. 2005. Optimal molecular profiling of tissue and tissue components - Defining the best processing and microdissection methods for biomedical applications. Mol Biotechnol 29: 119-152.

BURGOYNE CF. 2011. A biomechanical paradigm for axonal insult within the optic nerve head in aging and glaucoma. Exp Eye Res 93: 120-132.

BURNS JA, LI Y, CHENEY CA, OU Y, FRANLIN-PFEIFER LL, KUKLIN N AND ZHANG Z-Q. 2009. Choice of fixative is crucial to successful immunohistochemical detection of phosphoproteins in paraffin-embedded tumor tissues. J Histochem Cytochem 57: 257-264.

CARGNELLO M AND ROUX PP. 2011. Activation and function of the MAPKs and their substrates, the MAPK-activated protein Kinases. Microbiol Mol Biol Rev 75: 50-83.

CHIDLOW G, DAYMON M, WOOD JPM AND CASSON RJ. 2011a. Localization of a wide-ranging panel of antigens in the rat retina by immunohistochemistry: comparison of davidson's solution and formalin as fixatives. J Histochem Cytochem 59: 884-898.

CHIDLOW G, EBNETER A, WOOD JPM AND CASSON RJ. 2011b. The optic nerve head is the site of axonal transport disruption, axonal cytoskeleton damage and putative axonal regeneration failure in a rat model of glaucoma. Acta Neuropathol 121: 737-751.

CHIDLOW G, WOOD JPM, MANAVIS J, OSBORNE NN AND CASSON RJ. 2008. Expression of osteopontin in the rat retina: Effects of excitotoxic and ischemic injuries. Invest Ophthalmol Vis Sci 49: 762-771.

CUEVAS BD, ABELL AN AND JOHNSON GL. 2007. Role of mitogen-activated protein kinase kinase kinases in signal integration. Oncogene 26: 3159-3171.

CULBERT AA, SKAPER SD, HOWLETT DR, EVANS NA, FACCI L, SODEN PE, SEYMOUR ZM, GUILLOT F, GAESTEL M AND RICHARDSON JC. 2006. MAPK-activated protein kinase 2 deficiency in microglia inhibits pro-inflammatory mediator release and resultant neurotoxicity - Relevance to neuroinflammation in a transgenic mouse model of Alzheimer disease. J Biol Chem 281: 23658-23667.

DAPPER JD, CRISH SD, PANG IH AND CALKINS DJ. 2013. Proximal inhibition of p38 MAPK stress signaling prevents distal axonopathy. Neurobiol Dis 59: 26-37.

DAVIDSON B, KONSTANTINOVSKY S, KLEINBERG L, NGUYEN MTP, BASSAROVA A, KVALHEIM G, NESLAND JM AND REICH R. 2006. The mitogen-activated protein kinases (MAPK) p38 and JNK are markers of tumor progression in breast carcinoma. Gynecol Oncol 102: 453-461.

EBNETER A, CASSON RJ, WOOD JP AND CHIDLOW G. 2010. Microglial activation in the visual pathway in experimental glaucoma: spatiotemporal characterization and correlation with axonal injury. Invest Ophthalmol Vis Sci 51: 6448-6460.

EBNETER A, CHIDLOW G, WOOD JPM AND CASSON RJ. 2011. Protection of retinal ganglion cells and the optic nerve during short-term hyperglycemia in experimental glaucoma. Arch Ophthalmol 129: 1337-1344.

ESPINA V ET AL. 2008. A Portrait of Tissue Phosphoprotein Stability in the Clinical Tissue Procurement Process. Mol Cell Proteomics 7: 1998-2018.

FERNANDES KA, HARDER JM, FORNAROLA LB, FREEMAN RS, CLARK AF, PANG IH, JOHN SWM AND LIBBY RT. 2012. JNK2 and JNK3 are major regulators of axonal injury-induced retinal ganglion cell death. Neurobiol Dis 46: 393-401.

GROELZ D, SOBIN L, BRANTON P, COMPTON C, WYRICH R AND RAINEN L. 2013. Non-formalin fixative versus formalin-fixed tissue: a comparison of histology and RNA quality. Exp Mol Pathol 94: 188-194.

GUNDISCH S ET AL. 2012. Variability of protein and phosphoprotein levels in clinical tissue specimens during the preanalytical phase. J Proteome Res 11: 5748-5762.

HERNANDEZ MR. 2000. The optic nerve head in glaucoma; Role of astrocytes in tissue remodeling. Prog Retin Eye Res 19: 297.

HOLMAN MC, CHIDLOW G, WOOD JPM AND CASSON RJ. 2010. The Effect of Hyperglycemia on Hypoperfusion-Induced Injury. Invest Ophthalmol Vis Sci 51: 2197-2207.

IBRAHIM AS, EL-REMESSY AB, MATRAGOON S, ZHANG WB, PATEL Y, KHAN S, AL-GAYYAR MM, EL-SHISHTAWY MM AND LIOU GI. 2011. Retinal microglial activation and inflammation induced by amadori-glycated albumin in a rat model of diabetes. Diabetes 60: 1122-1133.

IRVING EA AND BAMFORD M. 2002. Role of mitogen- and stress-activated kinases in ischemic injury. J Cereb Blood Flow Metab 22: 631-647.

JOHNSON G. 2003. The p38 MAP kinase signaling pathway in Alzheimer's disease. Exp Neurol 183: 263-268.

JOHNSON GL AND LAPADAT R. 2002. Mitogen-activated protein kinase pathways mediated by ERK, JNK and p38 protein kinases. Science 298: 1911-1912.

KIM EK AND CHOI EJ. 2010. Pathological roles of MAPK signaling pathways in human diseases. Biochim Biophys Acta 1802: 396-405.

LATENDRESSE JR, WARBRITTION AR, JONASSEN H AND CREASY DM. 2002. Fixation of testes and eyes using a modified Davidson's fluid: Comparison with Bouin's fluid and conventional Davidson's fluid. Toxicol Pathol 30: 524-533.

LEVKOVITCH-VERBIN H. 2004. Animal models of optic nerve diseases. Eye 18: 1066-1074.

LEVKOVITCH-VERBIN H, QUIGLEY HA, MARTIN KRG, VALENTA D, BAUMRIND LA AND PEASE ME. 2002. Translimbal laser photocoagulation to the trabecular meshwork as a model of glaucoma in rats. Invest Ophthalmol Vis Sci 43: 402-410.

LIM MD, DICKHERBER A AND COMPTON CC. 2011. Before you analyze a human specimen, think quality, variability, and bias. Anal Chem 83: 8-13.

MAMMONE T, CHIDLOW G, CASSON RJ AND WOOD JP. 2017. Expression and activation of MAP kinases in the optic nerve head in a rat model of ocular hypertension. Mol Cell Neurosci: accepted.

MEHAN S, MEENA H, SHARMA D AND SANKHLA R. 2011. JNK: A stress-activated protein kinase therapeutic strategies and involvement in alzheimer's and various neurodegenerative abnormalities. J Mol Neurosci 43: 376-390.

MUELLER C ET AL. 2011. One-step preservation of phosphoproteins and tissue morphology at room temperature for diagnostic and research specimens. PLoS One 6.

PEARSON G, ROBINSON F, GIBSON TB, XU BE, KARANDIKAR M, BERMAN K AND COBB MH. 2001. Mitogen-activated protein (MAP) kinase pathways: Regulation and physiological functions. Endocr Rev 22: 153-183.

QI H, PRABAKARAN S, CANTRELLE FX, CHAMBRAUD B, GUNAWARDENA J, LIPPENS G AND LANDRIEU I. 2016. Characterization of neuronal tau protein as a target of extracellular signal-regulated kinase. J Biol Chem 291: 7742-7753.

ROSKOSKI R. 2012. ERK1/2 MAP kinases: Structure, function, and regulation. Pharmacol Res 66: 105-143.

ROTH S, SHAIKH AR, HENNELLY MM, LI Q, BINDOKAS V AND GRAHAM CE. 2003. Mitogen-activated protein kinases and retinal ischemia. Invest Ophthalmol Vis Sci 44: 5383-5395.

SONTAG E, LUANGPIROM A, HLADIK C, MUDRAK I, OGRIS E, SPECIALE S AND WHITE CL. 2004. Altered expression levels of the protein phosphatase 2A AB alpha C enzyme are associated with Alzheimer disease pathology. J Neuropathol Exp Neurol 63: 287-301.

TEZEL G, CHAUBAN BC, LEBLANC RP AND WAX MB. 2003. Immunohistochemical assessment of glial mitogen-activated protein kinase (MAPK) activation in glaucoma. Invest Ophthalmol Vis Sci 7: 3025-3033.

VOGELSBERG-RAGAGLIA V, SCHUCK T, TROJANOWSKI JQ AND LEE VM. 2001. PP2A mRNA expression is quantitatively decreased in Alzheimer's disease hippocampus. Exp Neurol 168: 402-412.

SUPPLEMENTAL FIGURES

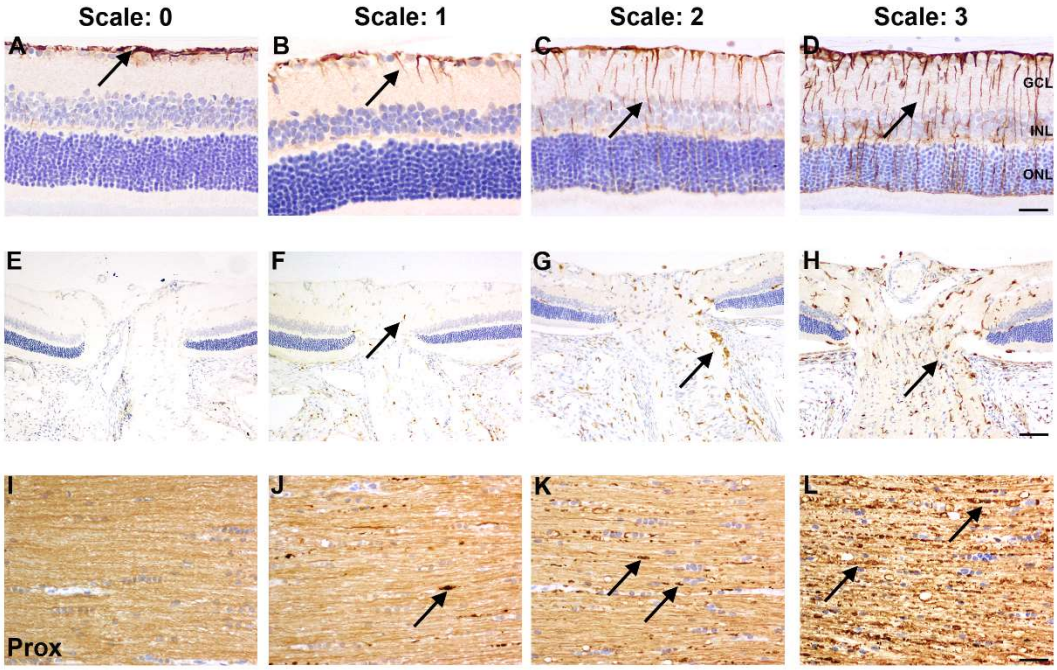

Supplementary Figure 1. The damage scale for classification of animals subjected to OHT for three days and perfused using saline alone. Immunohistochemical expression of GFAP (A-D) in the retina, the microglial marker, Iba1 (E-H) in the ONH and the axonal-based non-phosphorylated neurofilament heavy (npNFH; I-L) in the optic nerve, of treated animals; in each case example images are shown of the different grades used to categorise damage levels in tissue (see Methods Section). Grade 0 (A), grade 1 (B), grade 2 (C) and grade 3 (D), with grade 0 representing no damage and 3 representing a high level of damage. GCL, ganglion cell layer; INL, inner nuclear layer; ONL, outer nuclear layer. Direction of the optic nerve left to right; Prox, proximal to the retina. Scale bar (A-D) 50µm, (F-H) 100µm, (I-L) 50µm.

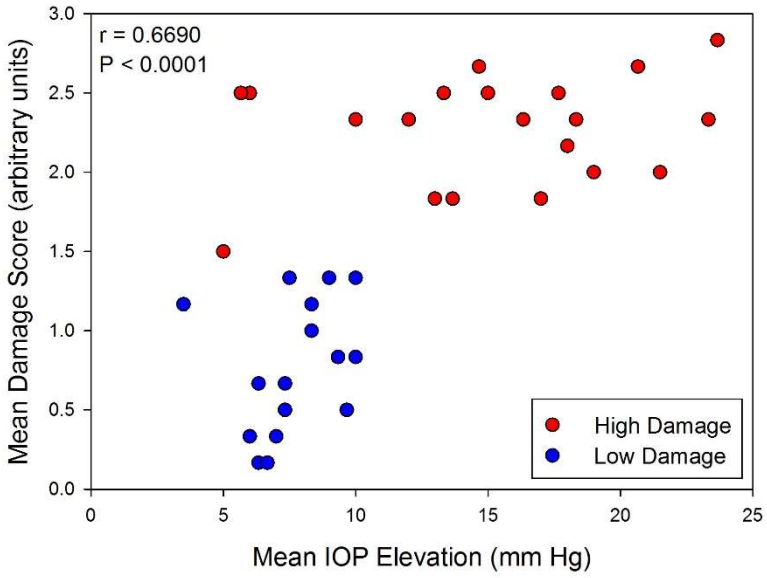

Supplemental Figure 2. Correlation of mean damage score with mean IOP elevation for animals included in the study. Animals with a mean damage score of less than 1.5 were defined as low damage and those with a mean damage score of greater than or equal to 1.5 were defined as high damage. There was a clear positive correlation between IOP increase and damage level in the model. High damage (●) *n*=20; low damage (●) *n*=16.

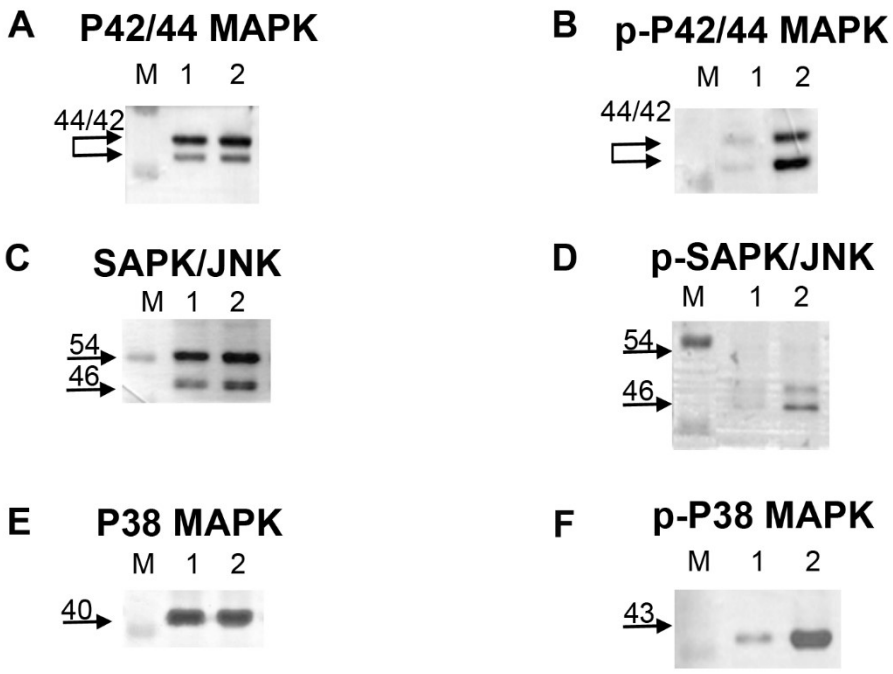

Supplementary Figure 3. Validation of antibodies used in the study. Identification of positive labelling of proteins for both total and phosphorylated MAPK as shown be Western immunoblot. Shown are control and treated ONH samples, which were validated as showing positive labelling for each respective MAPK species previously (Mammone et al. 2017). Lanes: M, molecular weight markers; lane 1, control ONH; lane 2, treated ONH after induction of OHT for three days. (A) P42/44 MAPK is detected in both control and treated ONH protein samples, (B) phospho-P42/44 MAPK (p-P42/44 MAPK) was only detected in treated samples (B; lane 2). Both total and phosphorylated P42/44 MAPK were detected at the predicted molecular masses of 42 and 44 kDa. (C) Labelling of SAPK/JNK and (D) phospho-SAPK/JNK (p-SAPK/JNK) in both control and treated ONH protein samples. Where present, both were detected at their predicted molecular masses of 54 and 46 kDa, but only the former is present in the control sample. (E) P38 MAPK and phospho-P38 MAPK (p-P38 MAPK; F) were detected at their predicted molecular mass of 40 and 43 respectively. Total P38 MAPK was detected in both samples whereas p-P38 MAPK protein was predominantly detected in the treated ONH sample. Protein masses shown by arrows.

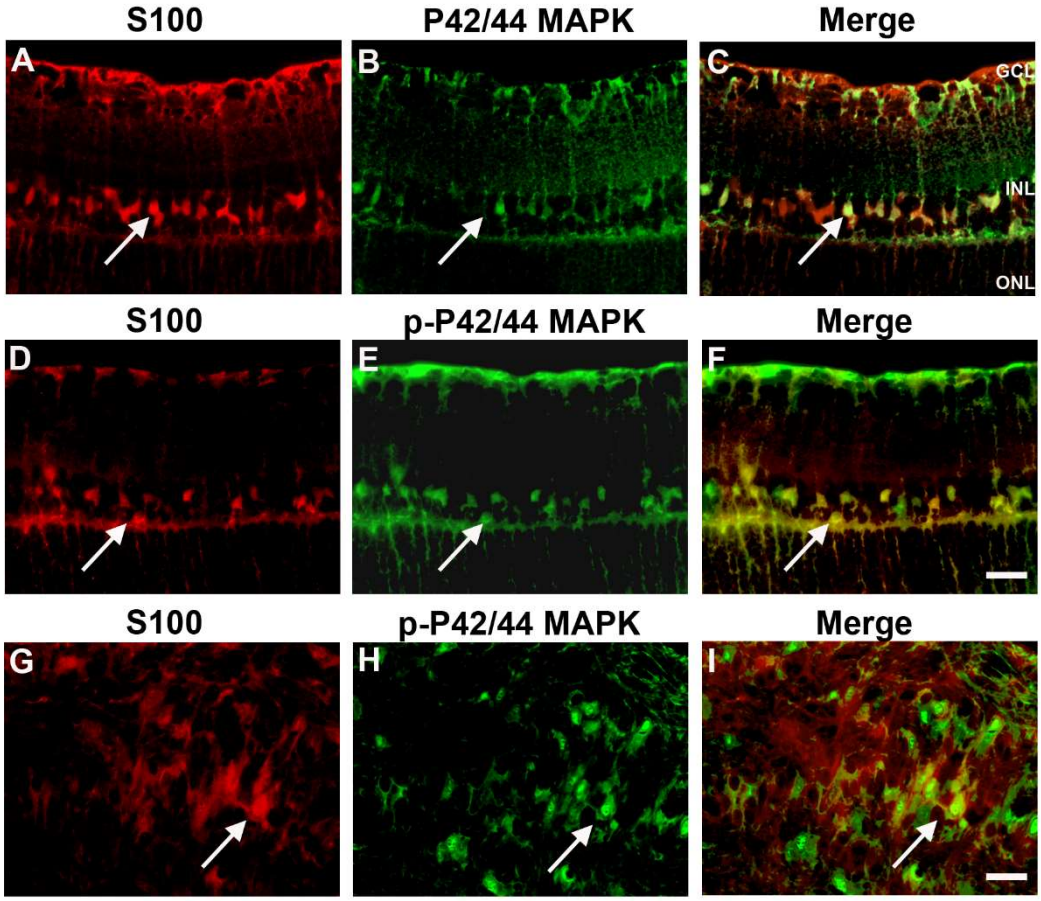

Supplementary Figure 4. Double-immunofluorescent labelling was used to confirm localisation of total P42/44 MAPK and phospho-P42/44 MAPK (p-P42/44 MAPK) in the presence of phosphatase inhibitors in the saline perfusate. Co-labelling was carried out with the glial cell (astrocyte and Müller cell) marker, S100. S100 (A; red) and P42/44 MAPK (B; green) within control retinas co-localise (arrow) in Müller glial cells as shown in the merged (C; yellow) image. Immunofluorescent labelling in retinas from animals subjected to OHT for three days also identified cellular location of p-P42/44 MAPK (green) when co-localised with the S100 glial cell marker. Co-localising with S100 (D), p-P42/44 MAPK (E) was located in a population of Müller glial cells and astrocytes within the retina (D-F) and some astrocytes within the optic nerve (G-I). GCL, ganglion cell layer; INL, inner nuclear layer; ONL, outer nuclear layer. Direction of the optic nerve shown: left to right, proximal to distal. Scale bar (A-F) 25µm, (G-I) 50µm.

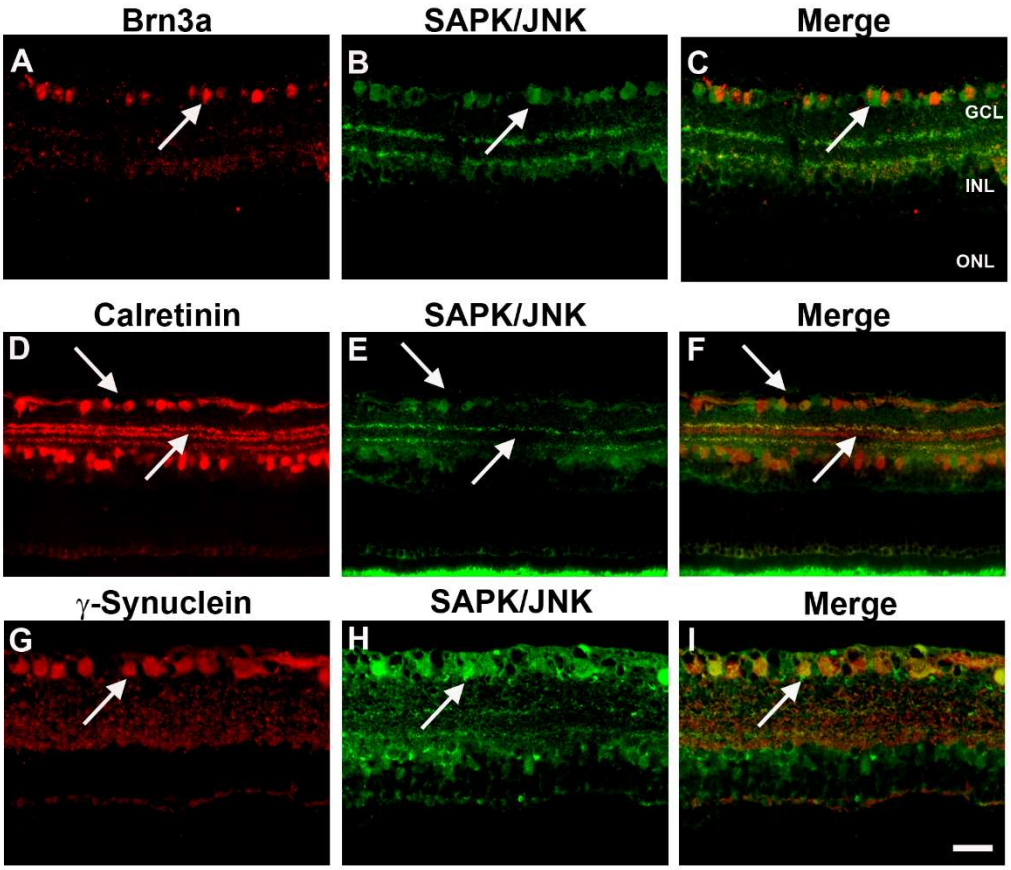

Supplementary Figure 5. Double-immunofluorescent labelling was used to determine the location of total SAPK/JNK in the presence of phosphatase inhibitors in the saline perfusate. Co-labelling (arrows) in control retinas (C; yellow) of ganglion cell specific Brn3a (A; red) and SAPK/JNK (B; green). Ganglion and amacrine cell-specific calretinin (D; red) expression partially co-localised with SAPK/JNK (E; green) in both perikarya and processes within the ganglion cell layer, the inner plexiform layer and the inner nuclear layer as shown in the merged image (F; yellow). The ganglion cell-specific marker protein, γ-synuclein (G; red), co-localised with SAPK/JNK (H; green) in ganglion cell bodies, (I; yellow). GCL, ganglion cell layer; INL, inner nuclear layer; ONL, outer nuclear layer. Scale bar (A-I) 25µm.

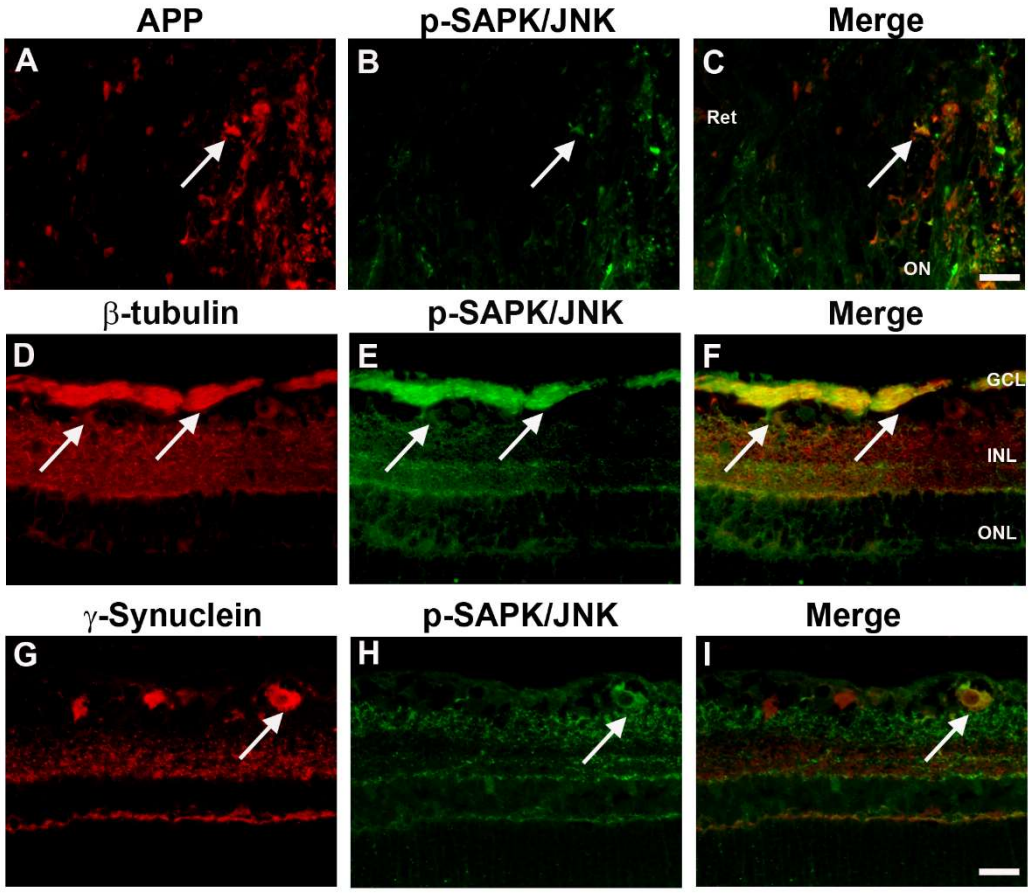

Supplementary Figure 6. Double-immunofluorescent labelling for phospho-SAPK/JNK (p-SAPK/JNK) in animals subjected to OHT for three days, to determine localisation in the presence of phosphatase inhibitors in the saline perfusate. Specific ganglion cell markers were used to confirm the expression of p-SAPK/JNK (green). APP (A; red), an axonal transport marker and p-SAPK/JNK (B) co-localise in axons in the ONH as shown by merged image (C; yellow). Another axonal marker, β-tubulin (D; red) and p-SAPK/JNK (E) co-label in the nerve fibre layer in the retina (F). γ-synuclein (G; red) labels ganglion cell bodes and co-labels with p-SAPK/JNK (H) in the treated retina (I). GCL, ganglion cell layer; INL, inner nuclear layer; ONL, outer nuclear layer. Scale bar (A-C) 25µm, (D-L) 50µm.

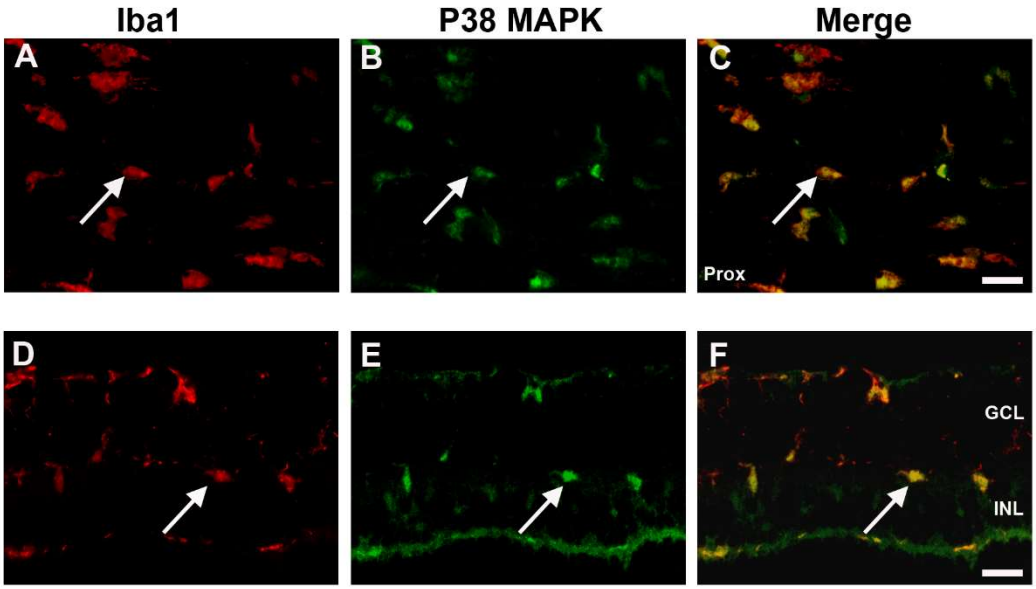

Supplemental Figure 7. Double-immunofluorescent labelling to ascertain the cellular location of total P38 MAPK in animals subjected to OHT for three days, in the presence of phosphatase inhibitors in the saline perfusate, in the optic nerve (A-C) and retina (D-F). Iba1 (A; red) and P38 MAPK (B; green) co-label in microglial cells (C; yellow) in the optic nerve. Iba1 (D) and P38 MAPK (E) also co-label in microglia in the retina (F). (A-C) Direction of optic nerve left to right; proximal to distal. (D-F) GCL, ganglion cell layer; INL, inner nuclear layer. Scale bar (A-C) 50µm, (D-F) 25µm.

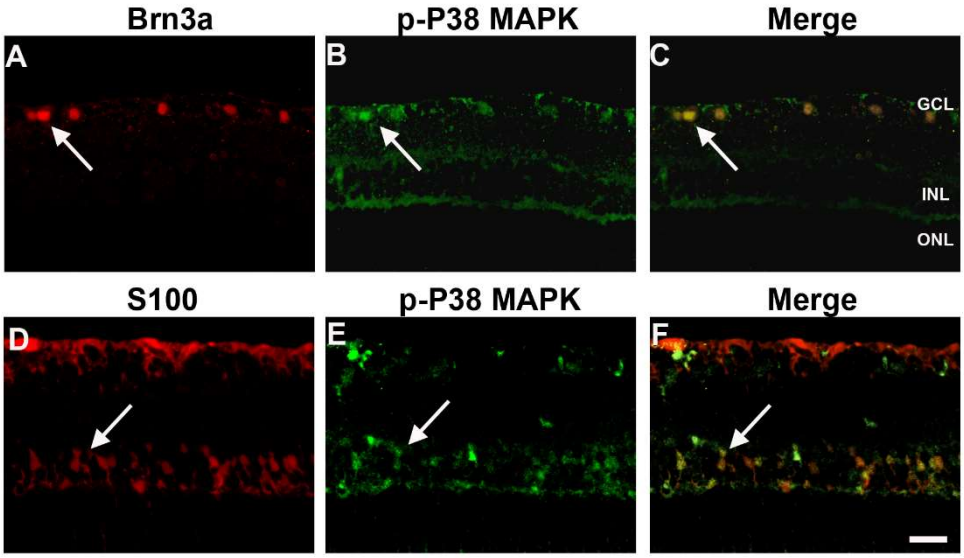

Supplemental Figure 8. Double-immunofluorescent labelling to ascertain the location of phospho-P38 MAPK (p-P38 MAPK) expression in the retinas (A-F) of animals subjected to OHT for three days in the presence of phosphatase inhibitors in the saline perfusate. Brn3a (A; red) and p-P38 MAPK (B; green) co-label in ganglion cell perikarya in the retina (C; yellow).Glial cell marker S100 (D; red) expressed in cell bodies within the inner nuclear layer co-localised with p-P38 MAPK (E) positive stained cells in the retina as indicated in the merge image (F). GCL, ganglion cell layer; INL, inner nuclear layer; ONL, outer nuclear layer. Scale bar (A-F) 25µm.

DISCUSSION

Context of the study and contribution to current knowledge

Glaucoma is the second highest cause of blindness worldwide, with the prevalence predicted to rise from 60.5 million people to 79.6 million people affected by 2020 (Quigley and Broman 2006). Glaucoma, which is often associated with ageing or elevated IOP, manifests as a clinically characteristic progressive optic neuropathy accompanied by gradual RGC loss. The pathogenesis of RGC loss in glaucoma, however, remains unclear (Casson et al. 2012). Research into the underlying causes of glaucoma is multi-faceted and although much work is being undertaken to understand the possible genetic background to this disease (Liu and Allingham 2017), an elucidation into molecular causes of the pathology remains crucial (Anders et al. 2017).

One such molecular target being investigated for a possible role in RGC loss in this disease is the MAPK family which is stimulated by extracellular influences to phosphorylate target proteins and thereby regulate cellular processes including proliferation, differentiation, survival and apoptosis (Cargnello and Roux 2011). MAPKs are divided into three major groups, depending on broad functionality: the P42/44 MAPK, the SAPK/JNK and the P38 MAPK isoenzyme groups. Each MAPK is activated by phosphorylation on at least one site and, therefore, detection of a phosphorylated MAPK isoenzyme after an experimental insult, for example, is a clear indication that this enzyme has been activated and can phosphorylate its own target proteins (Cargnello and Roux 2011). Furthermore, the involvement of MAPKs in development of retinal pathology has been documented in experimental models (Fernandes

et al. 2012, Dapper et al. 2013, Zhou et al. 2007), and alluded to in human glaucoma (Tezel et al. 2003).

The underlying aim of the laboratory where these studies were undertaken is to identify molecular targets for potential therapeutic intervention in glaucoma treatment. One such target identified was the MAPK enzyme family. In order to initiate investigations into the MAPK family, this thesis specifically aimed to determine whether different isoenzyme groups were affected in an experimental rat model of chronic OHT. This model, established by laser coagulation of the trabecular meshwork, exhibits moderate IOP elevation which can be sustained for up to at least two weeks following treatment. The model is associated with a characteristic pathological profile, exhibiting sectorial RGC loss and optic nerve damage as well as rapid axonal transport failure (Chidlow et al. 2011, Chidlow et al. 2012, Ebneter et al. 2010, Levkovitch-Verbin et al. 2003). Work undertaken in this thesis examined the P42/44 MAPK, SAPK/JNK and P38 MAPK isoenzyme groups and how they were affected in the OHT model. By employing a series of antibodies which only recognise phosphorylated, and, hence, activated MAPK isoenzymes, it was demonstrated that there was indeed an activation of this enzyme family; in fact each isoenzyme group was influenced in a distinct manner.

P42/44 MAPK was activated within 6 hours in the ONH in the model of OHT. Its activation within the ONH was limited to but not exclusive to astrocytes. Astrocytes are generally known to respond rapidly to injury (Harun-Or-Rashid et al. 2015, Roskoski 2012). This was also true in the present model: markers of astrocyte activation can be detected within hours of initiating IOP elevation by laser treatment (Chidlow et al. 2014). Future work will determine whether P42/44 MAPK is involved in the activation process of astrocytes or whether it is activated secondary to induction of astrogliosis.

Activated p-SAPK/JNK was present throughout RGC axons in the retina, ONH and optic nerve both in treated and untreated eyes. These data are novel and suggest that the presence of this enzyme is important in the physiological functioning of RGCs. As a result of elevating IOP, an increase in the quantity of activated p-SAPK/JNK was detected and a change in its location was also noted. We concluded that p-SAPK/JNK accumulated in the ONH in treated samples in RGC axons, which have abrogated transport as a result of IOP elevation (Chidlow et al. 2011). SAPK/JNK has been shown to be activated in RGC cell perikarya in response to different stressors (Kim et al. 2016, Kwong and Caprioli 2006), although our data were not fully in agreement with this. There are known to be several distinct SAPK/JNK isoforms, although our methods of detection did not differentiate between them. Differences in roles and cellular compartmentalisation for individual isoforms could therefore underlie differences in data obtained in this study compared with previous reports. It would therefore be pertinent to investigate possible changes in all SAPK/JNK isoforms in the present model. Future studies will address this.

P38 MAPK was abundant in both control and treated tissue. Data presented here demonstrated that P38 MAPK was expressed by a population of microglia which were significantly increased in number following IOP elevation. However, this enzyme was only significantly activated in microglia after 3 days, and then only in the ONH and optic nerve; in the retina it was solely activated in RGC perikarya. P38 MAPK has previously been localised to rat ocular microglia in a model of diabetes (Ibrahim et al. 2010, Ibrahim et al. 2011), after lipopolysaccharide treatment (Ahmad et al. 2014, Xu et al. 2012), and in response to optic nerve trauma (Katome et al. 2013) but data demonstrating the localisation of this enzyme to these cells, as well as its activation, after experimental elevation of IOP, are novel. Microglia are thought to be responders to and mediators of damage to neuronal tissues following

trauma, and P38 MAPK is known to play a key role in microglial phagocytosis (Hosmane et al. 2012). It is therefore possible that its activation here is related to removal of damaged axon tissue. With these data in mind, it would be of interest to apply P38 MAPK inhibitors to animals prior to establishment of the present model of OHT. Such an action could inhibit activation of (a subset of) microglia and this may well affect the pathological outcome.

Previous studies have also described a role for P38 MAPK in mediating apoptosis in RGC perikarya in an animal model of glaucoma (Dapper et al. 2013). Like this study, the present work describes an activation of P38 MAPK in RGC bodies a number of hours after induction of IOP elevation. Again, it is possible that different isoenzymes mediate the different effects of P38 MAPK in distinct locations within ocular tissues. As was the case for SAPK/JNK, dissemination of spatio-temporal activation or location changes in individual P38 MAPK isoenzymes in the present model would be of interest in future studies.

In order to determine whether there is any relationship between changes in ocular pressure in our glaucoma model and activation status for MAPKs, relative level of phosphorylation (from Western blot) for each group of isoenzymes was plotted separately against measured IOP level at each time point. When performing this comparison, we can see that the activation profile for both P42 MAPK and P44 MAPK (Figure 1A, B) follow the same general pattern of IOP pressure increase, ie. a peak followed by a gradual post-peak reduction, but with a temporal delay of several days. This could be explained by the primary site of P42/44 MAPK activation being in astrocytes at the ONH and although there being a pressure-dependent effect on these cells, there also being a delay in these cells both detecting an IOP elevation and their intracellular signalling system eliciting a response. Additionally, when comparing the activation of SAPK/JNK with the IOP profile over time, there are direct parallels as seen in figure 1C: the temporal pattern of protein activation shows an initial spike as well as

a regression at the later time points, concurrent with the same pattern in IOP. This likely relates to there being a direct effect of IOP on ganglion cells and their axons which rapidly activates SAPK/JNK, as demonstrated in chapter 1.

P38 MAPK demonstrated a significant delay in activation in the ONH after IOP elevation, reaching peak significance 2-3 days after achievement of maximum pressure at 3-7 days after laser treatment. However, similarly to SAPK/JNK, this activation also regressed to non-significance after 7 days (Figure 1D). Expression of activated P38 MAPK was found in selected microglia in the ONH. This delay in P38 MAPK activation in response to elevated IOP is likely due to there being a necessary sequence of events before the involvement of these cells in the damage cascade in a neuronal tissue. In the case of the present experiments, there was a significant time lag between pressure elevation, ensuing axonal breakdown and the resultant recruitment to and stimulation of microglia at this site (Chidlow et al. 2011b).

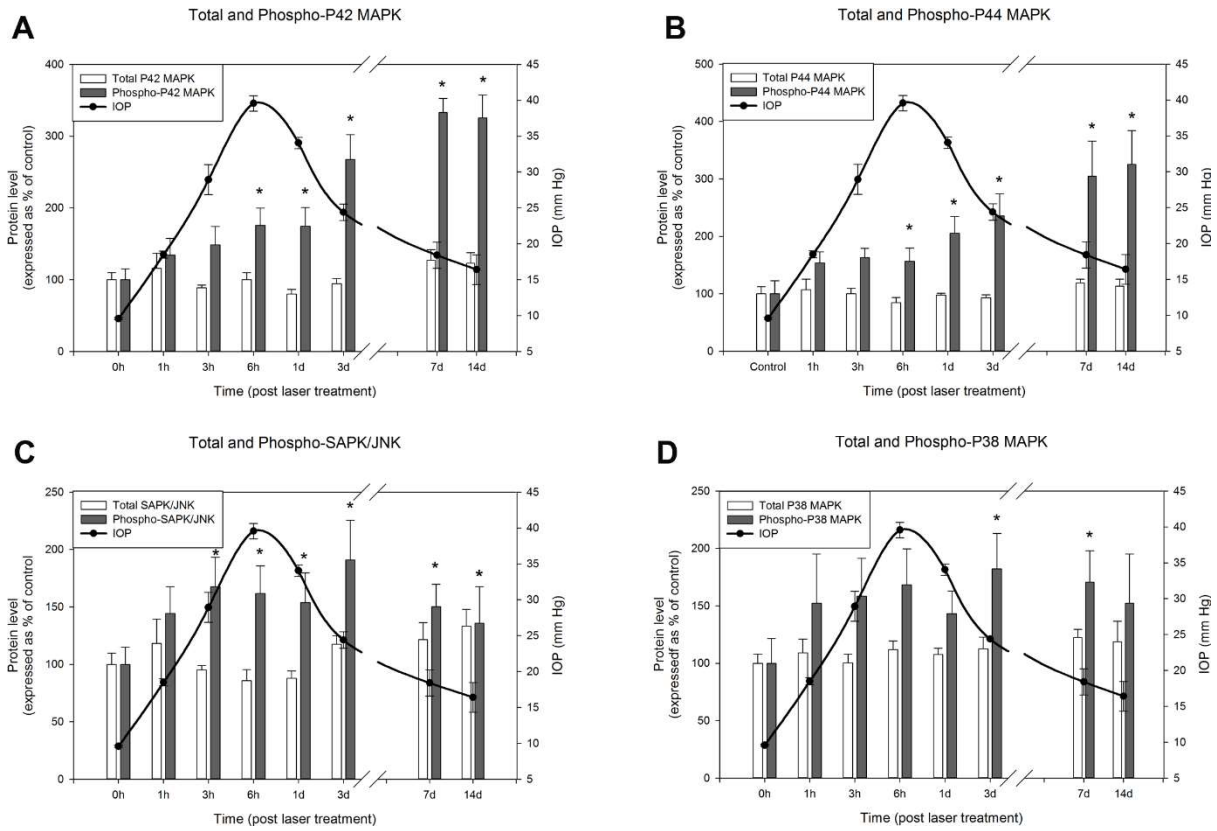

Figure 1. Expression and activation of individual MAPK proteins in the ONH and their relationship with IOP changes in treated eyes in our model. (A) Total protein expression and degree of activation of P42 MAPK expressed as a percentage of control levels, with IOP profile of treated eyes at corresponding times after induction of elevated IOP. (B) Total protein expression and degree of activation of P44 MAPK expressed as a percentage of control levels, with IOP profile of treated eyes at corresponding times after induction of elevated IOP. (C) Total protein expression and degree of activation of SAPK/JNK expressed as a percentage of control levels, with IOP profile of treated eyes at corresponding times after induction of elevated IOP. (D) Total protein expression and degree of activation of P38 MAPK expressed as a percentage of control levels, with IOP profile of treated eyes at corresponding times after induction of elevated IOP. Protein and IOP data are expressed as mean ± SEM values in each case (n=6 for protein data and n=15-25 for IOP data). **P* <0.05, when compared with sham, non-treated animals (time zero), by two sample paired t-test followed by a Bonferroni correction.

Data presented here along with that from previous studies demonstrate clearly that the MAPK enzyme family must play a key role in the developing pathology of neurological conditions such as glaucoma. However, in practical terms, inconsistencies in published data

will provide complications when analysing how to use such data for therapeutic benefit. As discussed above, discrepancies in data presented in this thesis do exist when comparing with some published data (eg. for SAPK/JNK). It was hypothesised that this could have been accounted for by differences in detection methods and their sensitivities (Bova et al. 2005), or the relative instability of phosphoproteins during tissue procurement for analysis (Burns et al. 2009, Mueller et al. 2011). In chapter two, therefore, a novel approach was taken to stabilise phosphoproteins in tissue procured for analysis. Inhibitors of phosphatases (PIs), the enzymes responsible for catalytic removal of phosphate groups from proteins, were added to saline which was used to perfuse experimental animals at the end-point of experiments before removing tissues for analysis. This procedure successfully stabilised and allowed detection of phosphorylated MAPK isoenzymes even after mild insults, where previously such analyses provided inconsistent results. This was the case for each of the different sub-groups of MAPKs. Data presented in chapter one identified clear MAPK changes following robust ocular pressure elevation. However, molecular tissue changes after less robust insults, for example at lower pressure elevations (as documented in chapter two), often provide more physiologically relevant information when potential therapeutic intervention strategies are being considered. Here, analysing tissue with a lower damage profile is vital in understanding initial stages of glaucoma pathology and determining if the MAPK activation is an all or nothing response.

The use of PIs during tissue collection and preservation has advantages for both diagnostic and research applications. The application of PIs provides researchers with the tools to assess phosphoprotein alterations in animal subjects after mild insults which may otherwise not have been accounted for.

Studying MAPKs in disease models is vital as these enzymes are critical in the functioning of many cellular processes. Overall, this study has furthered our knowledge as to

the roles that MAPKs may play in conditions such as glaucoma. Understanding cellular responses to adverse stimuli, such as elevated IOP in the present model, contributes to understanding the associated pathology and often help lead researchers to potentially useful therapeutic targets.

CONCLUSIONS AND FUTURE STUDIES

Data in this thesis has demonstrated activation of the three major sub-groups of MAPK: P42/44 MAPK, SAPK/JNK and P38 MAPK, in the retina, ONH and optic nerve, in a rat model of OHT. The spatio-temporal activation characteristics for each group of MAPKs differed markedly, implying that these enzymes have distinct roles in the physiological function and pathological response of ocular tissues. The current work also provides further evidence that the initial site of injury in the model of OHT employed, and therefore, perhaps, glaucoma itself, result from insults initiated in the ONH.

Future studies will employ specific inhibitors of each of the sub-groups of MAPK to see whether abrogating their activation has protective, or even enhancing, effects on development of pathology in the present model of experimental OHT. If it proves to be the case that MAPK activation is fundamental in the establishment of cellular signalling events which contribute to glaucomatous pathology, for example, then the protein targets for this group of enzymes must be identified in this system. Since the MAPK family has such a central role in many key cellular processes, it follows that there are a large number of protein substrates for their kinase action. Manipulation of such targets may also prove a useful therapeutic approach in the treatment of glaucoma.

REFERENCES

ADACHI M, TAKAHASHI K, NISHIKAWA M, MIKI H AND UYAMA M. 1996. High intraocular pressure-induced ischemia and reperfusion injury in the optic nerve and retina in rats. Graefes Arch Clin Exp Ophthalmol 234: 445-451.

ADDISON WHF AND HOW HW. 1926. Congenital hypertrophy of the eye in an albino rat. Anat Rec 32: 271-277.

AGAR A, LI S, AGARWAL N, CORONEO MT AND HILL MA. 2006. Retinal ganglion cell line apoptosis induced by hydrostatic pressure. Brain Res 1086: 191-200.

AGTHONG S, KAEWSEMA A AND CHENTANEZ V. 2012. Inhibition of p38 MAPK reduces loss of primary sensory neurons after nerve transection. Neurol Res 34: 714-720.

AHMAD S, ELSHERBINY NM, BHATIA K, ELSHERBINI AM, FULZELE S AND LIOU GI. 2014. Inhibition of adenosine kinase attenuates inflammation and neurotoxicity in traumatic optic neuropathy. J Neuroimmunol 277: 96-104.

AIHARA M, CHEN YN, UCHIDA S, NAKAYAMA M AND ARAIE M. 2014. Hyperbaric pressure and increased susceptibility to glutamate toxicity in retinal ganglion cells in vitro. Mol Vis 20: 606-615.

ANDERS F, TEISTER J, FUNKE S, PFEIFFER N, GRUS F, SOLON T AND PROKOSCH V. 2017. Proteomic profiling reveals crucial retinal protein alterations in the early phase of an experimental glaucoma model. Graefes Arch Clin Exp Ophthalmol 255: 1395-1407.

BACHSTETTER AD, ROWE RK, KANEKO M, GOULDING D, LIFSHITZ J AND VAN ELDIK LJ. 2013. The p38 alpha MAPK regulates microglial responsiveness to diffuse traumatic brain injury. J Neurosci 33: 6143-6153.

BENNETT BL ET AL. 2001. SP600125, an anthrapyrazolone inhibitor of Jun N-terminal kinase. Proc Natl Acad Sci U S A 98: 13681-13686.

BERKELAAR M, CLARKE DB, WANG YC, BRAY GM AND AGUAYO AJ. 1994. Axotomy results in delayed death and apoptosis of retinal ganglion-cells in adult-rats. J Neurosci 14: 4368-4374.

BJORKBLOM B, OSTMAN N, HONGISTO V, KOMAROVSKI V, FILEN JJ, NYMAN TA, KALLUNKI T, COURTNEY MJ AND COFFEY ET. 2005. Constitutively active cytoplasmic c-Jun N-terminal kinase 1 is a dominant regulator of dendritic architecture: Role of microtubule-associated protein 2 as an effector. J Neurosci 25: 6350-6361.

BOUHENNI RA, DUNMIRE J, SEWELL A AND EDWARD DP. 2012. Animal Models of Glaucoma. J Biomed Biotechnol.

BOVA GS, ELTOUM IA, KIERNAN JA, SIEGAL GP, FROST AR, BEST CJM, GILLESPIE JW, SU GH AND EMMERT-BUCK MR. 2005. Optimal molecular profiling of tissue and tissue components - Defining the best processing and microdissection methods for biomedical applications. Mol Biotechnol 29: 119-152.

BU XN, HUANG P, QI ZF, ZHANG N, HAN S, FANG L AND LI JF. 2007. Cell type-specific activation of p38 MAPK in the brain regions of hypoxic preconditioned mice. Neurochem Int 51: 459-466.

BURGOYNE CF. 2011. A biomechanical paradigm for axonal insult within the optic nerve head in aging and glaucoma. Exp Eye Res 93: 120-132.

BURKHARD K AND SHAPIRO P. 2010. Use of inhibitors in the study of MAP kinases. Methods Mol Biol 661: 107-122.

BURNS JA, LI Y, CHENEY CA, OU Y, FRANLIN-PFEIFER LL, KUKLIN N AND ZHANG Z-Q. 2009. Choice of fixative is crucial to successful immunohistochemical detection of phosphoproteins in paraffin-embedded tumor tissues. J Histochem Cytochem 57: 257-264.

CARGNELLO M AND ROUX PP. 2011. Activation and function of the MAPKs and their substrates, the MAPK-activated protein Kinases. Microbiol Mol Biol Rev 75: 50-83.

CASSON RJ, CHIDLOW G, WOOD JP, CROWSTON JG AND GOLDBERG I. 2012. Definition of glaucoma: clinical and experimental concepts. Clin Experiment Ophthalmol 40: 341-349.

CASSON RJ, WOOD JPM, HAN GG, KITTIPASSORN T, PEET DJ AND CHIDLOW G. 2016. M-type pyruvate kinase isoforms and lactate dehydrogenase A in the mammalian retina: metabolic implications. Invest Ophthalmol Vis Sci 57: 66-80.

CEDRONE C, MANCINO R, CERULLI A, CESAREO M AND NUCCI C. 2008. Epidemiology of primary glaucoma: prevalence, incidence, and blinding effects. Prog Brain Res 173: 3-14.

CHAMBARD JC, LEFLOCH R, POUYSSEGUR J AND LENORMAND P. 2007. ERK implication in cell cycle regulation. Biochimica Et Biophysica Acta-Molecular Cell Research 1773: 1299-1310.

CHANG LF, JONES Y, ELLISMAN MH, GOLDSTEIN LSB AND KARIN M. 2003. JNK1 is required for maintenance of neuronal microtubules and controls phosphorylation of microtubule-associated proteins. Dev Cell 4: 521-533.

CHIDLOW G, DAYMON M, WOOD JPM AND CASSON RJ. 2011a. Localization of a wide-ranging panel of antigens in the rat retina by immunohistochemistry: comparison of davidson's solution and formalin as fixatives. J Histochem Cytochem 59: 884-898.

CHIDLOW G, EBNETER A, WOOD JPM AND CASSON RJ. 2011b. The optic nerve head is the site of axonal transport disruption, axonal cytoskeleton damage and putative axonal regeneration failure in a rat model of glaucoma. Acta Neuropathol 121: 737-751.

CHIDLOW G, WOOD JP AND CASSON RJ. 2014. Expression of inducible heat shock proteins Hsp27 and Hsp70 in the visual pathway of rats subjected to various models of retinal ganglion cell injury. PLoS One 9: e114838.

CHIDLOW G, WOOD JPM AND CASSON RJ. 2007. Pharmacological neuroprotection for glaucoma. Drugs 67: 725-759.

CHIDLOW G, WOOD JPM, EBNETER A AND CASSON RJ. 2012. Interleukin-6 is an efficacious marker of axonal transport disruption during experimental glaucoma and stimulates neuritogenesis in cultured retinal ganglion cells. Neurobiol Dis 48: 568-581.

CHIDLOW G, WOOD JPM, MANAVIS J, OSBORNE NN AND CASSON RJ. 2008. Expression of osteopontin in the rat retina: Effects of excitotoxic and ischemic injuries. Invest Ophthalmol Vis Sci 49: 762-771.

CONSTABLE PA AND LAWRENSON JG. 2009. Glial cell factors and the outer blood retinal barrier. Ophthalmic Physiol Opt 29: 557-564.

COWAN KJ AND STOREY KB. 2003. Mitogen-activated protein kinases: new signaling pathways functioning in cellular responses to environmental stress. J Exp Biol 206: 1107-1115.

CUENDA A AND ROUSSEAU S. 2007. P38 MAP-Kinases pathway regulation, function and role in human diseases. Biochimica Et Biophysica Acta-Molecular Cell Research 1773: 1358-1375.

CULBERT AA, SKAPER SD, HOWLETT DR, EVANS NA, FACCI L, SODEN PE, SEYMOUR ZM, GUILLOT F, GAESTEL M AND RICHARDSON JC. 2006. MAPK-activated protein kinase 2 deficiency in microglia inhibits pro-inflammatory mediator release and resultant neurotoxicity - Relevance to neuroinflammation in a transgenic mouse model of Alzheimer disease. J Biol Chem 281: 23658-23667.

DANESH-MEYER HV. 2011. Neuroprotection in glaucoma: recent and future directions. Curr Opin Ophthalmol 22: 78-86.

DANG Y, XU Y, WU W, LI W, SUN Y, YANG J, ZHU Y AND ZHANG C. 2014. Tetrandrine suppresses lipopolysaccharide-induced microglial activation by inhibiting NF-kappa b and ERK signaling pathways in BV2 cells. PLoS One 9.

DAPPER JD, CRISH SD, PANG IH AND CALKINS DJ. 2013. Proximal inhibition of p38 MAPK stress signaling prevents distal axonopathy. Neurobiol Dis 59: 26-37.

DAVIDSON B, KONSTANTINOVSKY S, KLEINBERG L, NGUYEN MTP, BASSAROVA A, KVALHEIM G, NESLAND JM AND REICH R. 2006. The mitogen-activated protein kinases (MAPK) p38 and JNK are markers of tumor progression in breast carcinoma. Gynecol Oncol 102: 453-461.

DEGTEREV A AND YUAN J. 2008. Expansion and evolution of cell death programmes. Nature Reviews Molecular Cell Biology 9: 378-390.

EBNETER A, CASSON RJ, WOOD JP AND CHIDLOW G. 2010. Microglial activation in the visual pathway in experimental glaucoma: spatiotemporal characterization and correlation with axonal injury. Invest Ophthalmol Vis Sci 51: 6448-6460.

EBNETER A, CASSON RJ, WOOD JP AND CHIDLOW G. 2012. Estimation of axon counts in a rat model of glaucoma: comparison of fixed-pattern sampling with targeted sampling. Clin Exp Ophthalmol 40: 626-633.

EBNETER A, CHIDLOW G, WOOD JPM AND CASSON RJ. 2011. Protection of retinal ganglion cells and the optic nerve during short-term hyperglycemia in experimental glaucoma. Arch Ophthalmol 129: 1337-1344.

EDWARDS ME AND GOOD TA. 2001. Use of a mathematical model to estimate stress and strain during elevated pressure induced lamina cribrosa deformation. Curr Eye Res 23: 215-225.

ERGORUL C, RAY A, HUANG W, DARLAND D, LUO ZK AND GROSSKREUTZ CL. 2008. Levels of vascular endothelial growth factor-A(165b) (VEGF-A(165b)) are elevated in experimental glaucoma. Mol Vis 14: 1517-1524.

ESPINA V ET AL. 2008. A Portrait of Tissue Phosphoprotein Stability in the Clinical Tissue Procurement Process. Mol Cell Proteomics 7: 1998-2018.

FECHTNER RD AND WEINREB RN. 1994. Mechanisms of optic-nerve damage in primary open-angle glaucoma. Surv Ophthalmol 39: 23-42.

FERNANDES KA, HARDER JM, FORNAROLA LB, FREEMAN RS, CLARK AF, PANG IH, JOHN SWM AND LIBBY RT. 2012. JNK2 and JNK3 are major regulators of axonal injury-induced retinal ganglion cell death. Neurobiol Dis 46: 393-401.

FERNANDES KA, HARDER JM, JOHN SW, SHRAGER P AND LIBBY RT. 2014. DLK-dependent signaling is important for somal but not axonal degeneration of retinal ganglion cells following axonal injury. Neurobiol Dis 69: 108-116.

FERNANDES KA, HARDER JM, KIM J AND LIBBY RT. 2013. JUN regulates early transcriptional responses to axonal injury in retinal ganglion cells. Exp Eye Res 112: 106-117.

FITZGERALD M, BARTLETT CA, EVILL L, RODGER J, HARVEY AR AND DUNLOP SA. 2009. Secondary degeneration of the optic nerve following partial transection: The benefits of lomerizine. Exp Neurol 216: 219-230.

FLAMMER J, HAEFLIGER IO, ORGUL S AND RESINK T. 1999. Vascular dysregulation: A principal risk factor for glaucomatous damage? J Glaucoma 8: 212-219.

FLAMMER J, ORGUL S, COSTA VP, ORZALESI N, KRIEGLSTEIN GK, SERRA LM, RENARD JP AND STEFANSSON E. 2002. The impact of ocular blood flow in glaucoma. Prog Retin Eye Res 21: 359-393.

FLOOD DG, FINN JP, WALTON KM, DIONNE CA, CONTRERAS PC, MILLER MS AND BHAT RV. 1998. Immunolocalization of the mitogen-activated protein kinases p42(MAPK) and JNK1, and their regulatory kinases MEK1 and MEK4, in adult rat central nervous system. J Comp Neurol 398: 373-392.

FOX RR, CRARY DD, BABINO EJ AND SHEPPARD LB. 1969. Buphthalmia in rabbit - pleiotropic effects of (bu) gene and a possible explanation of mode of gene action. J Hered 60: 206-212.

FOXTON R, OSBORNE A, MARTIN KR, NG YS AND SHIMA DT. 2016. Distal retinal ganglion cell axon transport loss and activation of p38 MAPK stress pathway following VEGF-A antagonism. Cell Death Dis 7: e2212.

FU MM AND HOLZBAUR ELF. 2013. JIP1 regulates the directionality of APP axonal transport by coordinating kinesin and dynein motors. J Cell Biol 202: 495-508.

GIAUME C, KOULAKOFF A, ROUX L, HOLCMAN D AND ROUACH N. 2010. Astroglial networks: a step further in neuroglial and gliovascular interactions. Nature Reviews Neuroscience 11: 87-99.

GREWAL SS, YORK RD AND STORK PJS. 1999. Extracellular-signal-regulated kinase signalling in neurons. Curr Opin Neurobiol 9: 544-553.

GROELZ D, SOBIN L, BRANTON P, COMPTON C, WYRICH R AND RAINEN L. 2013. Non-formalin fixative versus formalin-fixed tissue: a comparison of histology and RNA quality. Exp Mol Pathol 94: 188-194.

GROSS RL, JI J, CHANG P, PENNESI ME, YANG Z, ZHANG J AND WU SM. 2003. A mouse model of elevated intraocular pressure: retina and optic nerve findings. Trans Am Ophthalmol Soc 101: 163-169; discussion 169-171.

GUNDISCH S ET AL. 2012. Variability of protein and phosphoprotein levels in clinical tissue specimens during the preanalytical phase. J Proteome Res 11: 5748-5762.

HANNA BL, SAWIN PB AND SHEPPARD LB. 1962. Recessive buphthalmos in rabbit. Genetics 47: 519-529.

HARADA T ET AL. 2007. The potential role of glutamate transporters in the pathogenesis of normal tension glaucoma. J Clin Invest 117: 1763-1770.

HARUN-OR-RASHID M, DIAZ-DELCASTILLO M, GALINDO-ROMERO C AND HALLBOOK F. 2015. Alpha2-Adrenergic-Agonist Brimonidine Stimulates Negative Feedback and Attenuates Injury-Induced Phospho-ERK and Dedifferentiation of Chicken Muller Cells. Invest Ophthalmol Vis Sci 56: 5933-5945.

HASHIMOTO K, PARKER A, MALONE P, GABELT BT, RASMUSSEN C, KAUFMAN PS AND HERNANDEZ MR. 2005. Long-term activation of c-Fos and c-Jun in optic nerve head astrocytes in experimental ocular hypertension in monkeys and after exposure to elevated pressure in vitro. Brain Res 1054: 103-115.

HERNANDEZ MR, MIAO HX AND LUKAS T 2008. Astrocytes in glaucomatous optic neuropathy. In: NUCCI, C, CERULLI, L, OSBORNE, NN AND BAGETTA, G (Eds.) Glaucoma: An Open Window to Neurodegeneration and Neuroprotection, Amsterdam: Elsevier Science Bv, p. 353-373.

HERNANDEZ MR. 2000. The optic nerve head in glaucoma; Role of astrocytes in tissue remodeling. Prog Retin Eye Res 19: 297.

HETMAN M AND GOZDZ A. 2004. Role of extracellular signal regulated kinases 1 and 2 in neuronal survival. Eur J Biochem 271: 2050-2055.

HOLMAN MC, CHIDLOW G, WOOD JPM AND CASSON RJ. 2010. The Effect of Hyperglycemia on Hypoperfusion-Induced Injury. Invest Ophthalmol Vis Sci 51: 2197-2207.

HORSLEY MB AND KAHOOK MY. 2010. Anti-VEGF therapy for glaucoma. Curr Opin Ophthalmol 21: 112-117.

HOSMANE S, TEGENGE MA, RAJBHANDARI L, UAPINYOYING P, KUMAR NG, THAKOR N AND VENKATESAN A. 2012. Toll/Interleukin-1 receptor domain-containing adapter inducing interferon-beta mediates microglial phagocytosis of degenerating axons. J Neurosci 32: 7745-7757.

HOWELL GR ET AL. 2007. Axons of retinal ganglion cells are insulted in the optic nerve early in DBA/2J glaucoma. J Cell Biol 179: 1523-1537.

HU DN, RITCH R, LIEBMANN J, LIU YZ, CHENG B AND HU MS. 2002. Vascular endothelial growth factor is increased in aqueous humor of glaucomatous eyes. J Glaucoma 11: 406-410.

HUNTWORK-RODRIGUEZ S, WANG B, WATKINS T, GHOSH AS, POZNIAK CD, BUSTOS D, NEWTON K, KIRKPATRICK DS AND LEWCOCK JW. 2013. JNK-mediated phosphorylation of DLK suppresses its ubiquitination to promote neuronal apoptosis. J Cell Biol 202: 747-763.

IBRAHIM AS, EL-REMESSY AB, MATRAGOON S, ZHANG WB, PATEL Y, KHAN S, AL-GAYYAR MM, EL-SHISHTAWY MM AND LIOU GI. 2011. Retinal microglial activation and inflammation induced by amadori-glycated albumin in a rat model of diabetes. Diabetes 60: 1122-1133.

IBRAHIM AS, EL-SHISHTAWY MM, PENA A AND LIOU GI. 2010. Genistein attenuates retinal inflammation associated with diabetes by targeting of microglial activation. Mol Vis 16: 2033-2042.

IRVING EA AND BAMFORD M. 2002. Role of mitogen- and stress-activated kinases in ischemic injury. J Cereb Blood Flow Metab 22: 631-647.

IWAMOTO K, MATA D, LINN DM AND LINN CL. 2013. Neuroprotection of rat retinal ganglion cells mediated through alpha7 nicotinic acetylcholine receptors. Neuroscience 237: 184-198.

JI RR AND SUTER MR. 2007. p38 MAPK, microglial signaling, and neuropathic pain. Mol Pain 3: 9.

JOACHIM SC, GRUS FH, KRAFT D, WHITE-FARRAR K, BARNES G, BARBECK M, GHANAATI S, CAO S, LI B AND WAX MB. 2009. Complex Antibody Profile Changes in an Experimental Autoimmune Glaucoma Animal Model. Invest Ophthalmol Vis Sci 50: 4734-4742.

JOHNSON B, HOUSE P, MORGAN W, SUN XH AND YU DY. 1999. Developing laser-induced glaucoma in rabbits. Aust N Z J Ophthalmol 27: 180-183.

JOHNSON EC, DEPPMEIER LMH, WENTZIEN SKF, HSU I AND MORRISON JC. 2000. Chronology of optic nerve head and retinal responses to elevated intraocular pressure. Invest Ophthalmol Vis Sci 41: 431-442.

JOHNSON G. 2003. The p38 MAP kinase signaling pathway in Alzheimer's disease. Exp Neurol 183: 263-268.

JOHNSON GL AND LAPADAT R. 2002. Mitogen-activated protein kinase pathways mediated by ERK, JNK and p38 protein kinases. Science 298: 1911-1912.

KATOME T ET AL. 2013. Inhibition of ASK1-p38 pathway prevents neural cell death following optic nerve injury. Cell Death Differ 20: 270-280.

KIKUCHI M, TENNETI L AND LIPTON SA. 2000. Role of p38 mitogen-activated protein kinase in axotomy-induced apoptosis of rat retinal ganglion cells. J Neurosci 20: 5037-5044.

KIM B-J, SILVERMAN SM, LIU Y, WORDINGER RJ, PANG I-H AND CLARK AF. 2016. In vitro and in vivo neuroprotective effects of cJun N-terminal kinase inhibitors on retinal ganglion cells. Mol Neurodegener 11.

KIM EK AND CHOI EJ. 2010. Pathological roles of MAPK signaling pathways in human diseases. Biochim Biophys Acta 1802: 396-405.

KIM MJ, FUTAI K, JO J, HAYASHI Y, CHO K AND SHENG M. 2007. Synaptic accumulation of PSD-95 and synaptic function regulated by phosphorylation of serine-295 of PSD-95. Neuron 56: 488-502.

KOISTINAHO M AND KOISTINAHO J. 2002. Role of p38 and p44/42 mitogen-activated protein kinases in microglia. Glia 40: 175-183.

KOKOTAS H, KROUPIS C, CHIRAS D, GRIGORIADOU M, LAMNISSOU K, PETERSEN MB AND KITSOS G. 2012. Biomarkers in primary open angle glaucoma. Clin Chem Lab Med 50: 2107-2119.

KUAN CY ET AL. 2003. A critical role of neural-specific JNK3 for ischemic apoptosis. Proc Natl Acad Sci U S A 100: 15184-15189.

KWONG JMK AND CAPRIOLI J. 2006. Expression of phosphorylated c-Jun N-terminal protein kinase (JNK) in experimental glaucoma in rats. Exp Eye Res 82: 576-582.

LATENDRESSE JR, WARBRITTION AR, JONASSEN H AND CREASY DM. 2002. Fixation of testes and eyes using a modified Davidson's fluid: Comparison with Bouin's fluid and conventional Davidson's fluid. Toxicol Pathol 30: 524-533.

LEE S, VAN BERGEN NJ, KONG GY, CHRYSOSTOMOU V, WAUGH HS, O'NEILL EC, CROWSTON JG AND TROUNCE IA. 2011. Mitochondrial dysfunction in glaucoma and emerging bioenergetic therapies. Exp Eye Res 93: 204-212.

LEVIN LA. 2001. Animal and culture models of glaucoma for studying neuroprotection. Eur J Ophthalmol 11: S23-S29.

LEVKOVITCH-VERBIN H 2015. Retinal ganglion cell apoptotic pathway in glaucoma: initiating and downstream mechanisms. In: BAGETTA, G AND NUCCI, C (Eds.) New Trends in Basic and Clinical Research of Glaucoma: A Neurodegenerative Disease of the Visual System, Pt A, p. 37-57.

LEVKOVITCH-VERBIN H, QUIGLEY HA, MARTIN KRG, VALENTA D, BAUMRIND LA AND PEASE ME. 2002. Translimbal laser photocoagulation to the trabecular meshwork as a model of glaucoma in rats. Invest Ophthalmol Vis Sci 43: 402-410.

LEVKOVITCH-VERBIN H, QUIGLEY HA, MARTIN KRG, ZACK DJ, PEASE ME AND VALENTA DF. 2003. A model to study differences between primary and secondary degeneration of retinal ganglion cells in rats by partial optic nerve transection. Invest Ophthalmol Vis Sci 44: 3388-3393.

LEVKOVITCH-VERBIN H. 2004. Animal models of optic nerve diseases. Eye 18: 1066-1074.

LI HY, LIANG YX, CHIU K, YUAN QJ, LIN B, CHANG RCC AND SO KF. 2013. Lycium barbarum (Wolfberry) reduces secondary degeneration and oxidative stress, and inhibits JNK pathway in retina after partial optic nerve transection. PLoS One 8: 13.

LIM MD, DICKHERBER A AND COMPTON CC. 2011. Before you analyze a human specimen, think quality, variability, and bias. Anal Chem 83: 8-13.

LIU CD, PENG M, LATIES AM AND WEN R. 1998. Preconditioning with bright light evokes a protective response against light damage in the rat retina. J Neurosci 18: 1337-1344.

LIU L, DORAN S, XU Y, MANWANI B, RITZEL R, BENASHSKI S, MCCULLOUGH L AND LI J. 2014. Inhibition of mitogen-activated protein kinase phosphatase-1 (MKP-1) increases experimental stroke injury. Exp Neurol 261: 404-411.

LIU Y AND ALLINGHAM RR. 2017. Major review: Molecular genetics of primary open-angle glaucoma. Exp Eye Res 160: 62-84.

LOBSIGER CS AND LEVELAND DW. 2007. Glial cells as intrinsic components of non-cell-autonomous neurodegenerative disease. Nat Neurosci 10: 1355-1360.

LUO XM, HEIDINGER V, PICAUD S, LAMBROU G, DREYFUS H, SAHEL J AND HICKS D. 2001. Selective excitotoxic degeneration of adult pig retinal ganglion cells in vitro. Invest Ophthalmol Vis Sci 42: 1096-1106.

LYE-BARTHEL M, SUN D AND JAKOBS TC. 2013. Morphology of astrocytes in a glaucomatous optic nerve. Invest Ophthalmol Vis Sci 54: 909-917.

MABUCHI F, LINDSEY JD, AIHARA M, MACKEY MR AND WEINREB RN. 2004. Optic nerve damage in mice with a targeted type I collagen mutation. Invest Ophthalmol Vis Sci 45: 1841-1845.

MAMMONE T, CHIDLOW G, CASSON RJ AND WOOD JP. 2017. Expression and activation of MAP kinases in the optic nerve head in a rat model of ocular hypertension. Mol Cell Neurosci: accepted.

MANABE S AND LIPTON SA. 2003. Divergent NMDA signals leading to proapoptotic and antiapoptotic pathways in the rat retina. Invest Ophthalmol Vis Sci 44: 385-392.

MANDELL JW AND VANDENBERG SR. 1999. ERK/MAP kinase is chronically activated in human reactive astrocytes. Neuroreport 10: 3567-3572.

MARTIN L, PAGE G AND TERRO F. 2011. Tau phosphorylation and neuronal apoptosis induced by the blockade of PP2A preferentially involve GSK3 beta. Neurochem Int 59: 235-250.

MCDONALD TO, HODGES JW, BORGMANN AR AND LEADERS FE. 1969. Water-loading test in rabbits - a method to detect potential ocular hypotensive drugs. Arch Ophthalmol 82: 381-&.

MCKAY JS, STEELE SJ, AHMED G, JOHNSON E AND RATCLIFFE K. 2009. An antibody panel for immunohistochemical analysis of the retina in Davidson's-fixed, paraffin-embedded eyes of rats. Exp Toxicol Pathol 61: 91-100.

MCMAHON C, SEMINA EV AND LINK BA. 2004. Using zebrafish to study the complex genetics of glaucoma. Comparative Biochemistry and Physiology C-Toxicology & Pharmacology 138: 343-350.

MEHAN S, MEENA H, SHARMA D AND SANKHLA R. 2011. JNK: A stress-activated protein kinase therapeutic strategies and involvement in alzheimer's and various neurodegenerative abnormalities. J Mol Neurosci 43: 376-390.

MELENA J, SANTAFE J AND SEGARRA J. 1997. Betamethasone-induced ocular hypertension in rabbits. Methods Find Exp Clin Pharmacol 19: 553-558.

MORGAN JE. 2000. Optic nerve head structure in glaucoma: astrocytes as mediators of axonal damage. Eye 14: 437-444.

MORIN PJ, ABRAHAM CR, AMARATUNGA A, JOHNSON RJ, HUBER G, SANDELL JH AND FINE RE. 1993. Amyloid precursor protein is synthesized by retinal ganglion-cells, rapidly trasported to the optic-nerve plasma-membrane and nerve-terminals, and metabolized. J Neurochem 61: 464-473.

MORRISON J, FARRELL S, JOHNSON E, DEPPMEIER L, MOORE CG AND GROSSMANN E. 1995. Structure and composition of the rodent lamina cribrosa. Exp Eye Res 60: 127-135.

MUELLER C ET AL. 2011. One-step preservation of phosphoproteins and tissue morphology at room temperature for diagnostic and research specimens. PLoS One 6.

MUNEMASA Y AND KITAOKA Y. 2013. Molecular mechanisms of retinal ganglion cell degeneration in glaucoma and future prospects for cell body and axonal protection. Front Cell Neurosci 6: 1-13.

MUNEMASA Y ET AL. 2005. Contribution of mitogen-activated protein kinases to NMDA-induced neurotoxicity in the rat retina. Brain Res 1044: 227-240.

MUNOZ L AND AMMIT AJ. 2010. Targeting p38 MAPK pathway for the treatment of Alzheimer's disease. Neuropharmacology 58: 561-568.

NAKAZAWA T, NAKAZAWA C, MATSUBARA A, NODA K, HISATOMI T, SHE H, MICHAUD N, HAFEZI-MOGHADAM A, MILLER JW AND BENOWITZ LI. 2006. Tumor necrosis factor-alpha mediates oligodendrocyte death and delayed retinal ganglion cell loss in a mouse model of glaucoma. J Neurosci 26: 12633-12641.

NAKAZAWA T, TAMAI M AND MORI N. 2002. Brain-derived neurotrophic factor prevents axotomized retinal ganglion cell death through MAPK and PI3K signaling pathways. Invest Ophthalmol Vis Sci 43: 3319-3326.

NEARY JT, KANG Y, WILLOUGHBY KA AND ELLIS EF. 2003. Activation of extracellular signal-regulated kinase by stretch-induced injury in astrocytes involves extracellular ATP and P2 purinergic receptors. J Neurosci 23: 2348-2356.

NICKELLS RW. 1996. Retinal ganglion cell death in glaucoma: The how, the why, and the maybe. J Glaucoma 5: 345-356.

NITZAN A, KERMER P, SHIRVAN A, BAHR M, BARZILAI A AND SOLOMON AS. 2006. Examination of cellular and molecular events associated with optic nerve axotomy. Glia 54: 545-556.

NOMURA-KOMOIKE K, SAITOH F, KOMOIKE Y AND FUJIEDA H. 2016. DNA Damage Response in Proliferating Muller Glia in the Mammalian Retina. Invest Ophthalmol Vis Sci 57: 1169-1182.

OSBORNE A, ALDARWESH A, RHODES JD, BROADWAY DC, EVERITT C AND SANDERSON J. 2015. Hydrostatic pressure does not cause detectable changes in survival of human retinal ganglion cells. PLoS One 10: e0115591.

OSBORNE NN, WOOD JPM, CHIDLOW G, BAE JH, MELENA J AND NASH MS. 1999. Ganglion cell death in glaucoma: what do we really know? Br J Ophthalmol 83: 980-986.

OZAWA H, SHIODA S, DOHI K, MATSUMOTO H, MIZUSHIMA H, ZHOU CJ, FUNAHASHI H, NAKAI Y, NAKAJO S AND MATSUMOTO K. 1999. Delayed neuronal cell death in the rat hippocampus is mediated by the mitogen-activated protein kinase signal transduction pathway. Neurosci Lett 262: 57-60.

PANG I-H, ZENG H, FLEENOR DL AND CLARK AF. 2007. Pigment epithelium-derived factor protects retinal ganglion cells. BMC Neurosci 8: 11.

PEARSON G, ROBINSON F, GIBSON TB, XU BE, KARANDIKAR M, BERMAN K AND COBB MH. 2001. Mitogen-activated protein (MAP) kinase pathways: Regulation and physiological functions. Endocr Rev 22: 153-183.

PITTMAN RN, WANG SL, DIBENEDETTO AJ AND MILLS JC. 1993. A system for characterizing cellular and molecular events in programmed neuronal cell-death. J Neurosci 13: 3669-3680.

PRODUIT-ZENGAFFINEN N, FAVEZ T, POURNARAS CJ AND SCHORDERET DF 2016. JNK inhibition reduced retinal ganglion cell death after ischemia/reperfusion in vivo and after hypoxia in vitro. In: RICKMAN, CB, LAVAIL, MM, ANDERSON, RE, GRIMM, C, HOLLYFIELD, J AND ASH, J (Eds.) Retinal Degenerative Diseases: Mechanisms and Experimental Therapy, Cham: Springer Int Publishing Ag, p. 677-683.

PURVES D AG, FITZPATRICK D, ET AL., EDITORS. . 2ND EDITION. SUNDERLAND (MA): SINAUER ASSOCIATES; 2001. THE RETINA. AVAILABLE FROM: HTTP://WWW.NCBI.NLM.NIH.GOV/BOOKS/NBK10885/ 2001. Neuroscience.

QI H, PRABAKARAN S, CANTRELLE FX, CHAMBRAUD B, GUNAWARDENA J, LIPPENS G AND LANDRIEU I. 2016. Characterization of neuronal tau protein as a target of extracellular signal-regulated kinase. J Biol Chem 291: 7742-7753.

QUIGLEY HA AND ADDICKS EM. 1980. Chronic experimental glaucoma in primates .2. Effect of extended intraocular-pressure elevation on optic-nerve head and axonal-transport. Invest Ophthalmol Vis Sci 19: 137-152.

QUIGLEY HA AND BROMAN AT. 2006. The number of people with glaucoma worldwide in 2010 and 2020. Br J Ophthalmol 90: 262-267.

RAY K AND MOOKHERJEE S. 2009. Molecular complexity of primary open angle glaucoma: current concepts. Journal of genetics 88: 451-467.

ROHRBACH JM, GRUB M AND SCHLOTE T. 2005. Neoplastic secondary glaucomas. Klinische Monatsblatter Fur Augenheilkunde 222: 788-796.

ROSKOSKI R. 2012. ERK1/2 MAP kinases: Structure, function, and regulation. Pharmacol Res 66: 105-143.

ROTH S, SHAIKH AR, HENNELLY MM, LI Q, BINDOKAS V AND GRAHAM CE. 2003. Mitogen-activated protein kinases and retinal ischemia. Invest Ophthalmol Vis Sci 44: 5383-5395.

SALVADOR-SILVA M, AOI S, PARKER A, YANG P, PECEN P AND HERNANDEZ MR. 2004. Responses and signaling pathways in human optic nerve head astrocytes exposed to hydrostatic pressure in vitro. Glia 45: 364-377.

SANDER EA AND NAUMAN EA. 2010. Effects of reduced oxygen and glucose levels on ocular cells in vitro: implications for tissue models. Cells Tissues Organs 191: 141-151.

SAPPINGTON RM, LOMONACO MB AND CALKINS DJ. 2003. Retinal glial cells produce vascular endothelial growth factor in an in vitro model of glaucoma. Society for Neuroscience

Abstract Viewer and Itinerary Planner 2003: Abstract No. 632.612-Abstract No. 632.612.

SAWAGUCHI K, NAKAMURA Y, NAKAMURA Y, SAKAI H AND SAWAGUCHI S. 2005. Myocilin gene expression in the trabecular meshwork of rats in a steroid-induced ocular hypertension model. Ophthalmic Res 37: 235-242.

SCHMIDT KG, PILLUNAT LE AND OSBORNE NN. 2004. Ischemia and hypoxia. An attempt to explain the different rates of retinal ganglion cell death in glaucoma. Ophthalmologe 101: 1071-1075.

SHACKELFORD DA AND YEH RY. 2006. Modulation of ERK and JNK activity by transient forebrain ischemia in rats. J Neurosci Res 83: 476-488.

SHIELDS MB. 2008. Normal-tension glaucoma: is it different from primary open-angle glaucoma? Curr Opin Ophthalmol 19: 85-88.

SOFRONIEW MV AND VINTERS HV. 2010. Astrocytes: biology and pathology. Acta Neuropathol 119: 7-35.

SONTAG E, LUANGPIROM A, HLADIK C, MUDRAK I, OGRIS E, SPECIALE S AND WHITE CL. 2004. Altered expression levels of the protein phosphatase 2A AB alpha C enzyme are associated with Alzheimer disease pathology. J Neuropathol Exp Neurol 63: 287-301.

STANCIU M AND DEFRANCO DB. 2002. Prolonged nuclear retention of activated extracellular signal-regulated protein kinase promotes cell death generated by oxidative toxicity or proteasome inhibition in a neuronal cell line. J Biol Chem 277: 4010-4017.

SUGINO T, NOZAKI K, TAKAGI Y, HATTORI I, HASHIMOTO N, MORIGUCHI T AND NISHIDA E. 2000. Activation of mitogen-activated protein kinases after transient forebrain ischemia in gerbil hippocampus. J Neurosci 20: 4506-4514.

SUN H, WANG Y, PANG IH, SHEN JQ, TANG X, LI Y, LIU CY AND LI B. 2011. Protective effect of a JNK inhibitor against retinal ganglion cell loss induced by acute moderate ocular hypertension. Mol Vis 17: 864-875.

TAKEDA K AND ICHIJO H. 2002. Neuronal p38 MAPK signalling: an emerging regulator of cell fate and function in the nervous system. Genes Cells 7: 1099-1111.

TEZEL G, CHAUBAN BC, LEBLANC RP AND WAX MB. 2003. Immunohistochemical assessment of glial mitogen-activated protein kinase (MAPK) activation in glaucoma. Invest Ophthalmol Vis Sci 7: 3025-3033.

TEZEL G, YANG XJ, YANG JJ AND WAX MB. 2004. Role of tumor necrosis factor receptor-1 in the death of retinal ganglion cells following optic nerve crush injury in mice. Brain Res 996: 202-212.

THANGARAJ G, GREIF A AND LAYER PG. 2011. Simple explant culture of the embryonic chicken retina with long-term preservation of photoreceptors. Exp Eye Res 93: 556-564.

TORIS CB, ZHAN GL, WANG YL, ZHAO J, MCLAUGHLIN MA, CAMRAS CB AND YABLONSKI ME. 2000. Aqueous humor dynamics in monkeys with laser-induced glaucoma. J Ocul Pharmacol Ther 16: 19-27.

TOURNIER C, POMERANCE M, GAVARET JM AND PIERRE M. 1994. MAP Kinase cascade in astrocytes. Glia 10: 81-88.

ULLIAN EM, BARKIS WB, CHEN S, DIAMOND JS AND BARRES BA. 2004. Invulnerability of retinal ganglion cells to NMDA excitotoxicity. Mol Cell Neurosci 26: 544-557.

VECINO E, DAVID RODRIGUEZ F, RUZAFA N, PEREIRO X AND SHARMA SC. 2016. Glia-neuron interactions in the mammalian retina. Prog Retin Eye Res 51: 1-40.

VLAHOPOULOS S AND ZOUMPOURLIS VC. 2004. JNK: A key modulator of intracellular signaling. Biochem-Moscow 69: 844-854.

VOGELSBERG-RAGAGLIA V, SCHUCK T, TROJANOWSKI JQ AND LEE VM. 2001. PP2A mRNA expression is quantitatively decreased in Alzheimer's disease hippocampus. Exp Neurol 168: 402-412.

WALSHE TE, LEACH LL AND D'AMORE PA. 2011. TGF-β signaling is required for maintenance of retinal ganglion cell differentiation and survival. Neuroscience 189: 123-131.

WANG L, CIOFFI GA, CULL G, DONG J AND FORTUNE B. 2002. Immunohistologic evidence for retinal glial cell changes in human glaucoma. Invest Ophthalmol Vis Sci 43: 1088-1094.

WANG L, COSSETTE SM, RARICK KR, GERSHAN J, DWINELL MB, HARDER DR AND RAMCHANDRAN R. 2013. Astrocytes directly influence tumor cell invasion and metastasis in vivo. PLoS One 8: 13.

WANG X ET AL. 2016. Requirement for Microglia for the Maintenance of Synaptic Function and Integrity in the Mature Retina. J Neurosci 36: 2827-2842.

WATKINS TA, WANG B, HUNTWORK-RODRIGUEZ S, YANG J, JIANG ZY, EASTHAM-ANDERSON J, MODRUSAN Z, KAMINKER JS, TESSIER-LAVIGNE M AND LEWCOCK JW. 2013. DLK initiates a transcriptional program that couples apoptotic and regenerative responses to axonal injury. Proc Natl Acad Sci U S A 110: 4039-4044.

WAX MB AND TEZEL G. 2009. Immunoregulation of retinal ganglion cell fate in glaucoma. Exp Eye Res 88: 825-830.

WEBER AJ AND ZELENAK D. 2001. Experimental glaucoma in the primate induced by latex microspheres. J Neurosci Methods 111: 39-48.

WELSBIE DS ET AL. 2013. Functional genomic screening identifies dual leucine zipper kinase as a key mediator of retinal ganglion cell death. Proc Natl Acad Sci U S A 110: 4045-4050.

WOOD JPM, MAMMONE T, CHIDLOW G, GREENWELL T AND CASSON RJ. 2012. Mitochondrial Inhibition in Rat Retinal Cell Cultures as a Model of Metabolic Compromise: Mechanisms of Injury and Neuroprotection. Invest Ophthalmol Vis Sci 53: 4897-4909.

XU YF, FU LL, JIANG CH, QIN YW, NI YQ AND FAN JW. 2012. Naloxone inhibition of lipopolysaccharide-induced activation of retinal microglia is partly mediated via the p38 mitogen activated protein kinase signalling pathway. J Int Med Res 40: 1438-1448.

YANG J-C, JI X-Q, LI C-L, LIN J-H AND LIU X-G. 2004. Impact of early-stage hepatic ischemia-reperfusion injury on other organs of rats. Di 1 jun yi da xue xue bao = Academic journal of the first medical college of PLA 24: 1019-1022.

YE X, REN H, ZHANG M, SUN Z, JIANG AC AND XU G. 2012. ERK1/2 signaling pathway in the release of VEGF from Muller cells in diabetes. Invest Ophthalmol Vis Sci 53: 3481-3489.

YONG HY, KOH MS AND MOON A. 2009. The p38 MAPK inhibitors for the treatment of inflammatory diseases and cancer. Expert Opin Investig Drugs 18: 1893-1905.

YUCEL YH, GUPTA N, ZHANG Q, MIZISIN AP, KALICHMAN MW AND WEINREB RN. 2006. Memantine protects neurons from shrinkage in the lateral geniculate nucleus in experimental glaucoma. Arch Ophthalmol 124: 217-225.

ZEKE A, MISHEVA M, REMENYI A AND BOGOYEVITCH MA. 2016. JNK signaling: Regulation and functions based on complex protein-protein partnerships. Microbiol Mol Biol Rev 80: 793-835.

ZHANG SSM, FU XY AND BARNSTABLE CJ. 2002. Tissue culture studies of retinal development. Methods 28: 439-447.

ZHOU RH, YAN H, WANG BR, KUANG F, DUAN XL AND XU Z. 2007. Role of extracellular signal-regulated kinase in glutamate-stimulated apoptosis of rat retinal ganglion cells. Curr Eye Res 32: 233-239.